INNOVATIVE METHOD OF PRESTRESSING STRUCTURES WITH EXTERNALLY BONDED FRP COMPOSITES

by

NIKOLA DESKOVIC

Diploma in Civil Engineering, University of Split
(1988)

SUBMITTED TO THE DEPARTMENT OF CIVIL ENGINEERING
IN PARTIAL FULFILLMENT OF THE REQUIREMENTS
FOR THE DEGREE OF

MASTER OF SCIENCE IN CIVIL ENGINEERING

at the

MASSACHUSETTS INSTITUTE OF TECHNOLOGY

February, 1991

Signature of Author_____
Department of Civil Engineering
February 1991

Certified by_____
Thanasis Triantafillou
Thesis Supervisor

Accepted by_____
Ole S. Madsen
Chairman, Departmental Graduate Committee

Innovative Method Of Prestressing Structures With Externally Bonded FRP Composites

by

Nikola Deskovic

Submitted to the Department of Civil Engineering
on January 18, 1991 in partial fulfillment of the
requirements for the Degree of Master of Science in
Civil Engineering

Abstract

The short term mechanical behavior of a novel prestressing technique is described. The technique involves external bonding of pretensioned fiber-reinforced plastic (FRP) composite sheets on the tension zones of structural elements. Analytical models are developed describing the maximum achievable prestress level so that the FRP-prestressed system does not fail near the anchorage zones. Both adhesive layer and beam material failures are considered. An experimental program was carried out and proved the validity of the analytical solution.

The effectiveness of the method on the flexural behavior of R/C and wood beams was studied both analytically and experimentally. FRP-prestressed structural members show improved strength and stiffness characteristics, while maintaining good ductility properties. The agreement between theory and experiments for the ultimate member loads was found to be satisfactory. The technique is applicable to the rehabilitation/strengthening of existing structures as well as the construction of new ones.

A new design concept, consisting of fiber-reinforced concrete prestressed by externally bonded CFRP sheets was developed and it is demonstrated that it has the potential to improve the traditional R/C design, creating a corrosion resistant and simple to fabricate system without conventional steel reinforcement.

Thesis Supervisor: Thanasis Triantafillou
Title: Assistant Professor of Civil Engineering

To my loving parents:

Mojim roditeljima, koji su mi svojom podrskom i ljubavlju omogucili sve sto sam ostvario, na cemu cu im zauvijek ostati zahvalan, sa zeljom da cu uvijek opravdati ukazano mi povjerenje.

AKNOWLEDGEMENTS

I would first like to express my warmest thanks to my mother, Dora, my brother Zarko, my whole family and my beloved Katja, whose love and encouragement constituted a priceless support.

I would like to express my profound gratitude to Professor Thanasis Triantafillou, my thesis supervisor, for his expert and invaluable guidance as well as his financial support throughout the course of this thesis, his abundant help, his never ending patience and at last his sincere friendship.

I would like to thank Professor Urs Meier, for having provided the opportunity to perform the essential experimental program at the EMPA (Swiss Federal Laboratories for Materials Testing and Research) as well as his financial support during my stay in Duebendorf.

Many thanks are due to Patrick Kim, Heinz Meier and Martin Deuring, who introduced me to the facilities at the EMPA and whose help and friendship I deeply appreciate.

I would also like to thank Mr. Jaene, Krebs and Waldvogel for their technical assistance at the EMPA.

I can not thank enough to all my good friends from the Department of Civil Engineering: Nicolaos Plevris, Hayat Tazir, Charis Gantes, Adrian Eterovic, Alan Brik, Riad Ghibril, Axel De La Beaumelle, Alex Elvin, Craig Schwitter, Mariano Valle, Gebran Karam, Gokan Goktuk, Patrick Kinnicutt, Ruadhri O'Connor, Nestor Agbayani, Antonio Tadeo, all the members of the soccer team Cosmos and all the others that I have unintentionally forgotten.

TABLE OF CONTENTS

LIST OF FIGURES

LIST OF SYMBOLS

A = area or

= coefficient;

A_s = tension steel area;

A_s' = compression steel area;

B = coefficient;

C = integration constant or

= FRC compression force;

C_b = geometric parameter;

C_C = compressive force in concrete block;

C_S = compressive force in steel reinforcement;

C_W = wood compression force;

E_b = Young's modulus of beam material;

E_c = Young's modulus of concrete;

E_f = Young's modulus of fibers;

E_{fc} = Young's modulus of fiber-composite;

E_m = Young's modulus of matrix;

E_s = Young's modulus of steel;

E_w = Young's modulus of wood;

$E_{||}$ = Young's modulus of FRP paralell to fiber direction;

F_{be} = bond factor;

F_{fc} = force in FRP sheet;

F_{fc}^o = total force in FRP sheet;

G_a = shear modulus of adhesive;

G_w = shear modulus of wood;

I = moment of inertia;

M_{CR} = FRC cracking moment;

M_{cr} = concrete first cracking moment;

M_u = ultimate moment capacity;

P_{el} = maximum elastic load in three point bending tests;

P_u = ultimate load;

P^* = failure load in three point bending tests;

T = FRC tension force;

T_C = tensile force in concrete;

T_g = glass transition temperature;

T_S = tensile force in steel reinforcement;

T_W = wood tension force;

V_C = concrete shear contribution;

V_F = prestressing shear contribution;

V_f = volume fraction of fibers;

V_S = steel shear contribution;

V_u = ultimate shear force;

a = geometric parameter for concrete compression force or
= shear span or
= depth of wood plastified zone;

a_f = concrete compression force lever arm;

a_o = concrete cover;

b = width of cross section;

b' = width of FRP sheet;

c = depth of neutral axis;

d = thickness of adhesive layer;

d_f = fiber diameter;

e = position in cross section where fiber pullout starts;

f_c = concrete stress at top face or
= wood compression strength;

f_c' = concrete compression strength;

f_r = concrete modulus of rupture;

$f_t^{'}$ = tensile strength of concrete;

f_y = steel yield strength;

h = height of cross section;

$h^{'}$ = distance from the centroid of the section to the extreme compressive fiber;

k = geometric parameter;

l = beam length;

l' = length of elastic region;

t = thickness of composite sheet;

t' = modified thickness of composite sheet;

u_b = displacement of the beam at the bottom fiber;

u_{fc} = displacement of fiber-composite after the pretension is released;

u_{fc}^{o} = initial displacement of fiber composite;

v_c = plain concrete ultimate shear stress;

v_s = shear reinforcement shear stress contribution;

x = distance from mid-span;

x' = distance from the origin of the nonlinear zone;

x^{*} = distance from beam end;

x^{o} = distance from nonlinear zone;

α = constant;

β_1 = compressive block hight ratio;

γ = shear strain in the adhesive;

γ_a^{*} = ultimate shear strain of adhesive;

γ_a^{el} = maximum elastic strain of adhesive;

γ_w^{el} = maximum elastic strain of wood;

γ_w^{*} = ultimate wood shear strain;

δ = shear slip or

= midspan deflection;

δ_{el} = maximum elastic starin in 3 point bending tests;

δ^* = characteristic shear slip;

ε_c = cocnrete strain at top face;

ε_{cu} = ultimate concrete compression strain;

ε_{fc} = normal strain in fiber-composite;

ε^o_{fc} = initial normal strain in fiber-composite;

ε^*_{fc} = uniaxial strain of fiber-composite at failure;

ε_s = strain in FRC at fiber pullout;

ε_{SC} = strain in compression steel;

ε_{ST} = strain in tension steel;

ε_T = strain at beam bottom fiber;

ν_{CF} = average shear strength in FRC;

ρ_{CS} = area fraction of compression reinforcement;

ρ_{fc} = FRP composite area fraction;

ρ_s^{max} = maximum steel area fraction;

ρ_s = area fraction of longitudinal steel;

ρ_{TS} = area fraction of tension reinforcement;

σ_f = stress in fibers at assumed bond stress;

σ^*_f = tensile strength of fibers;

σ_{fc} = normal stress in fiber-composite;

σ^o_{fc} = initial pretension in fiber-composite;

σ^*_{fc} = ultimate tensile strength of FRP comcpoite;

$\sigma^{initial}_{fc}$ = initial pretension of the FRP sheet;

σ'_m = stress in matrix at fracture strain of fibers;

σ_p = prestress at the bottom fiber of the beam;

σ_T = tensile stress in FRC;

τ = shear stress at the interface between the fiber-composite and the beam;

τ_a^* = shear strength of adhesive;

τ_c^* = shear strength of concrete;

τ_d = dynamic bond stress; and

τ_w^* = wood shear strength.

CHAPTER 1

INTRODUCTION

1.1 FIBER REINFORCED PLASTICS IN STRUCTURES

Fiber-reinforced composites have been used by man for a very long time. The first to be used were naturally occurring composites, such as wood. The issue was to use materials that would perform more efficiently in their specific application. Today engineers make artificial fiber-composite materials using glass, carbon or Kevlar fibers, bonded together with a matrix such as epoxy resin. By combining fibers and plastic matrix a bulk material is produced with a strength and stiffness close to that of the fibers and with the chemical resistance of the plastic. Among the properties of fiber-reinforced plastics (FRP) are high tensile strength, low weight, resistance to corrosion and high fatigue strength (Hull, 1981). Fiber-composites offer unique advantages for solving many civil engineering problems in areas where conventional materials do not perform well. Such areas include corrosive environments and structural elements required to have high strength/weight ratio.

Potential applications of FRP in structural engineering include: (a) development of high-strength lightweight cables in cable-supported bridges (e.g. Meier, 1987a; Aminian and White, 1988; Burgoyne, 1988; and Plecnik et al., 1989) or tendons in prestressed elements (e.g. Rubinsky and Rubinsky, 1954; Kaifasz, 1963; Somes, 1963; Rehm and Franke, 1974 and 1979; Weiser and Preis, 1984; Chambers, 1986; Preis and Bell, 1986; Waaser and Wolff, 1986; Gerritse et al., 1987; and Wolff and Miesseler, 1987); (b) replacement of steel used as reinforcement in concrete structures by composite rebars, offering corrosion resistance and providing non-conductive/magnetic fields (e.g. Fujisaki

et al., 1987; Saadatmanesh and Ehsani, 1989; Brown and Bartholomew, 1990; and Faza and GangaRao, 1990); (c) development of lightweight structural components such as framing and bridges (e.g. McCormick, 1978; Bakeri, 1989; Plecnik, 1989; Bank and Mosallam, 1990; and Fu et al., 1990); and (d) strengthening of existing structural members with epoxy-bonded fiber-composite sheets. The last application involves external bonding of thin FRP composite sheets on the tension face of beams using epoxy resins (Ranisch and Rostasy, 1986; Meier, 1987b; Kaiser, 1989; Saadatmanesh and Ehsani, 1989; and Triantafillou and Plevris, 1990). The composite sheets are made of unidirectional, continuous fibers bonded together with an epoxy resin matrix.

In this work, the spectrum of the use of FRP composites in structural design is expanded through a novel technique conceptualized at the EMPA (Swiss Federal Laboratories for Materials Testing and Research) (Kaiser, 1989; Deuring, 1990; Meier, 1990) of strengthening and/or reinforcing structural components. The technique can be thought of as a better way of strengthening structures using corrosion resistant and lightweight materials as well as a more economical alternative to prestressing methods used in new construction.

1.2 STRENGTHENING OF STRUCTURES

In general, a structure requires strengthening when its load-carrying capacity is not sufficient to resist the applied loads. When considering bridges, this might be due to increased traffic loads (e.g. by adding one additional lane), while in building construction strengthening may be required when a reconstruction (e.g. removal of a bearing wall or column to obtain larger spaces) is desired due to architectural layout changes. In concrete construction, this problem is highlighted with the loss of strength due to corrosion of reinforcement and spalling of concrete. Another typical reason for the need of strengthening is encountered when placement of steel reinforcement has been omitted by mistake or poor design. Among the known methods used to strengthen beams in existing bridges or buildings are external post-tensioning and the addition of epoxy-bonded steel

plates to the tension face. External post-tensioning by means of high-strength strands has been successfully employed to increase the load-bearing capacity of structures (e.g. Dunker et al., 1985; Saadatmanesh et al., 1989). This method, however, presents some difficulties in providing anchorage for the post-tensioning strands, maintaining the lateral stability of the girders during post-tensioning, and protecting the strands against corrosion. The addition of epoxy-bonded steel plates to the tension face of concrete girders is primarily used to repair and strengthen reinforced concrete elements with insufficient load carrying capacity due to mechanical damages, functional changes, or corrosion. The principles of this strengthening technique are obvious: epoxy-bonded steel plates on the tension face of a beam increase both its strength and stiffness. The advantages of this structural system include ease of application and elimination of the special anchorages needed in the post-tensioning method. A shortcoming of the method is the danger of corrosion at the epoxy-steel interface, which adversely affects the bond strength.

An effective way of eliminating the corrosion problem is to replace steel plates with corrosion resistant materials such as fiber composites (Meier, 1987b; Kaiser, 1989; Saadatmanesh and Eshani, 1989). When compared to other fiber composites, carbon FRP (CFRP) materials show superior characteristics in structural behavior. While glass FRP are sensitive to humid environments and Kevlar fibers are sensitive to sun light, carbon FRP have better durability, fatigue and creep characteristics. CFRP have been available since the early 1960's, their first application being in the aerospace industry, where the advantages of this high-performance material have been explored properly. The modulus-to-density ratio of CFRP is the highest available for structural materials and, hence, CFRP are found where maximum stiffness and light weight are essential. In bridge strenghtening applications, apart from the improvement in corrosion resistance, recent analysis has shown that the use of CFRP sheets permits considerable cost savings for the scaffolding needed (Meier, 1986). Because the composite sheets are extremely light, scaffolding is replaced by a hydraulic lift and the sheets are bonded from the working platform by pressing them on using a vacuum bag during the hardening process of the adhesive. Despite the much higher price of the CFRP sheet (approximately 40

times higher than steel), the total cost for this type of strengthening can be reduced by about 20% when compared to the method with steel plates. Another advantage was the enhanced fatigue life of CFRP materials when compared to steel. In addition, the composite sheets can be rolled and transported to construction sites easily. If high-strength steel plates were used instead, apart from restricted manufacturers availability, limited delivery lengths and restrictions to welding processes (high carbon contents of the steel plates) would impede the application on larger structures. On the other hand, prestressing of low strength steel with corresponding low elastic strains is not possible, since pretension losses due to creep, relaxation, shrinkage, etc. being of the same order of magnitude as the applied prestress levels, would cancel the initial pretension (Kaiser, 1989). Hence, the advantages of lower Young's modulus and high elastic strains of the CFRP sheets are obvious when they are used as prestressed reinforcement. It should be noticed that due to the high cost of the CFRP laminates, their beneficial properties have to be explored to their ultimate level and the efficiency in the application has to be maximized.

Combining these aspects and both strengthening techniques described above, a new method of external prestressing consisting of prestressed CFRP sheets epoxy-bonded on the tension face of structural elements is analyzed in this work. Motivated by the considerations mentioned above a study of the proposed strenghtening method was carried out. The analytical and experimental work performed can be summarized within two main guidelines. First, the maximum pretension stress was defined analytically such that upon releasing the prestress, failure of the system structural member-composite sheet does not occur; the analysis was accompanied by an experimental validation. Second, the improvement of the flexural behavior of members reinforced according to the new concept was investigated, focusing on the efficiency of the prestressing levels applied and comparing to equally reinforced, but unprestressed structures. The method was applied to both reinforced concrete and wood members and good agreement between experiment and analysis was found.

1.3 NEW CONSTRUCTION METHOD

Not only strengthening techniques but also reinforcing procedures applicable to the construction of new structural elements can be considered as potential applications of the new method. It appears that the technique can be implemented efficiently in the production of prefabricated prestressed elements. Simplicity of production process and low labor cost, high stiffness and low weight, high corrosion and fatigue resistance, electromagnetic neutrality etc. are sufficient factors to justify the high material cost. It should be mentioned that the cost of CFRP materials would decrease if its production were to increase. The high cost today is basically a result of the fabrication organization. Most manufacturers produce standard glass fiber materials and have to switch the production process in order to fulfill some small orders of CFRP materials. This is then associated with high expenses and thus, the market price is rather high. The author believes that in future the production of CFRP materials will increase and they will be used more widely in all engineering branches, including structural engineering.

The results obtained from the above study were used to create and implement an innovative design concept for the fabrication of concrete structures. The main objective here was to design a concrete beam without any traditional reinforcement, where the bending strength is provided by externally epoxy-bonded, prestressed CFRP sheets, while the shear loads are carried by fibrous inclusions in the concrete mix. From the analysis performed it is seen that the rather challenging idea can be implemented successfully and at a preliminary stage practical application can be anticipated.

1.4 ORGANIZATION OF THE THESIS

The present work is organized in eight chapters, with the main emphasis given in Chapters 3, 4, 5, 6 and 7 in which both the analytical and experimental work are described and an innovative prestressing method is presented.

Chapter 2 is devoted to a brief literature review. This review describes the

literature on : a) strengthening of structures with externally bonded reinforcement and b) the external prestressing techniques used in recent engineering practice.

A new method of external prestressing is presented in Chapter 3. Several failure mechanisms after the pretension is released are considered: a) adhesive shear failure and b) beam shear failure, the latter including a nonlinear model for concrete beams and both linear and nonlinear models for wood beams. The maximum pretension stress for all these failure modes was derived analytically and the equations for the distribution of the normal and shear stresses in the beam-adhesive interface are given. For the cases of adhesive and concrete shear failure a study of the method's efficiency was carried out.

In Chapter 4 the experimental verification of the analysis presented earlier is described. Both concrete and wood beams were reinforced with externally epoxy-bonded prestressed FRP sheets by means of a special prestressing apparatus and the magnitude of the ultimate prestress force causing failure of the system was recorded. The results from these tests are reported and correlated to the analytical values calculated using the procedures described in Chapter 3.

The influence of prestressing with externally bonded CFRP sheets on the flexural behavior of reinforced concrete members is studied in Chapter 5. The equations for the analysis of the bending behavior are derived for : a) first cracking of concrete; b) steel first yield and c) concrete crushing. Test results on four CFRP prestressed R/C beams in three point bending are compared to the analytical values. The efficiency of the prestressing method is studied using a computer program to analyze the ultimate moment capacity for various area fractions of the CFRP sheet.

The flexural behavior of wood beams prestressed with externally bonded CFRP sheets is investigated both analytically and experimentally in Chapter 6. Results from three point bending tests on 11 wood beams are compared to the analytical values for wood compression yielding and CFRP sheet rupture.

In Chapter 7 a new concept of hybrid FRP-concrete structural elements is presented. A brief review of the properties of fiber reinforced concrete and the equations for its ultimate strength in bending and shear is given first, followed by a study of the behavior of fiber reinforced concrete elements with externally bonded prestressed CFRP

sheets. Finally, a comparison of the structural performance of the new concept and the traditional design of reinforced concrete structures is carried out.

Chapter 8 summarizes the main findings that have come out of the research work. Conclusions regarding the effect of the prestressing procedure and the method's efficiency are given. A discussion on the possible improvements of the proposed method is presented and recommendations regarding future investigation expanding the presented research work are given.

CHAPTER 2

LITERATURE REVIEW

2.1 GENERAL

The work of structural engineers in the past has always been related to the construction and design of new structures, but later work on their maintenance, rehabilitation and upgrading gained in significance, and currently the latter became equally important. Only in the U.S. about one half of the approximately 600,000 highway bridges are in need of replacement or rehabilitation (Klaiber et al., 1987). A similar situation can be found in Europe where many post-war structures are inadequate to satisfy new serviceability requirements. Many bridges were originally developed for smaller vehicles, lighter loads and lower traffic volumes than common today, and hence, can not achieve the required load carrying capacity. Several solutions for this problem were found and the two most important strengthening techniques are bonding of reinforcing plates or sheets of various materials on the tension zones and external post-tensioning, which is also used in the construction of new structures.

2.2 STRENGTHENING OF STRUCTURES WITH EXTERNALLY BONDED REINFORCEMENT

Strengthening of reinforced concrete members in situ by externally bonded steel plates using epoxy resins has been recognized to be an efficient and convenient method of improving their structural performance. This technique has been used widely for both

bridges and buildings. Early research work established the static performance of beams and slabs with steel plates as tensile and shear reinforcement (L' Hermite and Bresson, 1967; Kaifasz, 1967; Fleming and King, 1967; and Lerchenthal, 1967). Jones et al. (1980) reported test results of reinforced concrete beams strengthened with externally epoxy-bonded steel plates on their tension face. They discussed the effects of adhesive type and steel strength on the deflection, mode of failure, load at first cracking and ultimate strength; and concluded that the range of elastic behavior, the stiffness and the flexural strength are all increased, the tension stresses in the concrete are reduced, and that the appearance of first cracking is delayed. MacDonald and Calder (1982) studied the behavior of concrete beams externally reinforced with steel plates bonded on their tension flanges. They concluded that substantial improvements in terms of ultimate load, crack control and stiffness can be achieved. Results of exposure tests, though, showed that the steel plates may corrode significantly during natural exposure, causing losses in the interface bond strength. A series of comprehensive test data on the effect of plate and adhesive thickness and layered and lapped plates were presented by Swamy et al. (1987a). From the analysis standpoint, the above studies verified the validity of the strain compatibility method for the prediction of the failure loads and concluded that external steel plates can be treated in a manner similar to conventional longitudinal reinforcement. Summarizing, it can be concluded that strengthening through external bonding of steel plates has several disadvantages. The most important ones include the deterioration of the bond at the steel-concrete interface caused by corrosion of steel and difficulties in manipulating the plates at the construction site and obtaining appropriate connections between single plates due to the limited delivery lengths.

These problems have led to the idea of replacing the steel plates by fiber reinforced composite sheets (e.g. Ranish and Rostasy, 1986; Meier, 1987b; Saadatmanesh and Ehsani, 1989; and Kaiser, 1989). The composite plates are made of unidirectional , continuous fibers such as glass, carbon and Kevlar, bonded together with an epoxy resin matrix. Saadatmanesh and Ehsani (1989) reported preliminary results from the study of reinforced concrete beams with glass FRP sheets bonded on the tensile zone. Their work emphasizes that selection of the appropriate adhesive is of primary

importance in the mechanical performance of the strengthened members. They suggest that the adhesive should have sufficient stiffness and strength to transfer the interface shear and also adequate toughness to prevent brittle bond failure as a result of cracking of concrete. The main disadvantages in the use of GFRP lies in its low tensile strength and sensitivity to humid environments.

CFRP sheets were employed for the first time in reinforced concrete strengthening applications by Kaiser (1989). His study includes the development of an analytical model for the composite plate anchoring which is in good agreement with experimental results. In his work he provides an extensive insight in the characteristics and behavior of the CFRP-reinforced concrete system. The main advantages of the CFRP composites, when used as external reinforcement of structures can be summarized as follows:

- No corrosion sensitivity and, therefore, no corrosion protection required, even in heavily salt saturated environments.
- High strength, dependent on the volume percentage and type of carbon fibers.
- Elastic behavior up to failure, and hence, a large elastic strain.
- Low density and hence easy manipulation and application procedures.
- The shear modulus and elastic shear strain allow for sufficient rotation such that the sheets can be rolled and transported to the construction site in a similar manner as prestressing tendons.

The main disadvantage of CFRP is its high cost which is based on the low amount produced, but, according to some predictions, should decrease in the future.

2.3 EXTERNAL PRESTRESSING

External prestressing implies the use of unbonded tendons outside the concrete section of a structural concrete member. It is considered to be a primary method for the rehabilitation and strengthening of existing structures. Because of the substantial economic savings and dramatic increase in rapidity of construction possible with this

technology, its application in the construction of concrete bridges is increasing. External prestressing was used for the first time in the early fifties, where for the first time the prestressing tendons were placed outside the concrete cross section (Magnel, 1953). Leonhard (1973) introduced external cables in prestressed box-girder bridges, constructed with the so-called launching method. In the 1960's and 1970's use of external prestressing was abandoned since several structures pretensioned with this method showed, some time after completion, corrosion problems due to insufficient protection of the prestressing tendons by the compacted mortar. In other cases, the pulling of the prestressing steel through holes in the steel deviators, during construction, and the stressing of the steel itself caused problems due to friction in the deviation zones.

The reason for redevelopment of external prestressing leads back to the demand for methods to repair prestressed concrete bridges with corroded prestressing tendons in concrete structures. Another beneficial property of the external prestressing method is its less complex construction procedure when compared to conventional prestressing procedures. In France, which is the mother-country of the prestressing technique in general, in the last ten years practically all large prestressed concrete road bridges have been built with external tendons (Virlogeux, 1990). This demonstrates that external prestressing offers great economical advantages for contractors. Recently this technique is developed in the U.S. (Muller, 1980), Germany, Switzerland and Belgium.

Some other applications of this technology are prestressed trusses, provisional prestressed concrete structures, cable-stayed bridges with short pilons, span by span in situ construction, continuous tendons of bridges executed according to the cantelevering construction method, prestressing of timber etc. Summarizing the advantages of external prestressing several properties have to be mentioned, such as the simple construction on the site, the possibility of inspection and replacement of the tendons etc. The main disadvantages, apart from corrosion, are vulnerability of the structure to fire, damage and sabotage. When considering the application of this method some special attention should be given to the anchorages, deviation zones, ducts and corrosion protection of the prestressing steel.

2.4 SUMMARY

From the literature review presented in this chapter it can be concluded that two concepts, namely the use of externally bonded FRP plates for the rehabilitation of structures and external prestressing, have the potential to become a technological "must" in future structural application. Combining the two concepts through the use of prestressed FRP sheets appears to be a promising way not only for strengthening of old structures but also for the rehabilitation of new ones. This concept is explored in this thesis.

CHAPTER 3

ANALYTICAL PREDICTION OF MAXIMUM PRESTRESS FORCE

3.1 INTRODUCTION

The new method of external prestressing is illustrated in Fig. 3.1. The composite sheet is first pretensioned and applied to the tension face of the beam (Fig. 3.1a, b). The two far ends of the composite are cut once the adhesive has fully hardened and the sheet is then transformed into a prestressing element (Fig. 3.1c). The effectiveness of the technique depends on a basic understanding of the member failure mechanisms after the pretension is released. Hence, the first problem that can be addressed is to determine the maximum pretension stress, for given geometry and material properties, so that, upon releasing it, failure of the system does not occur. In this chapter an analytical solution to this problem is given for the various failure modes that can be encountered.

3.2 ANALYTICAL SOLUTION FOR THE INTERFACE SHEAR

Consider the structural member (in the future text refered to as "beam") shown in Fig. 3.1b; it has a length l, a height h and a width b. The thicknesses of the composite sheet and the adhesive layer are t and d, respectively. The material properties are as follows:

E_b = Young's modulus of beam

E_{fc} = Young's modulus of fiber-composite sheet; and

G_a = shear modulus of adhesive.

It is assumed that the FRP is pretensioned at a stress level σ^o_{fc}. Upon releasing the tension (Fig. 3.1c), the normal stress in the FRP drops to $\sigma_{fc}(x)$ and a compressive stress $\sigma_p(x)$ develops at the bottom fiber of the beam; the stress transfer from the FRP sheet to the beam is achieved through shearing of the adhesive layer, the shear stress at a distance x from the origin being $\tau(x)$.

Figure 3.2 illustrates the displacements at x of the three different components (FRP, adhesive, beam) before and after the pretension is released. The following notation is used: $u^o_{fc}(x)$=initial extension of the FRP; $u_{fc}(x)$=extension of the FRP shortly after the pretension is released; and $u_b(x)$=shortening of the beam at the bottom fiber. The analysis presented next is based on the following assumptions:

a) the materials are linear elastic;
b) the governing deformation mode in the adhesive layer is shear; and
c) the FRP sheet and the beam have only axial deformations, which are uniform along their height.

The shear strain in the interface at a distance x from the origin can be written as:

$$\gamma = \frac{u^o_{fc} - u_{fc} + u_b}{d} \tag{3.1}$$

and the interface shear is:

$$\tau = \frac{G_a}{d}\left(u^o_{fc} - u_{fc} + u_b\right) \tag{3.2}$$

Differentiation of the shear stress with respect to x gives:

$$\frac{d\tau}{dx} = \frac{G_a}{d}\left(\frac{du^o_{fc}}{dx} - \frac{du_{fc}}{dx} + \frac{du_b}{dx}\right) = \frac{G_a}{d}\left(\frac{\sigma^o_{fc}}{E_{fc}} - \frac{\sigma_{fc}}{E_{fc}} + \frac{\sigma_p}{E_b}\right) \tag{3.3}$$

As illustrated in Fig. 3.3, the prestress at the bottom fiber of the beam, σ_p, can be expressed in terms of the normal stress in the composite, σ_{fc}, as follows:

$$\sigma_p = -\frac{bt}{A}\sigma_{fc} - \frac{bt(h')^2}{I}\sigma_{fc} = -\alpha\sigma_{fc} \tag{3.4}$$

where A and I is the area and second moment of inertia of the cross section, respectively; h' is the distance from the centroid of the section to the extreme compressive fiber. For a rectangular cross section α can be calculated as:

$$\alpha = \frac{bt}{A} + \frac{bt(h')^2}{I} = \frac{bt}{bh} + \frac{bt}{bh^3}\frac{12h^2}{4} = \frac{4t}{h}$$

By combining eqns (3.3) and (3.4) we obtain:

$$\frac{d\tau}{dx} = \frac{G_a}{d}\left(\frac{\sigma^o_{fc}}{E_{fc}} - \frac{\sigma_{fc}}{E_{fc}} - \frac{\alpha\sigma_{fc}}{E_b}\right) \tag{3.5}$$

and

$$\frac{d^2\tau}{dx^2} = -\frac{G_a}{d}\left(\frac{1}{E_{fc}} + \frac{\alpha}{E_b}\right)\frac{d\sigma_{fc}}{dx} \tag{3.6}$$

Furthermore,

$$t\frac{d\sigma_{fc}}{dx} = -\tau \tag{3.7}$$

so that eqn. (3.6) is written as:

$$\frac{d^2\tau}{dx^2} = \omega^2\tau \quad , \quad \omega^2 = \frac{G_a}{dt}\left(\frac{1}{E_{fc}} + \frac{\alpha}{E_b}\right) \tag{3.8}$$

The solution of the last differential equation is of the form:

$$\tau = Ae^{\omega x} + Be^{-\omega x} \tag{3.9}$$

which represents the shear stress distribution in the interface.

In the next sections we calculate the initial prestress σ^o_{fc} which, when released, will just initiate failure of the system. Failure of the system can be controlled by several failure modes, dependent upon which of the constituent materials has the lowest shear capacity. It is seen that the following cases are to be considered:

a) *Adhesive failure*: applicable if the shear capacity of the beam is higher than that of the adhesive (e.g., aluminium, steel , high-strength wood (see Fig 3.4a)).

b) *Beam shear failure:* applicable to low shear strength materials such as concrete and low-strength wood (Fig. 3.4b).

c) *FRP interlaminar failure*: This failure mode might occur when the shear capacity of the FRP matrix is low. In this case the assumption that the FRP sheet undergoes axial deformations only must be relaxed. Shear strains become important and failure occurs in a similar way as described under a) above, and, hence, this failure mechanism will not be studied separately (Fig. 3.4c).

It should be noted that an additional constraint to the maximum pretension stress is the ultimate tensile stress that the FRP sheet can withstand in uniaxial tension (see Fig. 3.4d). This constraint will be used as a "cutoff" in the analysis that follows.

3.3 ADHESIVE SHEAR FAILURE

Let us assume that the beam is made of a material characterized by shear capacity higher than that of the adhesive (e.g. aluminium, steel, high-strength wood). A typical relationship between shear stress and shear strain for common structural epoxy adhesives is given in Fig. 3.5. Fracture of the adhesive in shear occurs after the material *yields plastically*. This phenomenon is often due to the presence of rubbery particles commonly used to toughen structural epoxy adhesives (Kinloch, 1987). The true shear stress-strain relationship can be approximated by a bilinear curve describing two regimes of behavior: a linear elastic and a perfectly plastic (Fig. 3.5, dashed lines).

After the pretension is released, the shear strains in the adhesive are high near the two ends of the member. When failure of the system is imminent the two end zones of the adhesive layer become fully plastic, as suggested by the shear stress-strain constitutive law for the adhesive (Fig. 3.5). The interface shear stress distribution at failure of the system is illustrated in Fig. 3.6; the shear strain at x=l'/2 and x=l/2 is γ_a^{el} and γ_a^*, respectively. The shear stress is described by eqn. (3.9) for $0 \le x \le l'/2$ and is constant (equal to the shear strength of the adhesive, τ_a^*) for $l'/2 \le x \le l/2$. Equation (3.9) along with the boundary conditions

$$\begin{aligned} &\tau(x=0)=0 \\ &\gamma(x=l'/2)=\frac{\tau(x=l'/2)}{G_a}=\gamma_a^{el} \end{aligned} \tag{3.10}$$

gives the elastic shear stress distribution as follows:

$$\tau=\frac{\gamma_a^{el}G_a}{\sinh\frac{\omega l'}{2}}\sinh\omega x \quad , \quad 0\le x\le\frac{l'}{2} \tag{3.11}$$

The corresponding shear strain distribution is:

$$\gamma = \frac{\gamma_a^{el}}{\sinh \frac{\omega l'}{2}} \sinh \omega x \qquad , \qquad 0 \le x \le \frac{l'}{2} \tag{3.12}$$

Although the shear stress is constant for $l'/2 \le x \le l/2$, this is not so for the interface shear strains. The analysis herein assumes that the strain distribution described by eqn. (3.12) is valid not only in the elastic but also in the plastic zone:

$$\gamma = \frac{\gamma_a^{el}}{\sinh \frac{\omega l'}{2}} \sinh \omega x \qquad , \qquad 0 \le x \le \frac{l}{2} \tag{3.13}$$

This assumption is consistent with the commonly employed hypothesis that the strains in materials in the inelastic regime of behavior are approximately described by the same relationship characterizing elastic response. A typical example is the assumption of linear strain profiles in members subject to bending, even after yielding has occurred.

From the condition $\gamma(x = l/2) = \gamma_a^*$, the length of the elastic zone, l', is calculated as follows:

$$l' = \frac{2\ln\left[\left(\beta + \sqrt{\beta^2 + 4}\right)/2\right]}{\omega} \qquad , \qquad \beta = \frac{2\gamma_a^{el}}{\gamma_a^*} \sinh \frac{\omega l}{2} \tag{3.14}$$

The normal stress distribution, σ_{fc}, along the FRP sheet can be obtained from eqn. (3.5):

$$\sigma_{fc} = \frac{\sigma_{fc}^o - \frac{E_{fc} d}{G_a} \frac{d\tau}{dx}}{1 + \alpha \frac{E_{fc}}{E_b}} \qquad , \qquad 0 \le x \le \frac{l'}{2} \tag{3.15}$$

Furthermore, eqn. (3.11) gives:

$$\frac{d\tau}{dx} = \frac{\gamma_a^{el} G_a \omega}{\sinh \frac{\omega l'}{2}} \cosh \omega x \qquad , \qquad 0 \le x \le \frac{l'}{2} \tag{3.16}$$

Combining eqns (3.15) and (3.16) we obtain:

$$\sigma_{fc} = \frac{\sigma^{o}_{fc} - \dfrac{E_{fc} d\omega \gamma^{el}_{a}}{\sinh \dfrac{\omega l'}{2}} \cosh \omega x}{1 + \alpha \dfrac{E_{fc}}{E_{b}}} \quad , \qquad 0 \le x \le \frac{l'}{2} \tag{3.17}$$

The normal stress in the FRP must drop from $\sigma_{fc}(x=l'/2)$ to zero at x=l/2. Considering that the interface shear, τ, in the plastic zone, (l-l')/2, is constant and that the size of that zone is small for practical cases, a linear distribution of the normal stress, σ_{fc}, can be realized for $l'/2 \le x \le l/2$ (Fig. 3.7). Then, by imposing the condition of slope continuity of σ_{fc} at x=l'/2 we write:

$$\left.\frac{d\sigma_{fc}}{dx}\right|_{x=l'/2} = \frac{-\sigma_{fc}|_{x=l'/2}}{(l-l')/2} \tag{3.18}$$

where σ_{fc} is described by eqn. (3.17). Finally, eqn. (3.18) can be solved for σ^{o}_{fc}, the initial prestress level that will just cause failure of the system once the pretension at the end of the FRP composite is released:

$$\sigma^{o}_{fc} = E_{fc} d\gamma^{el}_{a} \omega \left[\coth \frac{\omega l'}{2} + \frac{\omega(l-l')}{2} \right] \tag{3.19}$$

3.4 BEAM SHEAR FAILURE

Two different failure mechanisms were considered for two widely used structural materials, namely concrete and wood. The major differences in the approach for the calculation of the failure loads are related to the softening behavior in the shear stress-strain diagram. In this section the maximum FRP pretension stress has been derived for various beam material softening models.

3.4.1 Maximum Pretension for Concrete Beams

When the beam is made of a low shear strength material such as concrete, failure due to pretension release will occur at the two end zones due to high shear stresses in the concrete layer above the FRP sheet (Fig. 3.4b). The interface shear stress at failure of the system is schematically illustrated in Fig. 3.8. In the *linear region* ($0 \le x \le l'/2$), the shear stress, τ, is described by eqn. (3.9). The descending portion of the shear stress distribution in the *nonlinear region* ($0 \le x' \le (l-l')/2$) is due to the softening behavior of concrete in shear. A qualitative description of the shear stress vs. slip curve for concrete subjected to shear through pulling an externally bonded plate is shown in Fig. 3.9 (e.g. Ladner and Weder, 1981; Ranisch and Rostasy, 1986; and Kaiser, 1989). The softening branch in Fig. 3.9 is described by the peak strength, τ_c^*, and the characteristic slip, δ^*, after which the shear resistance levels-off at a value near zero.

Applying the boundary conditions:

$$\tau(x = 0) = 0$$
$$\tau(x = l'/2) = \tau_c^* \tag{3.20}$$

in eqn. (3.9) for the shear stress we obtain:

$$\tau = \frac{\tau_c^*}{\sinh \frac{\omega l'}{2}} \sinh \omega x \quad , \quad 0 \le x \le \frac{l'}{2} \tag{3.21}$$

and

$$\frac{d\tau}{dx} = \frac{\tau_c^* \omega}{\sinh \frac{\omega l'}{2}} \cosh \omega x \quad , \quad 0 \le x \le \frac{l'}{2} \tag{3.22}$$

Furthermore, the normal stress in the FRP, σ_{fc}, is described by eqn. (3.15) with $d\tau/dx$ given by eqn. (3.22):

$$\sigma_{fc} = \frac{\sigma^{o}_{fc} - \dfrac{E_{fc} d\omega \tau^{*}_{c}}{G_a \sinh \dfrac{\omega l'}{2}} \cosh \omega x}{1 + \alpha \dfrac{E_{fc}}{E_b}} \quad , \qquad 0 \le x \le \frac{l'}{2} \tag{3.23}$$

Next, assuming that the system concrete/epoxy in the nonlinear region is infinitely rigid, the shear slip, δ, at a cross section x' is solely due to straining of the FRP sheet. The same assumption was successfully employed by Kaiser (1989) in calculating the required anchorage length of thin sheets externally bonded on the tension face of concrete beams subjected to bending. When the pretension is released, the FRP cross section at x' moves a distance u^{o}_{fc}-u_{fc} (see Fig. 3.2) and the associated strain is:

$$\frac{d(u^{o}_{fc} - u_{fc})}{dx'} = \frac{du^{o}_{fc}}{dx'} - \frac{du_{fc}}{dx'} = \varepsilon^{o}_{fc} - \varepsilon_{fc} \tag{3.24}$$

Therefore, the shear slip $\delta(x')$ is calculated as follows:

$$\delta(x') = \int_0^{x'} (\varepsilon^{o}_{fc} - \varepsilon_{fc}) dx' = \frac{\sigma^{o}_{fc}}{E_{fc}} x' - \int_0^{x'} \frac{\sigma_{fc}}{E_{fc}} dx' \tag{3.25}$$

Approximating the interface shear in the nonlinear region by a linearly varying function (Fig. 3.8, dashed line) and considering the equilibrium of the FRP element shown in Fig. 3.10 we obtain:

$$t\sigma_{fc} = \frac{1}{2} \tau \left[\frac{(1 - l')}{2} - x' \right] \quad , \qquad 0 \le x' \le \frac{1 - l'}{2} \tag{3.26}$$

where

$$\tau = \tau^{*}_{c} \left[1 - \frac{x'}{(1 - l')/2} \right] \quad , \qquad 0 \le x' \le \frac{1 - l'}{2} \tag{3.27}$$

Equations (3.26) and (3.27) can be combined to solve for the normal stress σ_{fc}:

$$\sigma_{fc} = \frac{\tau_c^*}{t(l-l')}\left[\frac{(l-l')}{2} - x'\right]^2 \quad , \quad 0 \le x' \le \frac{l-l'}{2} \tag{3.28}$$

Substituting eqn. (3.28) into eqn. (3.25) gives:

$$\delta(x') = \frac{\sigma_{fc}^o}{E_{fc}}x' - \int_0^{x'} \frac{\tau_c^*}{E_{fc}t(l-l')}\left[\frac{(l-l')}{2} - x'\right]^2 dx'$$

$$= \frac{\sigma_{fc}^o}{E_{fc}}x' - \frac{\tau_c^*(l-l')}{4E_{fc}t}x' + \frac{\tau_c^*}{2E_{fc}t}(x')^2 - \frac{\tau_c^*}{3E_{fc}t(l-l')}(x')^3 + C \tag{3.29}$$

From the condition $\delta(x'=0)=0$ and eqn. (3.29) we calculate C=0. Moreover, the displacement δ at the end of the member (x'=(l-l')/2) is taken equal to δ^* (see Fig. 3.9) and eqn. (3.29) is written as:

$$\delta^* = \frac{\sigma_{fc}^o(l-l')}{2E_{fc}} - \frac{\tau_c^*(l-l')^2}{24E_{fc}t} \tag{3.30}$$

Finally, we use the condition that the normal stress in the FRP evaluated from eqn. (3.28) for x'=0 should identically reduce to that evaluated from eqn. (3.23) for x=l'/2; the result is:

$$\frac{\sigma_{fc}^o - \frac{E_{fc}d\omega\tau_c^*}{G_a}\coth\frac{\omega l'}{2}}{1+\alpha\frac{E_{fc}}{E_b}} = \frac{(l-l')\tau_c^*}{4t} \tag{3.31}$$

Equations (3.30) and (3.31) can be solved for the length of the linear region, l', and the initial pretension stress, σ_{fc}^o, which, when released, will just cause failure of the system. Since the equations are highly nonlinear and no closed form solution can be obtained, a numerical procedure was implemented in a computer program and the solution was obtained by iteration through the unknown variable l'. It should be noted that the hyperbolic function coth(x) can easily produce overflow during the iteration

procedure and hence, the appropriate iteration limits have to be defined.

Substitution of l' in eqns (3.23) and (3.28) gives the normal stress distribution in the FRP, σ_{fc}, shown qualitatively in Fig. 3.11; when σ_{fc} is known, the maximum prestress at the beam's bottom fiber is calculated from eqn. (3.4).

3.4.2 Maximum Pretension for Wood Beams

If the shear strength of the FRP-prestressed wood beam is less than the shear strength of the adhesive used, failure due to pretension release will occur in the beam itself. The failure will start at the far ends where the shear stress distribution is maximum. This type of failure may be encountered when either a low shear strength wood or a high shear strength adhesive is employed. Two models describing failure of FRP-prestressed wood beams were analyzed and the maximum pretension stress to cause failure in the wood beam after releasing the prestressing force was obtained.

3.4.2.1 *Linear Elastic Wood Model*

Considering wood to behave as a linear elastic continuum, we can adopt the solution obtained for the interface shear stress distribution as described by eqn. (3.9). At failure, the maximum interface shear stress occuring at x=l/2 reaches the shear strength of wood, τ_w^* (see Fig. 3.12).

From the boundary conditions

$$\tau(x=0)=0$$
$$\tau(x=l/2)=\tau_w^* \qquad (3.32)$$

the elastic shear stress distribution is obtained as follows:

$$\tau = \frac{\tau_w^*}{\sinh\frac{\omega\, l}{2}}\sinh\omega\, x \qquad , \qquad 0 \le x \le \frac{l}{2} \tag{3.33}$$

Differentiating with respect to x we find:

$$\frac{d\tau}{dx} = \frac{\tau_w^*\,\omega}{\sinh\frac{\omega\, l}{2}}\cosh\omega\, x \tag{3.34}$$

Combining eqns (3.5) and (3.34) gives:

$$\sigma_{fc} = \frac{\sigma_{fc}^o - \frac{E_{fc} d\omega \tau_w^*}{G_a \sinh\frac{\omega l}{2}}\cosh\omega x}{1+\alpha\frac{E_{fc}}{E_b}} \qquad , \qquad 0 \le x \le \frac{l}{2} \tag{3.35}$$

Now, considering equilibrium at any cross section we get (see Fig. 3.13):

$$\sigma_{fc}(x^*)t = \int_0^{x^*} \tau\left(\frac{l}{2} - x^*\right)dx^* \tag{3.36}$$

The above integral is calculated as follows:

$$\sigma_{fc}(x^*) = \frac{1}{t\omega}\frac{\tau_w^*}{\sinh\frac{\omega l}{2}}\left[\cosh\frac{\omega l}{2} - \cosh\omega\left(\frac{l}{2} - x^*\right)\right] + C \tag{3.37}$$

Since the boundary condition $\sigma_{fc}(x^* = 0) = 0$ and eqn. (3.37) give C=0, we can derive the normal stress distribution in the FRP sheet as:

$$\sigma_{fc}(x^*) = \frac{1}{t\omega}\frac{\tau_w^*}{\sinh\frac{\omega l}{2}}\left[\cosh\frac{\omega l}{2} - \cosh\omega\left(\frac{1}{2} - x^*\right)\right] \tag{3.38}$$

Equation (3.38) evaluated at midspan ($x^* = l/2$) along with the definition of ω (see eqn. (3.8)) gives:

$$\sigma_{fc}^o = \frac{\tau_w^* d\,\omega E_{fc}}{G_a}\coth\frac{\omega l}{2} \tag{3.39}$$

which is the maximum pretension stress required to initiate wood shear failure when the pretension is transmitted from the two end zones into the beam.

3.4.2.2 *Nonlinear Wood Model*

Assuming some softening behavior of the wood after the peak shear stress is reached (see Fig. 3.14) the interface shear stress distribution in the wood bottom fiber can be represented as shown in Fig. 3.15.

Note that the softening branch is assumed to vary linearly from τ_w^* at l'/2 to 0 at the beam's edge. The solution for the shear stress distribution corresponding to linear behavior ($0 \le x \le l'/2$) is described by eqn. (3.33), where the value of l has to be substituted by l'. Hence, we obtain

$$\tau = \frac{\tau_w^*}{\sinh\frac{\omega l'}{2}}\sinh\omega x \quad , \quad 0 \le x \le \frac{l'}{2} \tag{3.40}$$

corresponding to shear strains:

$$\gamma = \frac{\tau_w^*}{G_w\sinh\frac{\omega l'}{2}}\sinh\omega x \quad , \quad 0 \le x \le \frac{l'}{2} \tag{3.41}$$

Assuming that eqn. (3.41) holds not only for the linear but also for the nonlinear zone,

(i.e. for all $0 \le x \le l/2$, see Fig. 3.16) we can write:

$$\gamma = \frac{\tau_w^*}{G_w \sinh\frac{\omega l'}{2}} \sinh\omega x \qquad , \qquad 0 \le x \le \frac{l}{2} \tag{3.42}$$

From eqn. (3.42) and the condition $\gamma(x = l/2) = \gamma_w^*$ we can solve for l':

$$l' = \frac{2\ln\left[\left(\beta + \sqrt{\beta^2 + 4}\right)/2\right]}{\omega} \qquad , \qquad \beta = \frac{2\gamma_w^{el}}{\gamma_w^*}\sinh\frac{\omega l}{2} \tag{3.43}$$

Furthermore, by considering equilibrium of forces at any cross section as shown in Fig. 3.17, the following relationship is obtained:

$$\sigma_{fc}(x^o)t = \frac{l - l'}{4}\tau_w^* + \int_0^{x^o} \tau\left(\frac{l'}{2} - x^o\right)dx^o \tag{3.44}$$

where $\tau(x)$ is described by eqn. (3.40). At midspan ($x^o = l'/2$) eqn. (3.44) gives:

$$\sigma_{fc}(x^o = l'/2) = \frac{\tau_w^*}{t}\left(\frac{l - l'}{4} + \frac{\cosh\frac{\omega l'}{2} - 1}{\omega\sinh\frac{\omega l'}{2}}\right) \tag{3.45}$$

Also from eqn. (3.40) we find:

$$\frac{d\tau}{dx} = \frac{\tau_w^*\,\omega}{\sinh\frac{\omega\, l'}{2}}\cosh\omega\, x \qquad , \qquad 0 \le x \le \frac{l'}{2} \tag{3.46}$$

and at midspan ($x = 0$):

$$\frac{d\tau}{dx} = \frac{\tau_w^* \omega}{\sinh \frac{\omega l'}{2}} \tag{3.47}$$

Finally, inserting eqn. (3.47) into eqn. (3.5) we can solve for σ_{fc}^o:

$$\sigma_{fc}^o = \tau_w^* \left\{ \left(1 + \frac{\alpha E_{fc}}{E_b} \right) \left(\frac{\cosh \frac{\omega l'}{2} - 1}{\omega t \sinh \frac{\omega l'}{2}} + \frac{1 - l'}{4t} \right) + \frac{E_{fc} d \omega}{G_a \sinh \frac{\omega l'}{2}} \right\} \tag{3.48}$$

where l' is defined by eqn. (3.43).

3.5 DISCUSSION OF RESULTS

To illustrate the potential of the technique discussed above we assume that a high performance composite sheet made of unidirectional carbon fibers and epoxy matrix (CFRP) is employed to prestress two different beams: one is made of wood and the other is made of normal strength concrete. The material properties used are summarized in Table 3.1.

Table 3.1 Material properties used to obtain the numerical results

Property	E_{fc}	E_b (concrete)	E_b (wood)	G_a	γ_a^*	γ_a^{el}	τ_c^*	δ^*
Value	185 GPa	28 GPa	10 GPa	0.9 GPa	0.03	0.08	8 MPa	20μm

In all cases the pretension level, σ_{fc}^o, is taken equal to that required to just initiate failure of the system, the member aspect ratio, l/h, is assumed equal to 10 and the cross sections are considered rectangular.

3.5.1 Wood Beams

In the results presented next it is assumed that the beam consists of high-strength wood and the adhesive has a low shear strength. Therefore, the adhesive shear failure solution, as described in Section 3.3, applies. Figure 3.18 illustrates the relationship between the ratio of the length of the linear zone to the total length, l'/l, and the adhesive thickness normalized with respect to the cross section height, d/h, for various CFRP area fractions. It is seen that an increase in either the adhesive thickness or the composite area fraction results in an increased yield zone in the adhesive.

The relationship between the initial prestress level resulting in failure normalized with respect to the FRP elastic modulus, σ^{o}_{fc}/E_{fc} (=initial strain), and the d/h ratio is given in Fig. 3.19. The figure shows that σ^{o}_{fc}/E_{fc} increases by increasing the adhesive thickness and/or decreasing the FRP area fraction. Note that the initial pretension strain is limited by the ultimate FRP strain, ε^{*}_{fc}, indicated in Fig. 3.19 by the horizontal dashed line.

A measure of the technique's effectiveness is given by the maximum achievable prestress level, σ_p, at the bottom fiber of the beam. The distribution of the prestress along the member, σ_p, normalized with respect to the elastic modulus, E_b, is illustrated in Fig. 3.20 for two adhesive thicknesses, namely d/h=0.004 and 0.01. It is remarkable that the prestress is almost constant along the beam and drops almost suddenly to zero near the two ends (anchorage zones). Furthermore, the maximum achievable prestress level increases as both the adhesive thickness and the composite sheet area fraction increase. The dashed lines in Fig. 3.20 correspond to FRP area fractions less than the minimum values required to ensure that the composite sheet does not fracture during the pretension.

3.5.2 Concrete beams

The set of results obtained for FRP-pretensioned wood beams is repeated in Figs 3.21-3.23 for members made of normal strength concrete, assuming a member length of 5 m. The behavior is quite similar to that described earlier with one exception concerning

the relationship between the length of the nonlinear zone and the adhesive thickness (Fig. 3.21a). Here, the length of the nonlinear zone increases with the FRP area fraction but decreases with the adhesive thickness, unless the adhesive layer is extremely thin in which case failure of the prestressed system is the result of adhesive shear failure and the equations for members with high shear strength apply (note the discontinuity in Fig. 3.21b for small d/h ratios).

Comparison of Figs 3.19 and 3.22 reveals that for the same geometrical characteristics a FRP-prestressed concrete system will fail at a pretension level, σ^{o}_{fc}, which is 4-5 times lower than the corresponding for the FRP-wood system. The initial prestress level in Fig. 3.22 is obtained from the system of eqns (3.30) and (3.31) except for very small d/h ratios when eqn. (3.19) controls.

3.6 CONCLUSIONS

The mechanics associated with the short term behavior of a new method of prestressing has been studied. The analytical models developed describe the maximum achievable prestress level so that the FRP-prestressed system does not fail near the anchorage zones, when the pretension is released from the load source. Account is taken for the failure of either the adhesive layer or the beam material, depending on which of the two is characterized by the lowest shear strength. The solution for four different failure modes was found, describing adhesive shear failure, concrete shear failure, wood shear failure when wood is assumed to behave in a linear elastic manner, and wood shear failure when wood is assumed to behave nonlinearly.

The results suggest that the method's efficiency is improved by increasing the thickness of the adhesive layer and/or increasing the area fraction of the composite material, efficiency here being defined as the level of prestress at the bottom fiber of the member. While the achievable levels of prestress are moderate when the method is applied to concrete beams, they are quite high when materials with increased shear

resistance, such as high-strength wood, are under consideration. The solutions obtained need to be verified experimentally, which follows in the next chapter.

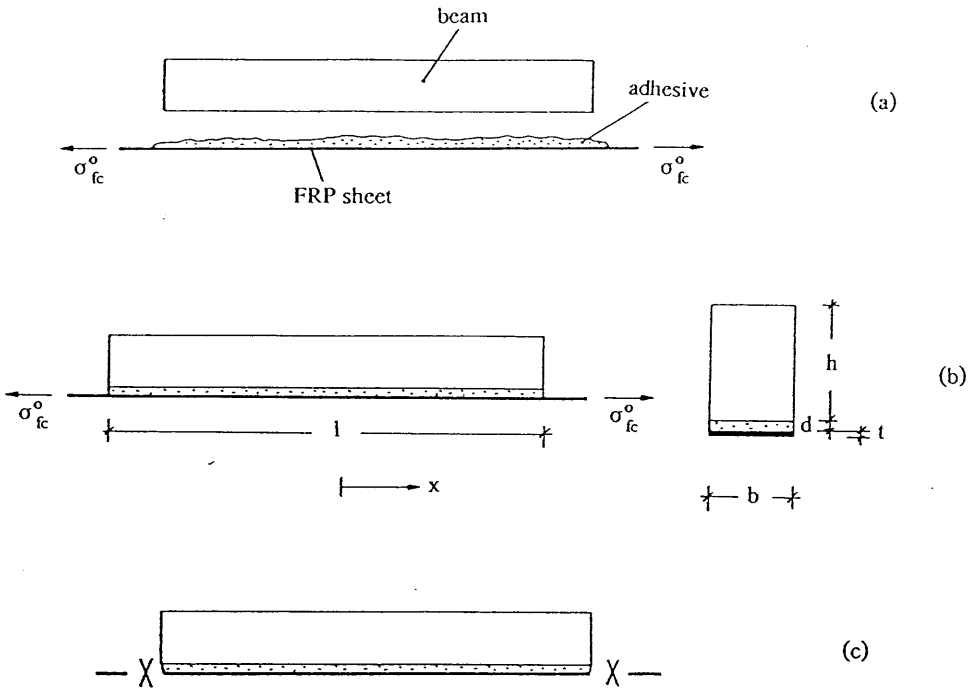

Figure 3.1 Post-reinforcing with pretensioned FRP sheets: (a) FRP prestressing; (b) curing of the adhesive; (c) FRP ends released.

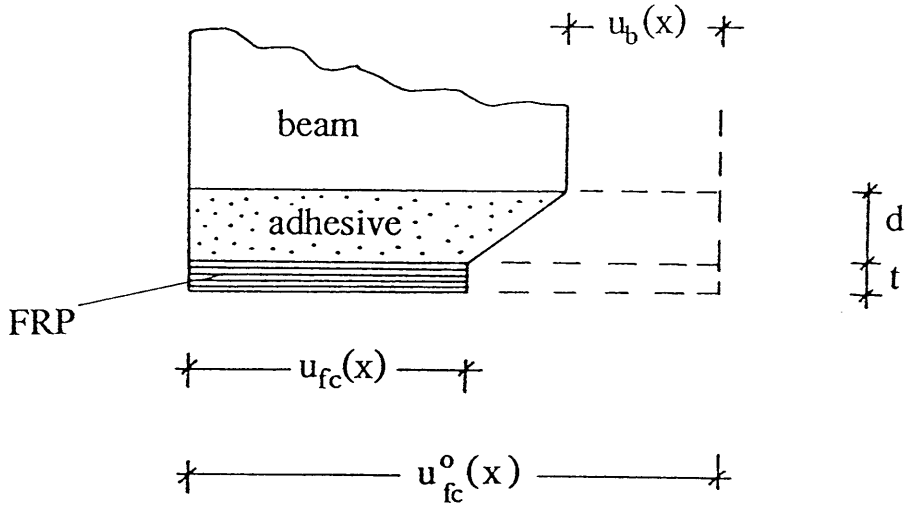

Figure 3.2 The deformation pattern of the FRP-adhesive system upon releasing the pretension at the ends of the FRP. Dashed lines: configuration during pretensioning; solid lines: pretension is released.

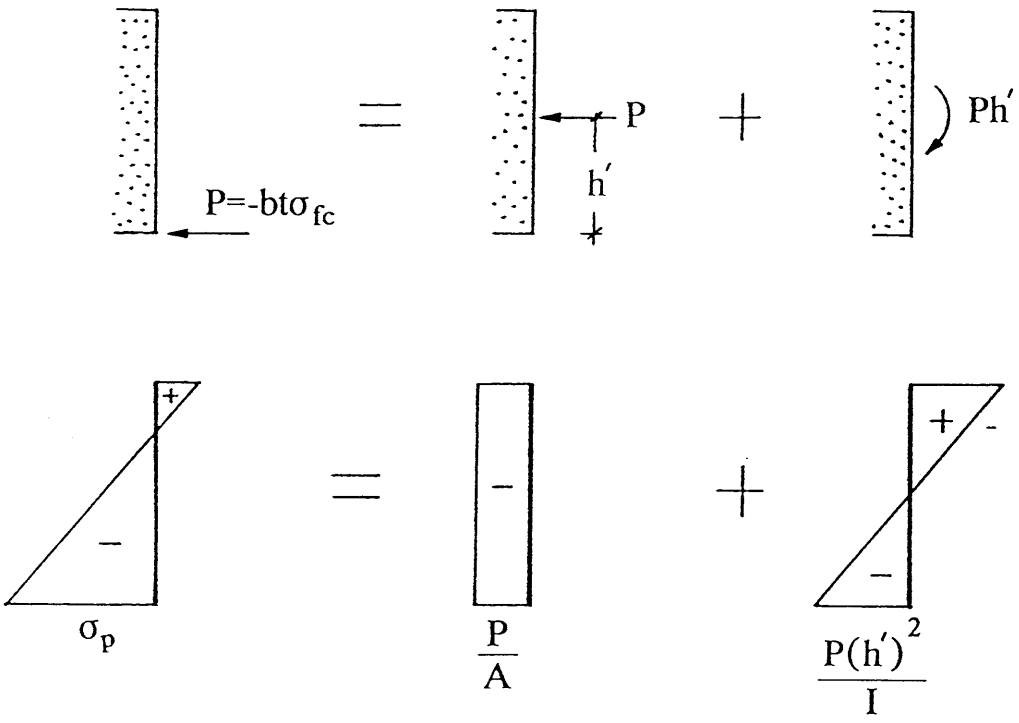

Figure 3.3 The normal stress distribution at the cross section of the beam after the pretension has been released.

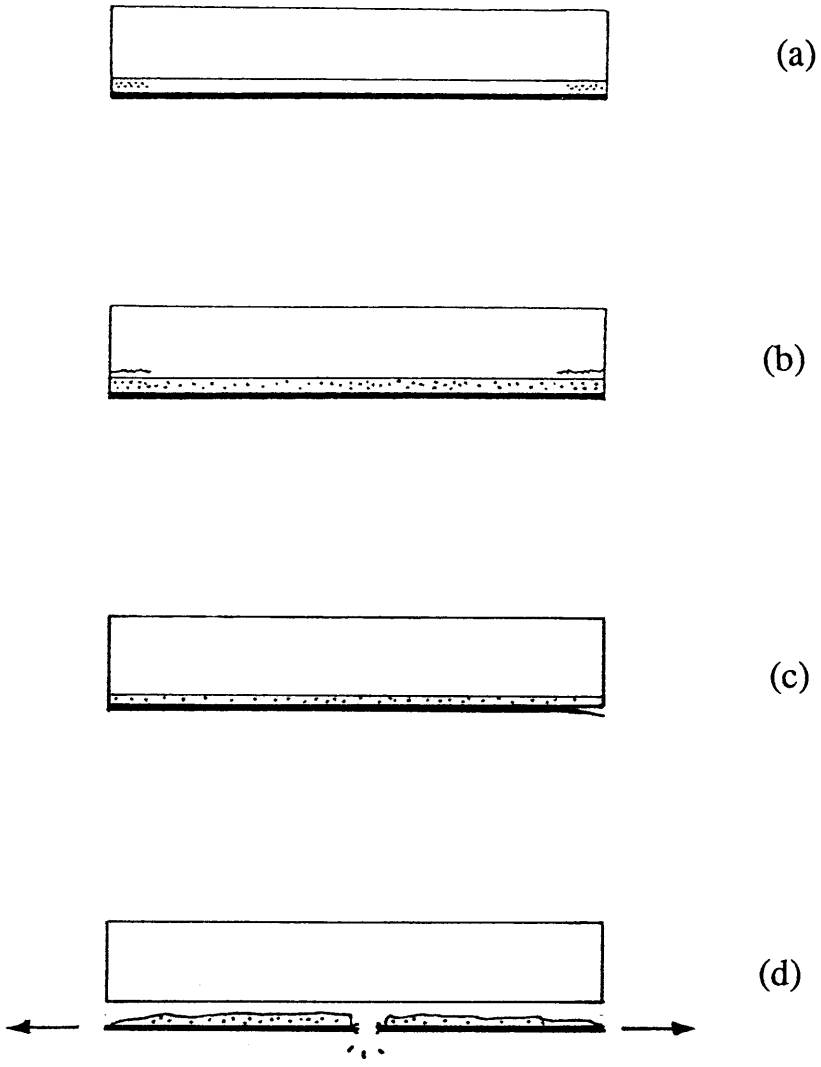

Figure 3.4 Failure mechanisms of beams with external pretensioned FRP sheets: (a) adhesive shear strength < beam shear strength; (b) adhesive shear strength > beam shear strength; c) FRP interlaminar failure; and d) FRP tension rupture.

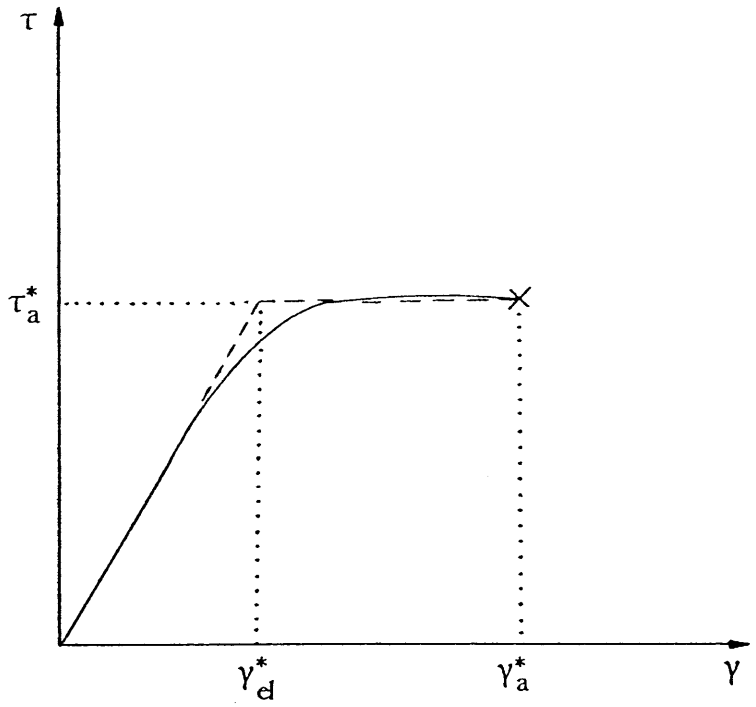

Figure 3.5 Shear stress-shear strain relationship for structural epoxy adhesives. Solid line: true relationship; dashed line: idealized relationship.

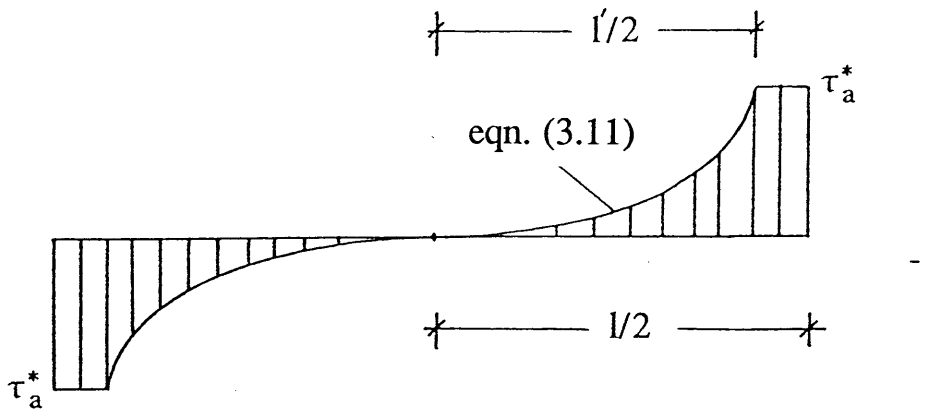

Figure 3.6 Distribution of the shear stress at the interface between the FRP sheet and the beam: adhesive shear strength < beam shear strength.

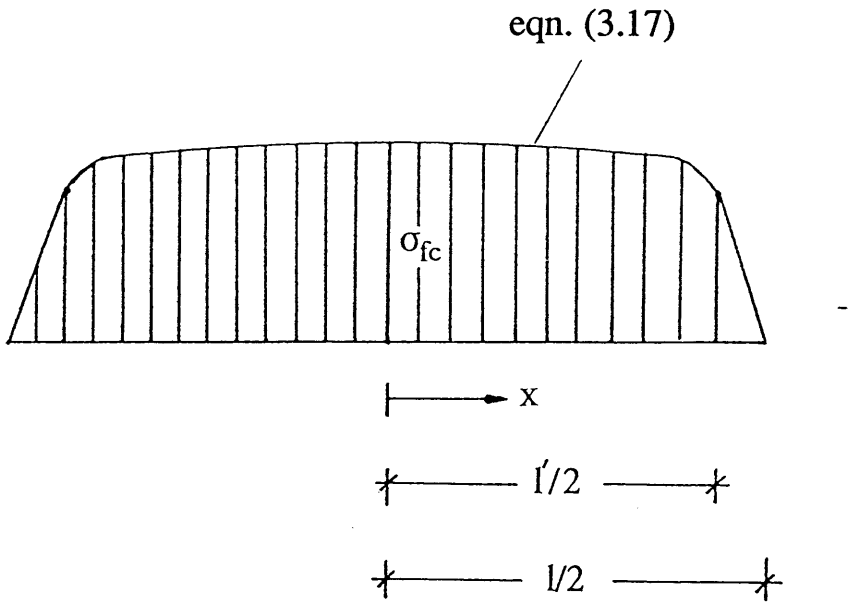

Figure 3.7 Distribution of the normal stress in the FRP sheet: adhesive shear strength < beam shear strength.

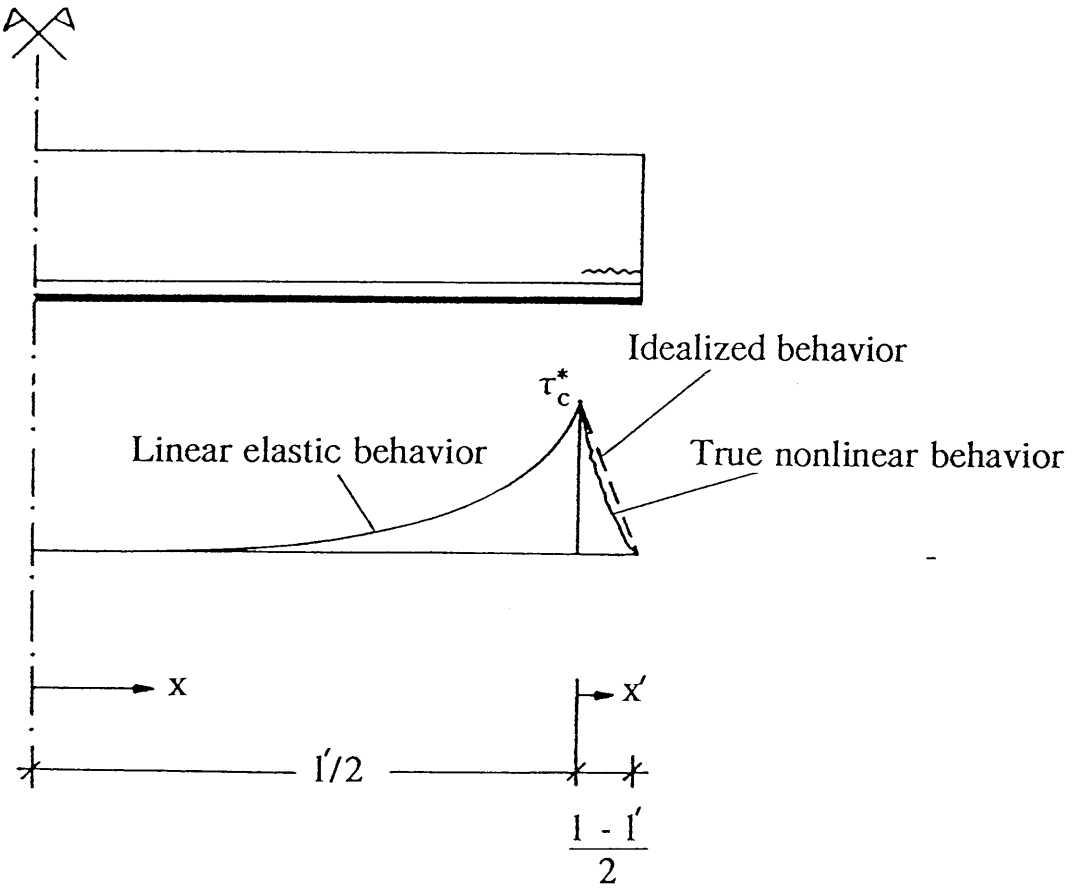

Figure 3.8 Distribution of the shear stress at the interface between the FRP sheet and the beam: adhesive shear strength > beam shear strength.

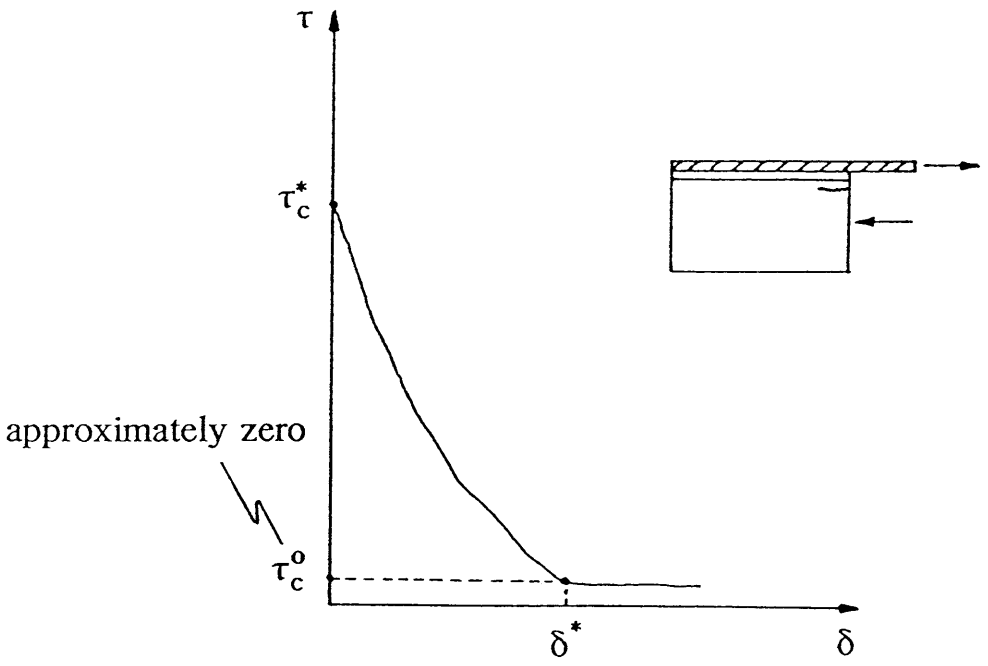

Figure 3.9 Softening branch of the shear stress-slip relationship for concrete.

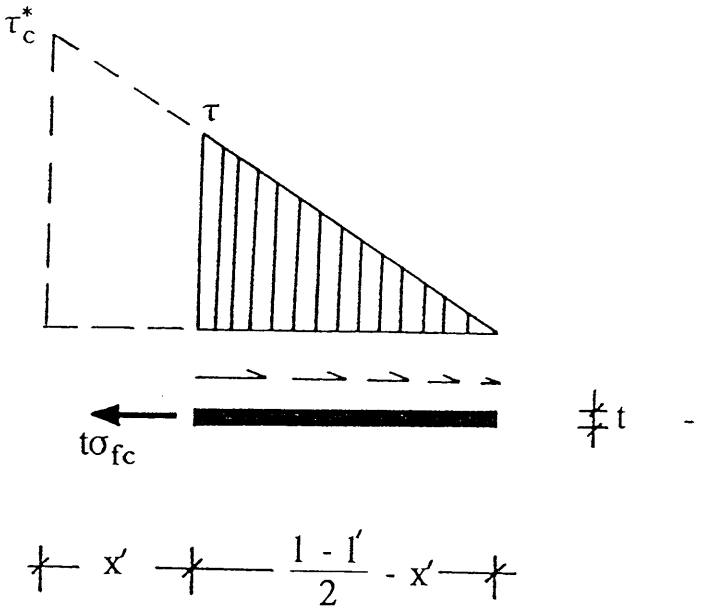

Figure 3.10 Equilibrium of a FRP element under interface shear and normal stresses.

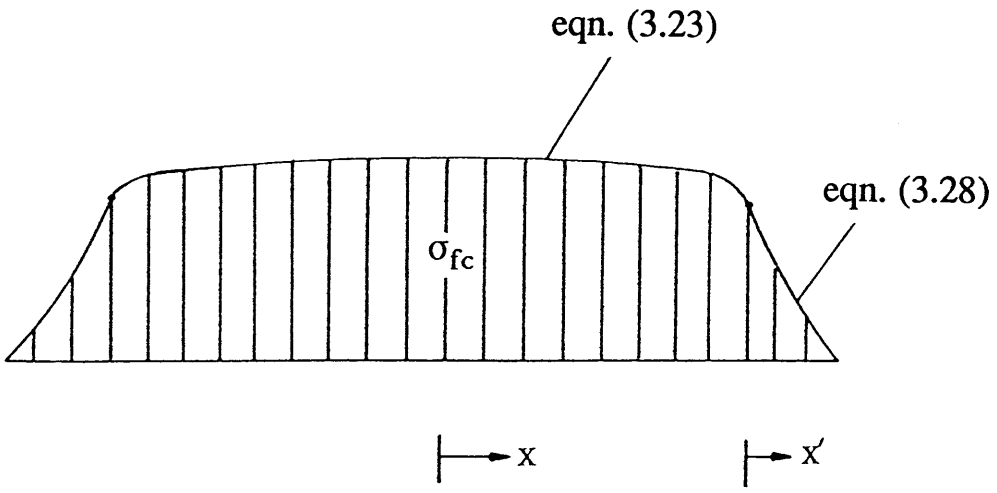

Figure 3.11 Distribution of the normal stress in the FRP sheet: adhesive shear strength > beam shear strength.

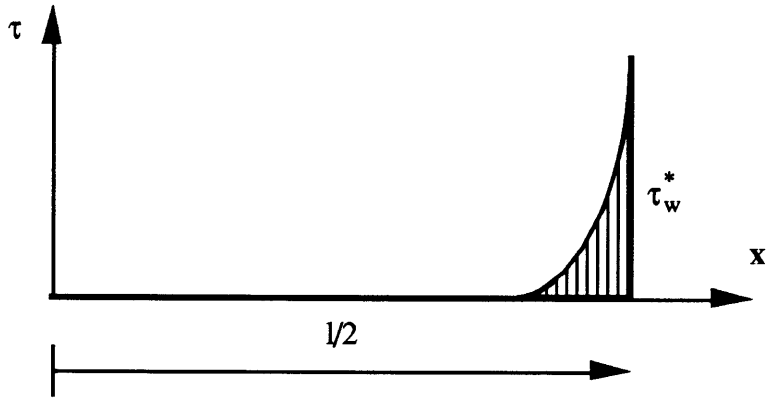

Figure 3.12 Wood linear model, shear stress distribution.

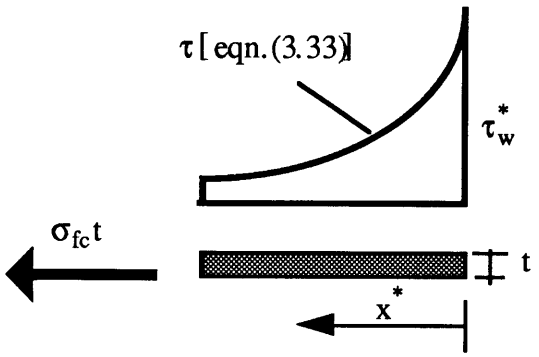

Figure 3.13 Wood linear model, equilibrium of forces in cross section.

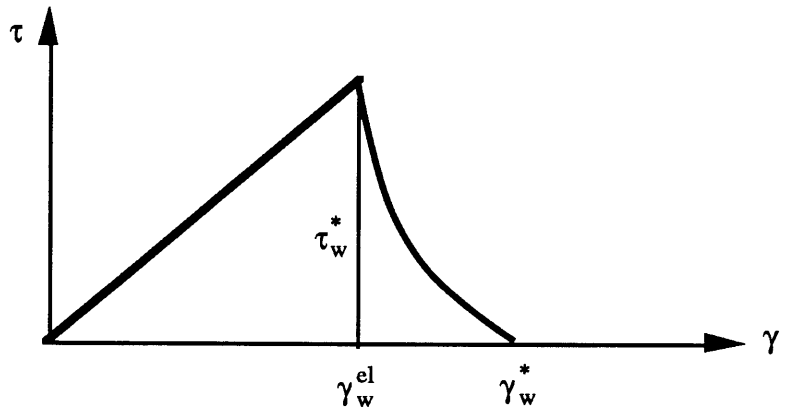

Figure 3.14 Wood linear model, shear stress/strain relationship.

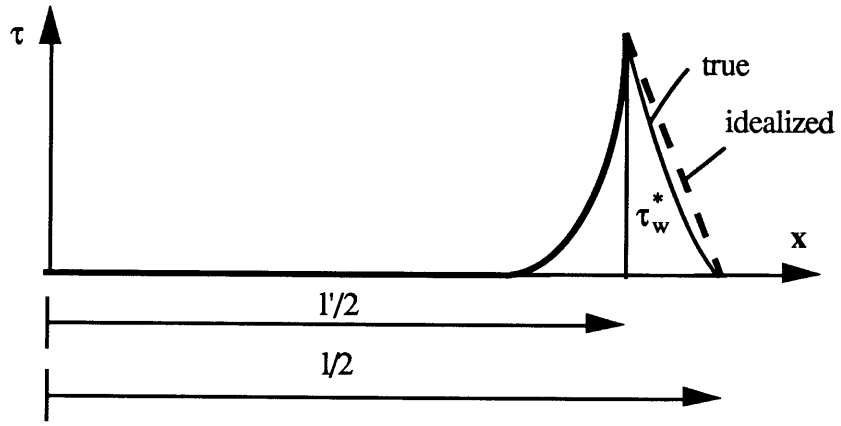

Figure 3.15 Wood nonlinear model, shear stress distribution.

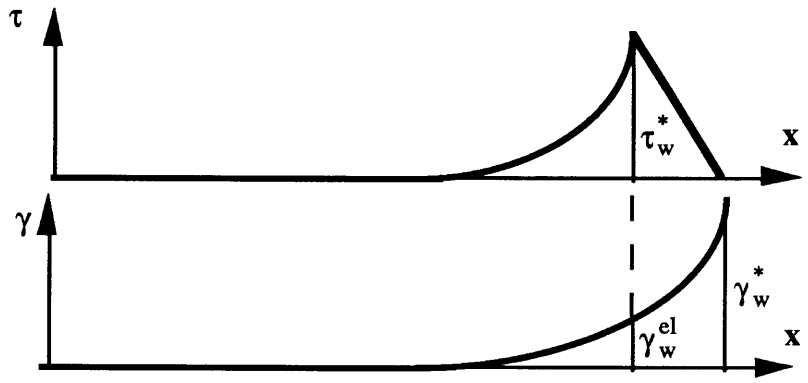

Figure 3.16 Wood nonlinear model, shear stress and strain distribution.

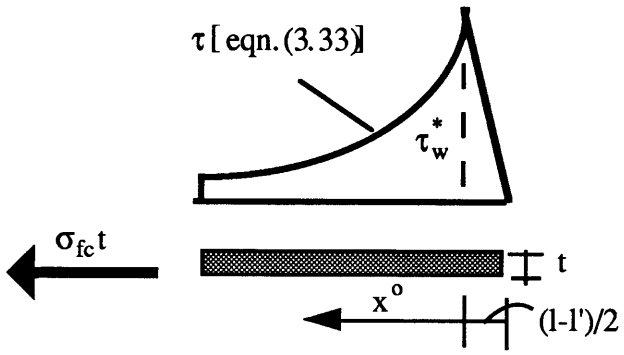

Figure 3.17 Wood nonlinear model, equilibrium of cross section forces.

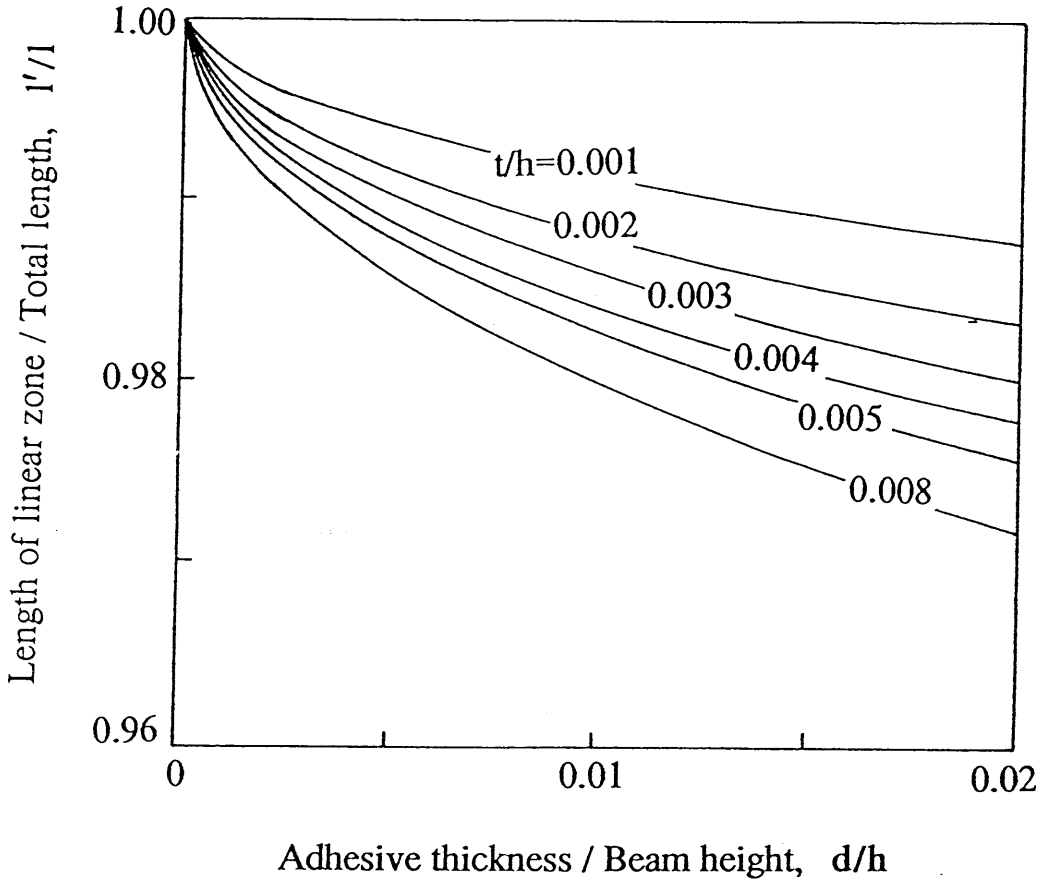

Figure 3.18 Length of the nonlinear zone vs. adhesive thickness for various FRP area fractions - wood beams with l/h=10.

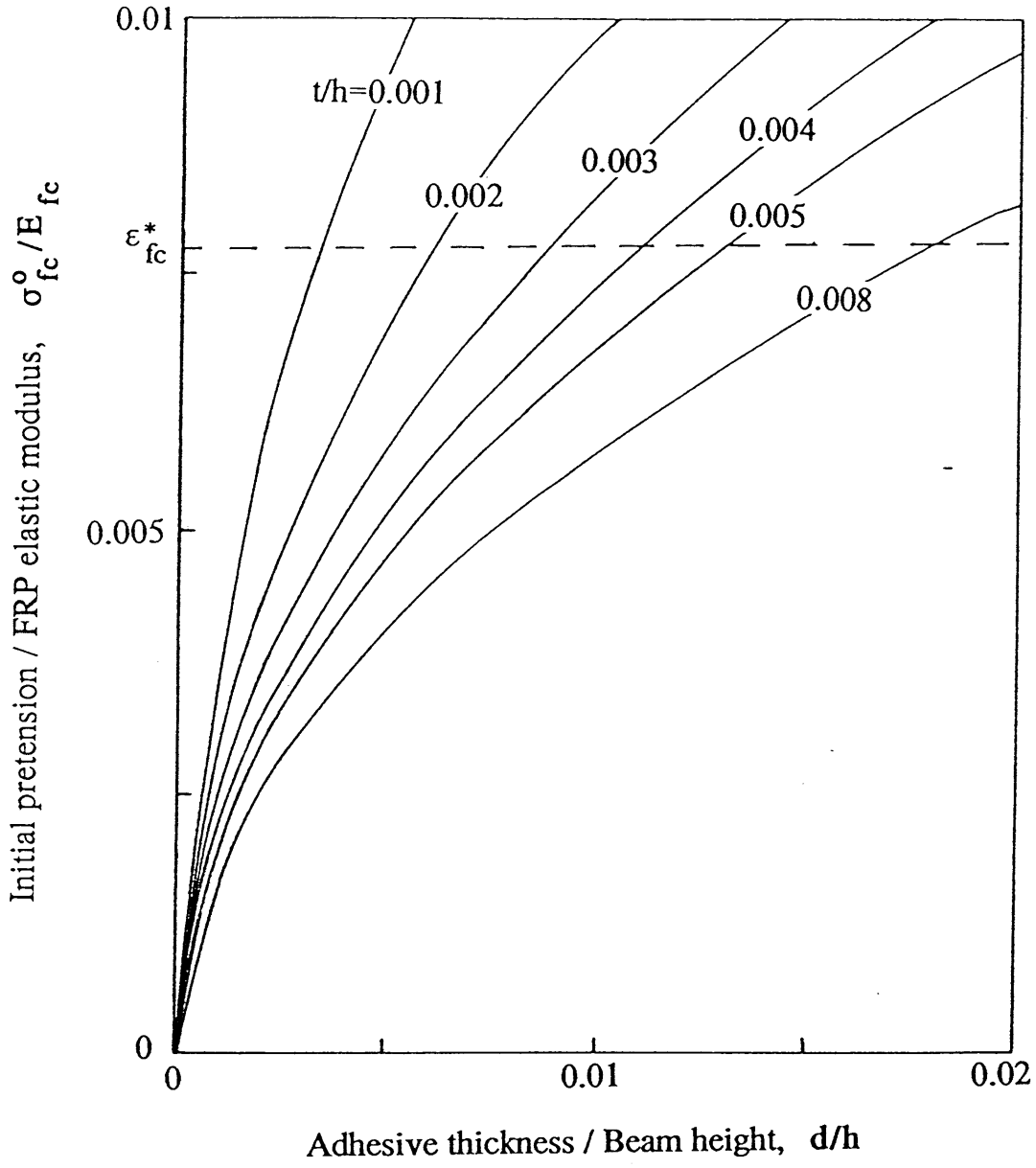

Figure 3.19 Initial prestress level vs. adhesive thickness for various FRP area fractions - wood beams with l/h=10.

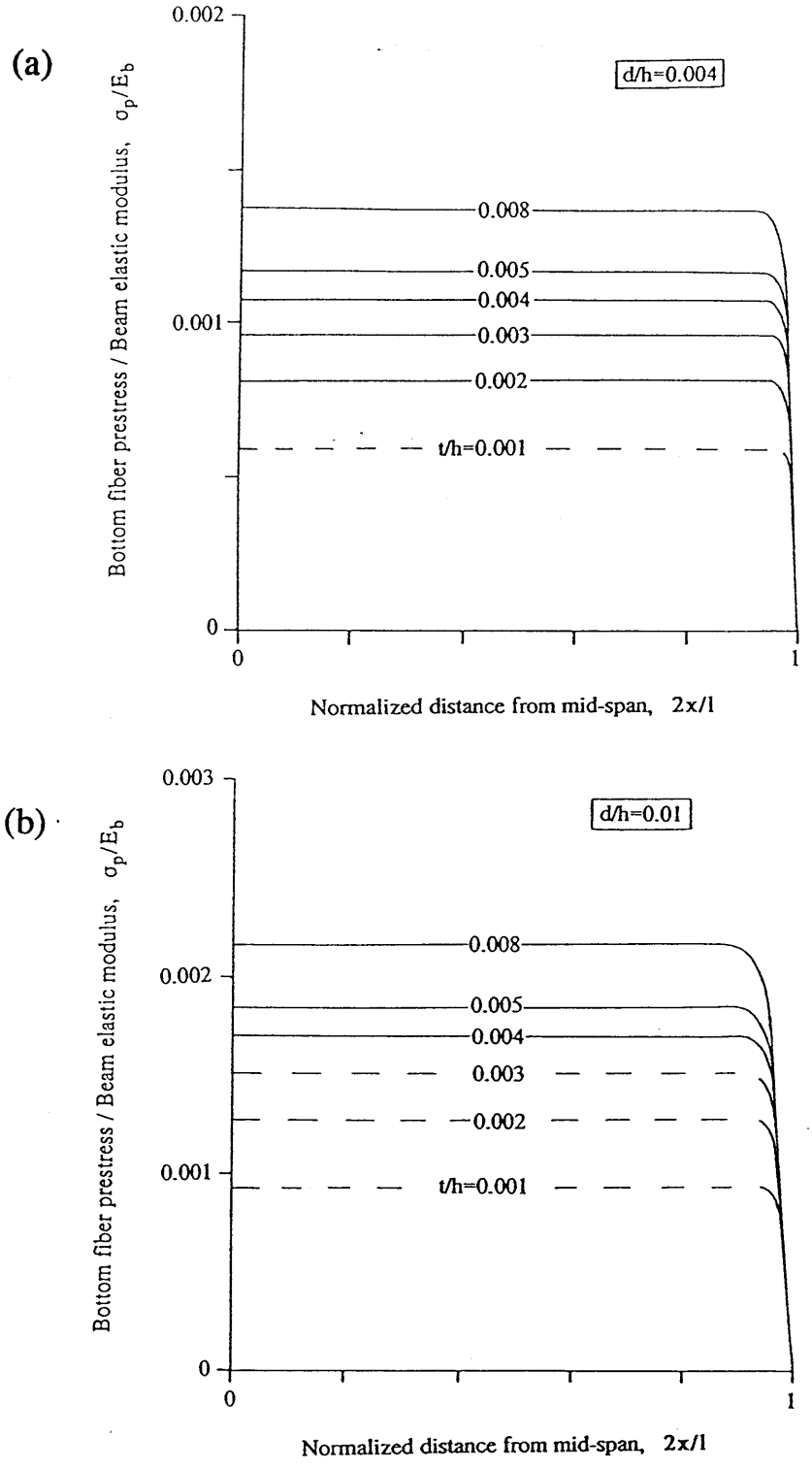

Figure 3.20 Bottom fiber prestress distribution along the member for various FRP area fractions - wood beams with l/h=10; (a) d/h=0.004 and (b) d/h=0.01.

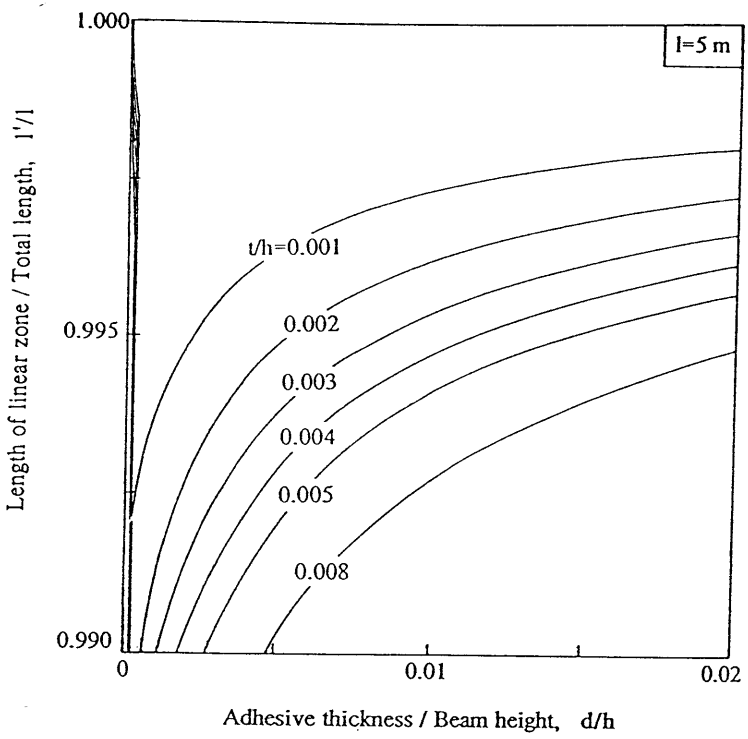

(a)

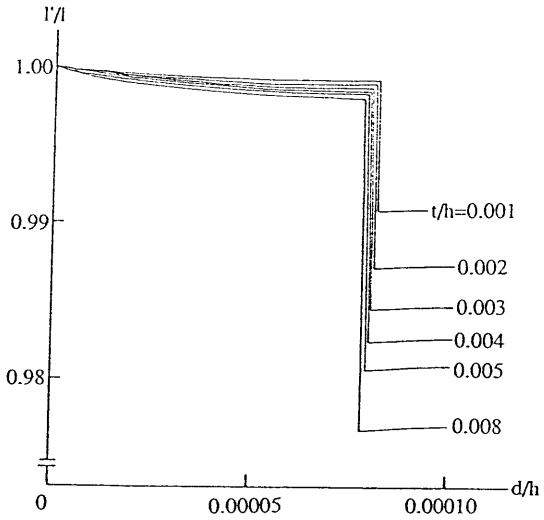

(b)

Figure 3.21 Length of the nonlinear zone vs. adhesive thickness for various FRP area fractions - concrete beams with l/h=10 and l=5 m.

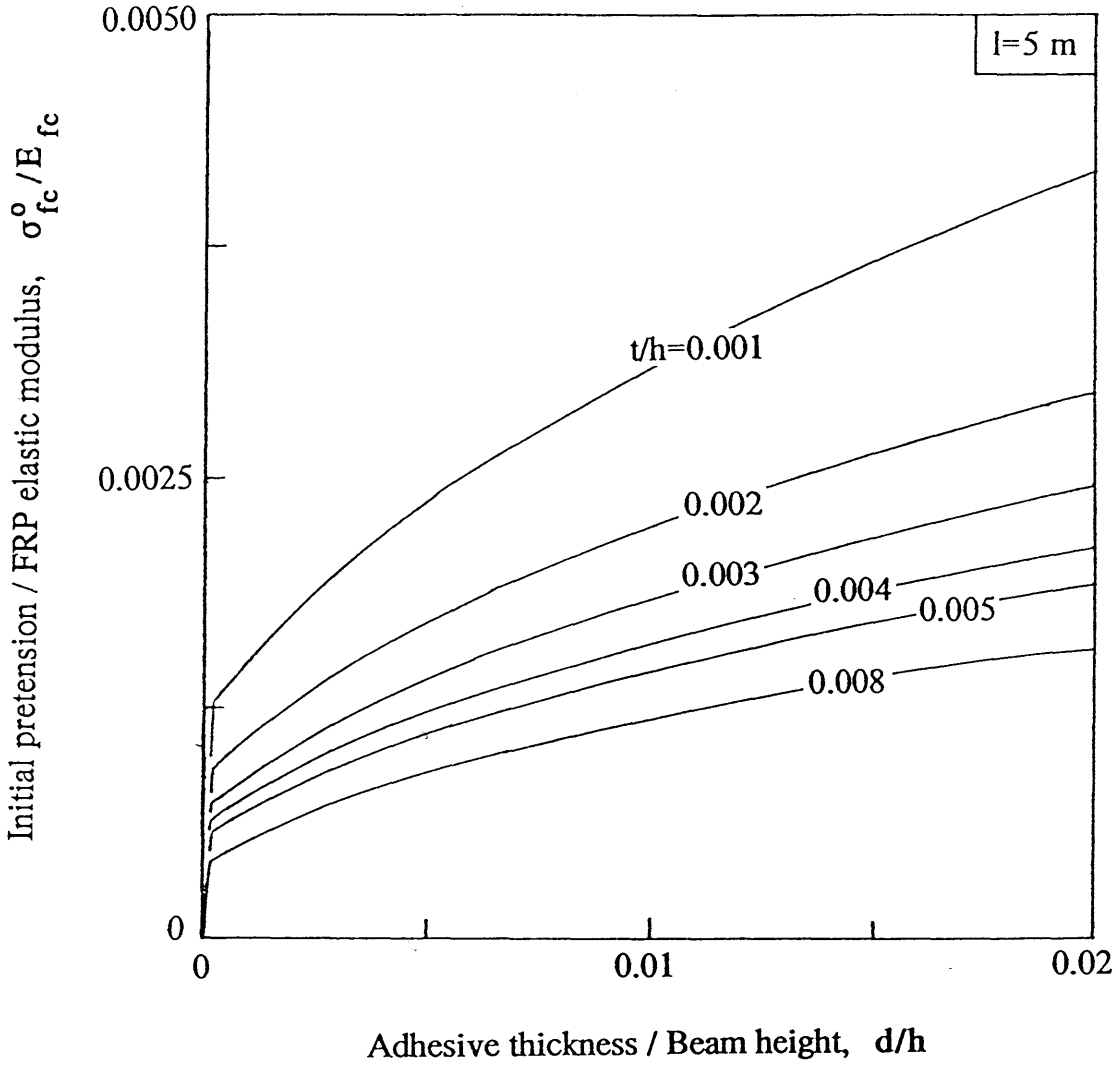

Figure 3.22 Initial prestress level vs. adhesive thickness for various FRP area fractions - concrete beams with l/h=10 and l=5 m.

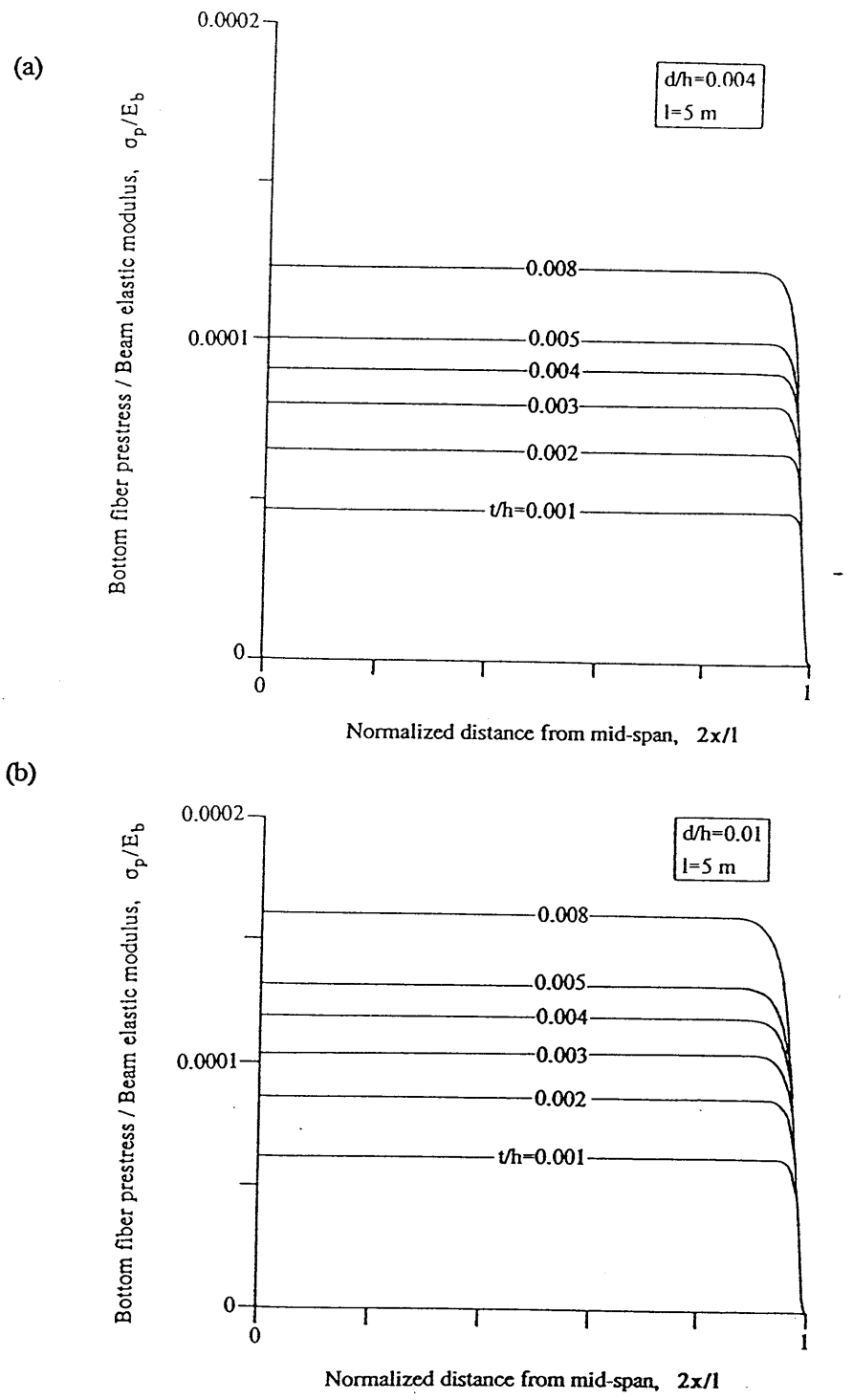

Figure 3.23 Bottom fiber prestress distribution along the member for various FRP area fractions - concrete beams with l/h=10 and l=5 m; (a) d/h=0.004 and (b) d/h=0.01.

CHAPTER 4

EXPERIMENTAL VALIDATION OF ANALYSIS

4.1 INTRODUCTION

This chapter describes the experimental verification of the analysis presented earlier. For this purpose, concrete and wood beams were reinforced with externally epoxy-bonded prestressed FRP sheets. A special prestressing apparatus designed by Deuring (1990) at the EMPA was employed in order to prestress the sheets before gluing them onto the beams. The magnitude of the ultimate prestress force causing failure of the system after releasing the pretension was measured and then correlated to the analytical values calculated using the procedures described in the previous chapter. It is concluded that the agreement between analysis and experiment is satisfactory.

4.2 MATERIAL PROPERTIES

4.2.1 Carbon Fiber Reinforced Plastic Sheets

Unidirectional fiber reinforced plastics (FRP) are made of continuous, aligned fibers embedded into a resin matrix. Depending on the type of fibers and matrix used, several FRP materials can be obtained. Typical fiber materials are glass, aramid and carbon, which can be used separately or as a mixture, while epoxies or polyesters are

often employed as matrix materials. If several different fiber types are used, then the fiber reinforced plastic is referred to as a hybrid laminate. In the experimental program described in this section only carbon fibers (T 300, Toray Industries) were used as reinforcement of the FRP sheets; their properties are given in Table 4.1.

Table 4.1 Material properties of T 300 fibers

Young's Modulus	[MPa]	235000
Tensile Strength	[MPa]	3200
Density	[g/cm^3]	1.76
Fiber Diameter	[10^{-6} m]	7

Carbon fibers behave in tension in a linear elastic manner up to failure, and a yield plateau does not exist; their response when loaded is quite brittle. The modulus of elasticity depends on the production process and the raw material. The most widely used raw material is Polyacrylonitrile (PAN). The elastic modulus and tensile strength of carbon fibers are inversely proportional to each other and, therefore, very stiff fibers have usually a lower tensile strength than those with a lower elastic modulus. The properties of the fibers and the matrix can be described by their unidirectional elastic constants. Unidirectionality in the composite material results from the layout of fibers, which are placed continuous and parallel to each other. The Young's modulus ($E_{\parallel}$, parallel to the fiber direction) and the Poisson's ratio ($\nu_{\perp\parallel}$, perpendicular to the fiber direction when the traction is in the fiber direction) of unidirectional FRP sheets can be calculated by the rule of mixtures as follows:

$$E_{\parallel} = E_f\, V_f + E_m(1 - V_f)$$
$$\nu_{\perp\parallel} = \nu_f\, V_f + \nu_m(1 - V_f) \qquad (4.1)$$

where the subscripts f and m refer to the fibers and the matrix, respectively, and V_f is the volume fraction of fibers.

The ultimate tensile stress of the FRP composite for fiber failure can be expressed as:

$$\sigma_{fc}^{*} = \sigma_{f}^{*} V_f + \sigma_{m}^{'}(1 - V_f) \tag{4.2}$$

where σ_f^* is the tensile strength of the fibers and $\sigma_m^{'}$ is the stress in the matrix at the fracture strain of the fibers. The last equation is valid if the applied stresses are parallel to the direction of the fibers and no shear forces are induced in the composite material. On the other hand, if the principal stresses are not parallel to the principal material directions, shearing of the matrix governs the failure load. In this case the failure load is highly decreased. It is concluded that unidirectional FRP sheets are most efficient and their use is optimized when bonded to the sides of structural components where the stresses are predominantly tensile. The properties of the matrix used in this study are summarized in Table 4.2.

Table 4.2 Mechanical properties of epoxy resin matrix

Young's modulus	[MPa]	3500
Tensile Strength	[MPa]	90
Density	[g/cm^3]	1.2

The elastic modulus, tensile strength and ultimate strain of the carbon fiber reinforced plastic (CFRP) sheet used in the experimental program of this chapter were measured by Kaiser (1989). The results reported on 20 mm wide CFRP sheets are given in Table 4.3.

Table 4.3 Mechanical properties of CFRP sheets

CFRP sheet thickness [mm]	Young's modulus $E_{\|\|}$ [GPa]	Tensile strength σ^*_{fc} [MPa]	Ultimate strain ε^*_{fc} [%]
0.5	110.5	1450	1.27
0.75	115.0	1470	1.22
1.0	120.5	1525	1.22

The volume fraction of fibers was found to have average values of 55.5%, 58.5% and 52.2% for the thicknesses of 1.0, 0.75 and 0.5 mm, respectively. Figure 4.1 illustrates typical uniaxial stress-strain curves for CFRP sheets and their relation to the uniaxial response of A36 structural steel.

4.2.2 Adhesive

The epoxy adhesive Sikadur 30 from Sika AG was employed in this testing program to provide shear transfer from the FRP sheet to the beam. The hardening process of this adhesive is a poly-addition. The resin and the hardener components have to be mixed in an exact proportion of 3:1 by weight. The hardening reaction uses a certain activation energy, which has to be provided in the form of heat. The speed of the reaction is highly sensitive to the external temperature. A temperature increase of 10 ^{o}C only can reduce the time to reach full strength by 50%.

The adhesive Sikadur 30 contains filler materials that substantially influence its properties. This filler is mainly quartz powder and quartz sand and is primarily used to improve the mechanical properties (creep resistance) and reduce the price. The properties of the adhesive are summarized in Table 4.4.

Table 4.4 Mechanical Properties of Adhesive

Young's modulus	[MPa]	7500
Modulus of Rupture	[MPa]	50-60
Compression Strength of Cube	[MPa]	90-100
Tensile Strength	[MPa]	30-40
Shear Modulus	[MPa]	2700
Shear Strength	[MPa]	25-30

Since the shear modulus of the adhesive represents an important parameter in the analysis described in Chapter 3, the torsion pendulum test was employed to determine its magnitude and establish its relation to temperature. The specimens used for the torsion pendulum test consisted of thin prisms with dimensions of 1x10x100 mm. The prisms were clamped on one side in the vertical direction, while a mass was attached on their free end. During the test, the mass was given a certain amount of torque, which was consequently released and its free vibration recorded. From the oscillation period and amplitude decrement of the system, the frequency and the damping were calculated, resulting in the shear modulus. The test was repeated at various temperatures in the range -100 ^{o}C to 150 ^{o}C, and the shear modulus-temperature dependence as shown in Fig. 4.2 was obtained. It is seen that the glass transition temperature (T_g) is approximately 60 ^{o}C, beyond which the shear modulus suddenly drops. It must be noted that the temperatures at which this adhesive can be efficiently used have to be below 60 ^{o}C, since at higher temperatures additional creep effects would be expected.

4.2.3 Concrete

The validity of the analytical solution for the maximum pretension of FRP sheets bonded on the tension face of concrete beams was verified from experiments on four

plain concrete beams. The beams were cut out of an approximately one year old concrete wall. The concrete mix was not known, but the maximum aggregate size was found to be 32 mm. The material properties were established from uniaxial tests on cylinders (diameter = height = 50 mm) that were also drilled out of the same wall. The ultimate compressive strength had an average value of 61.9 MPa (5 test results) while the tensile splitting test gave an average tensile strength of 4.9 MPa. The elastic modulus was calculated according to the ACI 318 formula:

$$E_c = 4730\sqrt{f_c'} \tag{4.3}$$

to be equal to 37.2 GPa.

4.3 THE EXPERIMENT SETUP AND METHOD

4.3.1 Anchorage of CFRP Sheets

The anchoring of FRP sheets has always been a problem when tensile tests are performed. Bone-shaped specimens are not appropriate since the shear strength of the FRP sheet is low and the increased cross section would detach at a lower load than the tensile strength (core pull-out effect). If friction clamps are used, the stress applied perpendicular to the fiber direction would have to be very high to provide for sufficient friction. This stress would damage the FRP sheet at the anchorage location and the FRP sheet would fail locally, again without reaching its tensile strength. Another possibility for the anchoring procedure is the application of high-performance adhesives. Here the FRP sheet is glued between two steel plates connected to the load source. The problem of stress concentration next to the anchorage can be solved by gradually decreasing the thickness of the plates so that their stiffness decreases towards their end, and a more uniform shear stress distribution is obtained. This concept was implemented by Deuring(1990) who designed an efficient prestressing apparatus. It consists of a rigid

steel beam with proper end fittings to hold a load cell on one end and a hydraulic jack on the other side (see Fig. 4.3). The FRP sheet is glued between two steel plates on both ends and then inserted into the end hinges, which are connected to the loading cell and the hydraulic jack (see Fig. 4.4). The adhesive used in the tests was a product of 3M. The steel plates were sandblasted and the CFRP sheet surface was roughened with sandpaper before the adhesive was applied over them. The overlapping length in the adhesive connection was 100 mm. The hardening process was accelerated by an increase in temperature. The sandwich consisting of two plates and the CFRP sheet was cured in a hydraulic press at constant pressure (10 atm) and temperature (65 ^{o}C) for two hours.

4.3.2 Surface Preparation

In the process of reinforcing of structural elements with externally bonded CFRP sheets the quality of the bond is of essential importance. Therefore, both surfaces have to be adequately prepared to reduce the risk of interface failures.

When concrete beams are to be reinforced by externally bonded sheets, a perfect bond can be achieved only if the external concrete surface, which contains a high amount of very fine particles (cement cover), has been removed. This is necessary to provide for a penetration and interlock of the adhesive into the compact aggregate configuration. A pneumatic hammer was employed to "clean" the concrete surface from this undesired cement paste, until a surface where the aggregate particles were clearly visible was obtained. Consequently the loose particles were removed using a strong vacuum cleaner.

It should be noted that two of the beams were cut from one free end of the concrete wall (beam no. 1 and 2) while the others (no. 3 and 4) were cut from the central part of the wall and, therefore, no free surfaces were covered by cement paste. Furthermore, some of the larger aggregates on the surface of beams 3 and 4 were cut through and after the hammering was performed a clearly better surface was obtained than for beams 1 and 2. The roughness was more uniform and a higher aggregate surface over mortar surface ratio was obtained for beams 3 and 4.

Similarly to the concrete surface, the CFRP sheet surface has also a resin surface that has worse mechanical properties than the core portion and is therefore undesired. This layer was removed using sandpaper. Shortly before the adhesive was applied the CFRP sheet surface was cleaned with acetone.

4.3.3 Test Procedure and Results

The CFRP sheet with the anchorage plates on both sides was spanned over the steel frame (see Fig. 4.3) and pin-connected to the hydraulic jack on one end and the load cell on the other. The pretension force was introduced in the sheet through the hydraulic jack up to the desired value and the adhesive was then applied on the CFRP and beam surfaces. The beam was then placed on top of the pretensioned sheet. The dead weight of the beam was increased by placing lead weights on the top, so that a surface pressure of approximately 0.06 MPa was reached. A continuous support for the CFRP sheet was provided with a soft wood plank.

The adhesive hardened in three days. The additional weights and the wooden support were removed. The pretension force was then gradually released from one end with the hydraulic jack and transmitted to the beam. In order to be able to pick up the failure load at which the prestressed system beam - CFRP sheet fails as accurately as possible, the decrement of load was very small (of the order of 5% of the initial pretension). To eliminate the effect of the dead load of the beam (lateral pressure on the CFRP-concrete interface) on the failure load, the beam was supported at the two ends so that it would not load the FRP sheet. At every load decrement , both of the vertical sides of the beam near the ends were checked for the appearance of cracks. Finally, the load at which the first visible crack appeared was recorded. The difference between this load and the initial pretension load gave the ultimate pretension level that could be achieved. The results obtained from the four experiments on the plain concrete members are summarized in Table 4.5.

Table 4.5 Test results on pretensioning concrete beams

BEAM	Position from wall	Prestressing force [KN]	$\sigma_{fc}^{initial}$ [MPa]	Force at failure [KN]	σ_{fc}^{o} [MPa]
1	bottom	13.0	347	12.0	290
2	bottom	11.0	293	10.5	280
3	center	14.0	373	14.0	373
4	center	16.5	440	13.5	360

The final state of the four beams after the pretension was fully released is shown in Fig. 4.5. It is seen that beams 2 and 3 had a small crack, since the initial prestressing load was close to the failure load, while beams 1 and particularly 4 show substantial peeling-off. It can be noticed that the initial crack propagates almost parallel to the FRP sheet and through the concrete, but then stops at a certain point. This phenomenon can be explained from the analysis in Chapter 3. From there it is seen that the ultimate pretension stress, σ_{fc}^{o}, increases when the beam length decreases (eqns 3.30 and 3.31). Hence, it can be concluded that the crack propagated decreasing the bonded length l, until the uncracked portion reached the maximum length required to withstand the imposed prestress level of $\sigma_{fc}^{initial}$ and create equilibrium. In addition to that, some strain energy was dissipated to bend the debonded part as seen in Fig. 4.5. Consequently, since the difference between $\sigma_{fc}^{initial}$ and σ_{fc}^{o} for beams 2 and 3 was small, the crack propagated by far less than in beams 1 and 4, where that difference was significant.

4.4 COMPARISON OF ANALYSIS WITH EXPERIMENTS

Using the computer program developed in this study and described in Section 3.4.1, the maximum pretension stress for the four concrete beams tested can be predicted

analytically. The material and geometric properties used here are given in Table 4.6.

Table 4.6 Geometric and material properties used in analysis

l[m]	t[mm]	h[m]	b[m]	b'[m]	E_{fc}[GPa]	E_c[GPa]	G_a[GPa]	τ_c^*[MPa]	δ^*[mm]
0.6	0.75	0.1	0.085	0.05	115	37	2.7	8.0	0.03

The value b' denotes the width of the CFRP sheet and the values for τ_c^* and δ^* were taken as mean values from results obtained by Ranish and Rostasy (1986), Ladner and Weder (1981) and Kaiser (1989). They performed tests on concrete subject to shear through pulling an externally bonded plate and recorded the shear stress τ_c^* and slip δ^* at failure. The equations developed in Section 3.1.3 assume that the width of the beam, b, and the FRP sheet , b', are equal. This was not the case in the experimental method. To account for this discrepancy, the thickness t of the FRP sheet was modified such that the FRP sheet area fraction remains constant. The modified thickness, t', can be found from the following equation:

$$t' = t\frac{b'}{b} \tag{4.4}$$

The total force, F_{fc}^o, in the FRP sheet required to cause failure of the system when the pretension is released can be calculated from the ultimate pretensioning stress σ_{fc}^o using the following equation:

$$F_{fc}^o = b\, t'\, \sigma_{fc}^o \tag{4.5}$$

Figure 4.6 shows the analytical curve defining the ultimate prestress force for different adhesive thicknesses. Since the concrete surface in the interface with the adhesive is quite rough and nonuniform, the adhesive thickness can only be estimated. Therefore, the experimentally obtained points were plotted as lines over an adhesive thickness ranging from 0.75 to 1.75 mm (minimum and maximum estimated values). If

the adhesive thickness is defined at an average value of 1.25 mm for all the beams tested, the experimental and analytical values for the ultimate pretension in the FRP sheet can be compared as illustrated in Fig. 4.7. It is seen that the analytical solution provides fairly good estimates of the experimentally obtained values and it can be concluded that the analysis gives satisfactory results. The average deviation between analysis and experiment is only 3.6% while the maximum deviation (beam 2) is 19%.

4.5 PRESTRESSING TESTS ON WOOD BEAMS

In order to evaluate experimentally the ultimate prestress levels that can be applied to wood beams, three beams were prestressed with externally bonded CFRP sheets. The wood type was beech and all beams were cut out from the same wood plank. The same apparatus and test procedure as described in Section 4.3.3 was employed. Following the recommendations by the manufacturer, the same adhesive as for the concrete beams was used. Shortly before the application of the adhesive, the wood surfaces were cleaned using acetone only (as solvent), since any mechanical roughening of the surface (e.g. application of sandpaper or sandblasting) would create loose wood particles which would decrease the performance of the bond. The length of all beams was $l = 800$ mm, while the cross section dimensions of the beams and the composite sheets varied. The geometric characteristics and the results from the prestressing procedure for the three experiments are summarized in Table 4.7 (notation as defined earlier).

Table 4.7 Geometric properties and test results on pretensioning wood beams

BEAM	h	t [mm]	b	b'	Prestressing force [KN]	$\sigma_{fc}^{initial}$ [MPa]	Force at failure [KN]	σ_{fc}^{o} [MPa]
1	60	0.75	45	43	28.5	883	25.5	790
2	60	0.50	45	45	18.5	822	18.0	800
3	80	0.5	45	44	20.5	932	18.0	818

The failure occurred in all beams through shearing of the wood. A crack propagated from the end of one side only, initiating close to the CFRP sheet interface, and running parallel to it. In the most heavily stressed beam (No. 3) the crack propagated to the middle of the member, while in the other two beams it stopped at a shorter distance. It is seen that the adhesive was strong enough to withstand the applied pretension and, although a high strength wood was used, the failure occurred in the beam. Therefore, the analysis performed in Section 3.4.2 applies for this case. Since, the shear strength of wood τ_w^* and the shear strain at failure γ_w^* need to be defined for the analysis, these values have to be obtained experimentally, first. The test method could be similar to the one employed by Kaiser (1989) to pull-out externally bonded FRP sheets on concrete surfaces or, as a simplified alternative, a shear test of wood specimen, bonded with the same adhesive, between two steel plates. Unfortunately, these tests were not carried out in this study and therefore the comparison between experiment and analysis is a subject of future work.

4.6 DISCUSSION

From the experiments carried out in this study it is seen that prestressing through external bonding of CFRP sheets on concrete and wood beams is a viable method for

strengthening and/or reinforcing structures. It must be emphasized that surface preparation at the beam-FRP interface is an important factor for the maximum achievable pretension level and hence, for practical applications this might play a crucial role. The ultimate prestress level that can be applied to concrete elements can be predicted analytically using the equations derived in Chapter 3, since good agreement (average deviation = 3.6%) between experiment and analysis is obtained. The results obtained here encourage the use of these analytical solutions for the calculation of ultimate prestress levels in further investigations on the flexural behavior of FRP-prestressed concrete structures. These issues will be addressed in the following chapter.

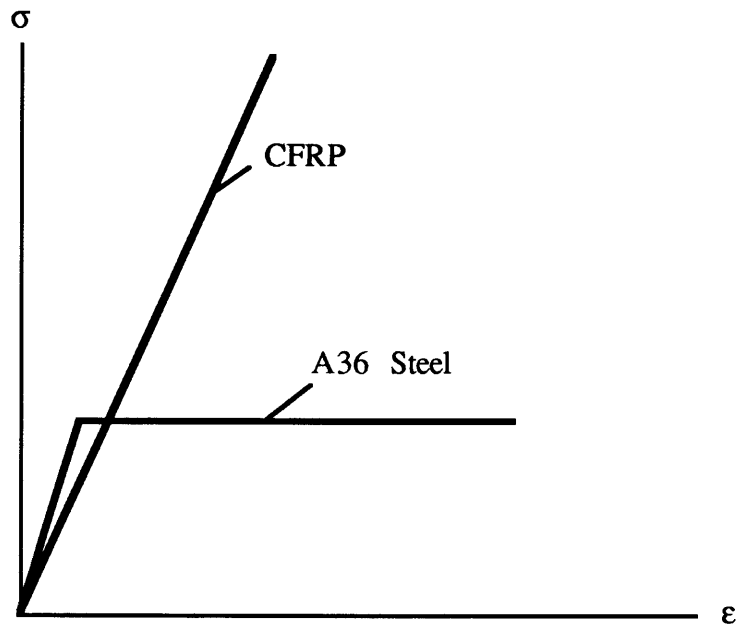

Figure 4.1 Uniaxial stress-strain relationship for CFRP sheets and A36 steel.

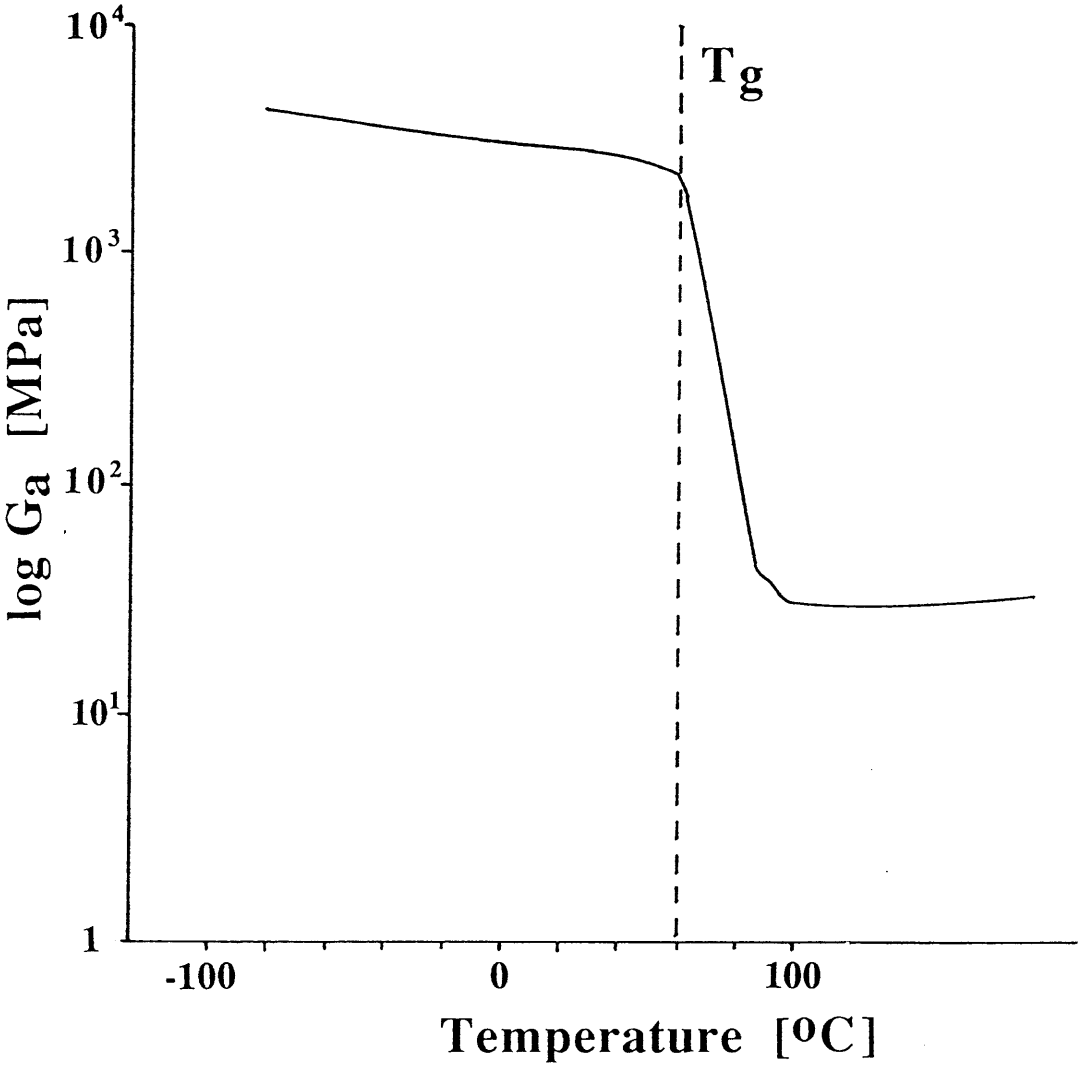

Figure 4.2 Adhesive torsion pendulum test results. Shear modulus as a function of temperature.

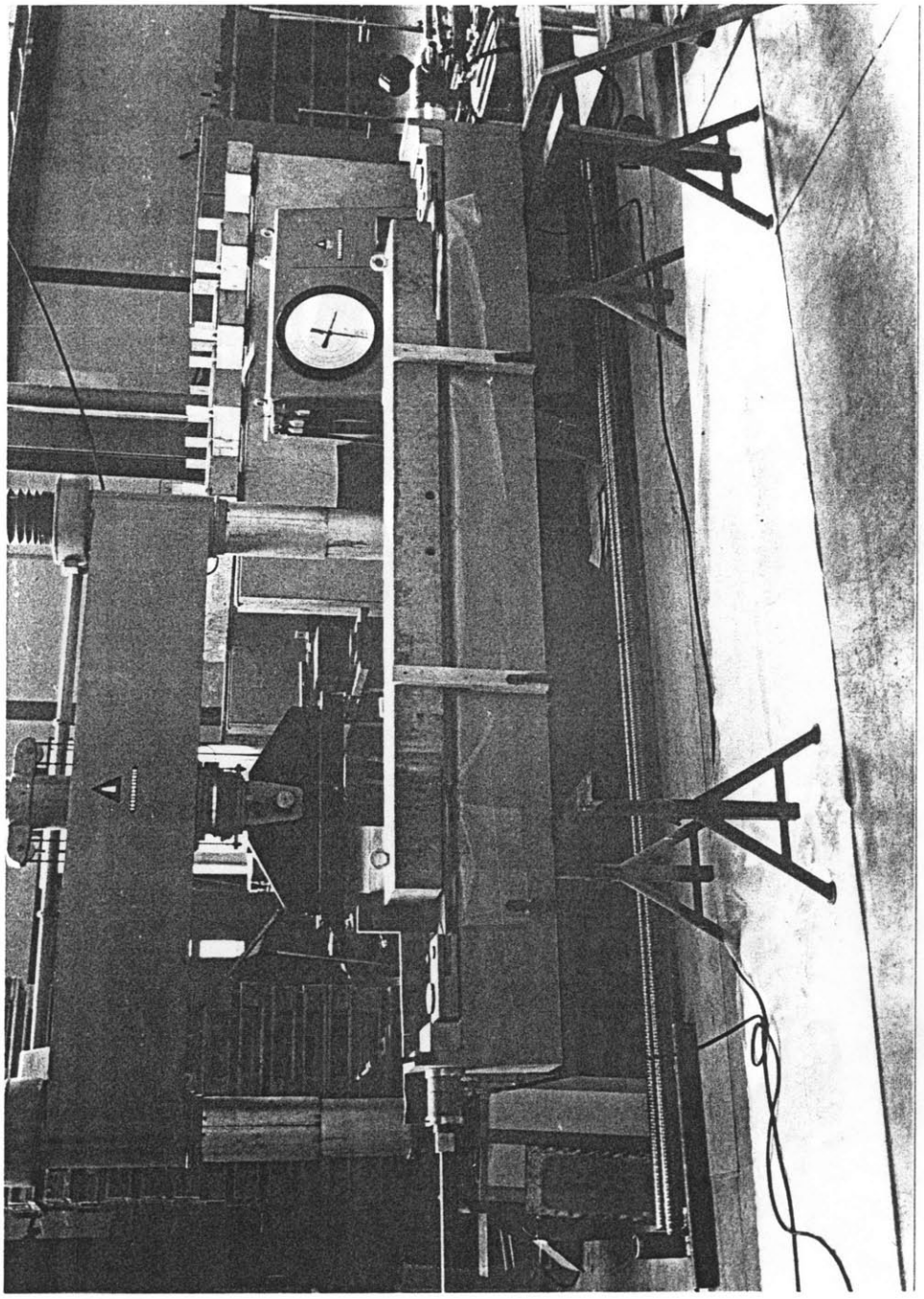

Figure 4.3 The prestressing apparatus.

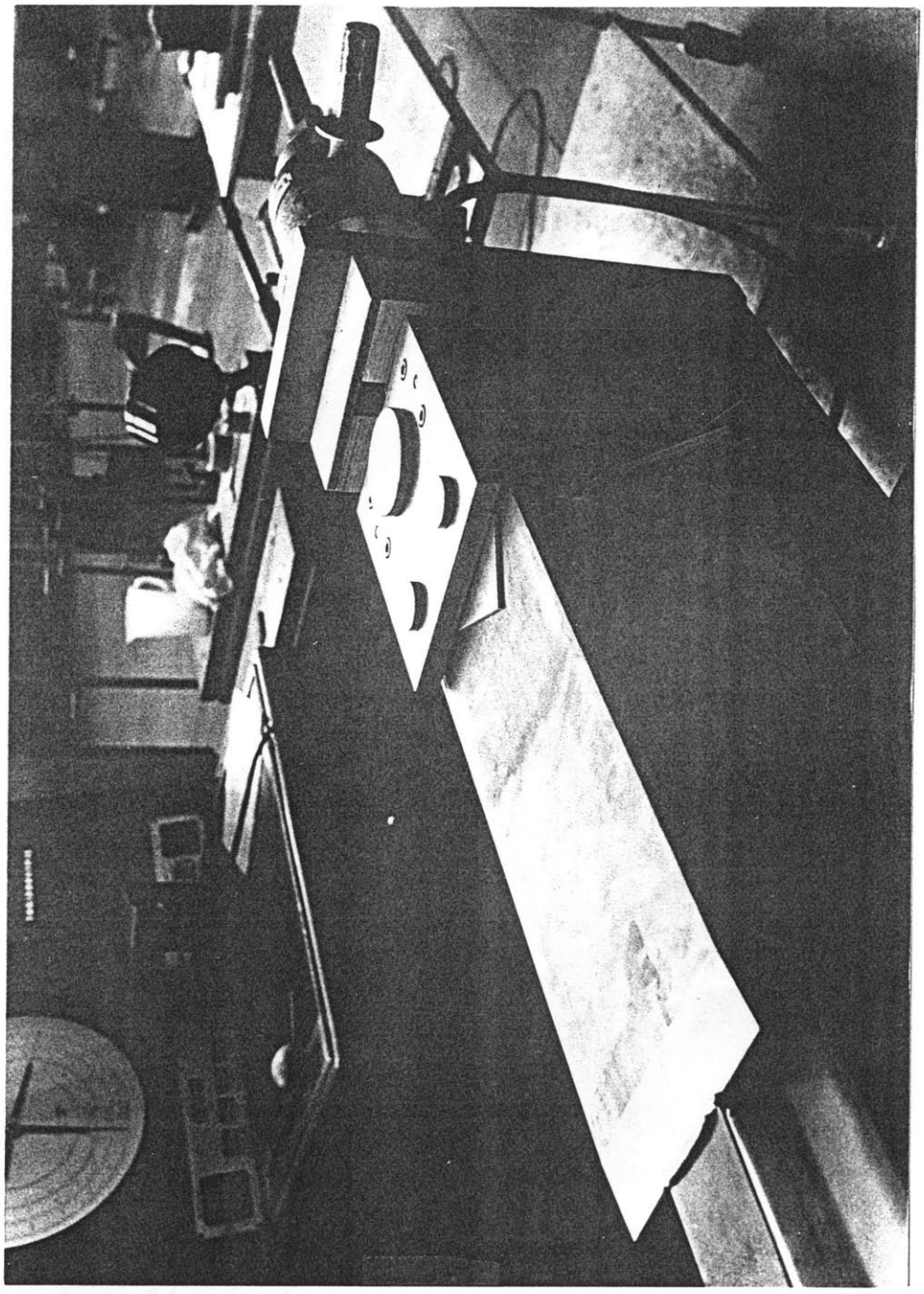

Figure 4.4 The anchorage detail.

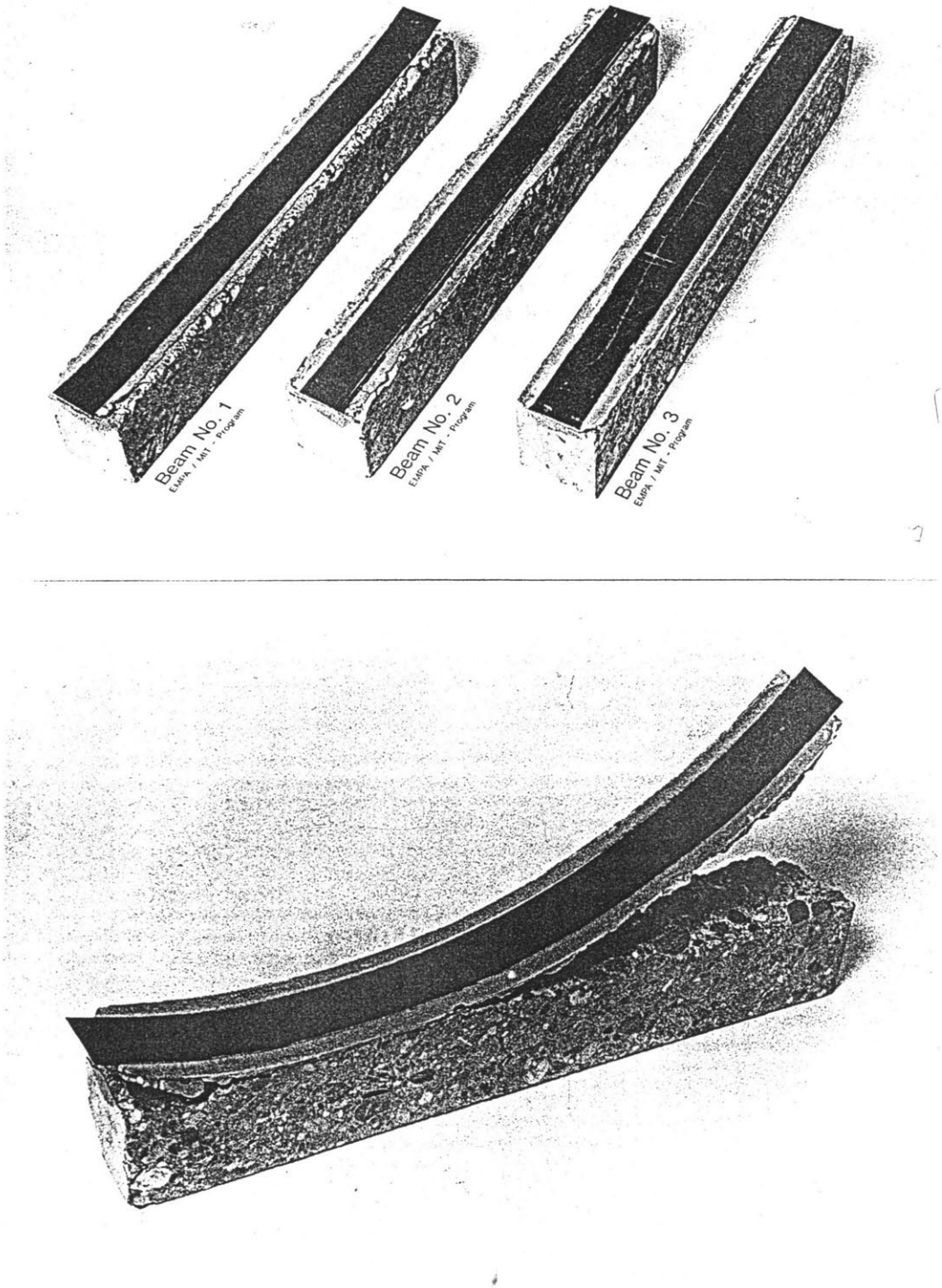

Figure 4.5 The concrete beams after prestressing was released.

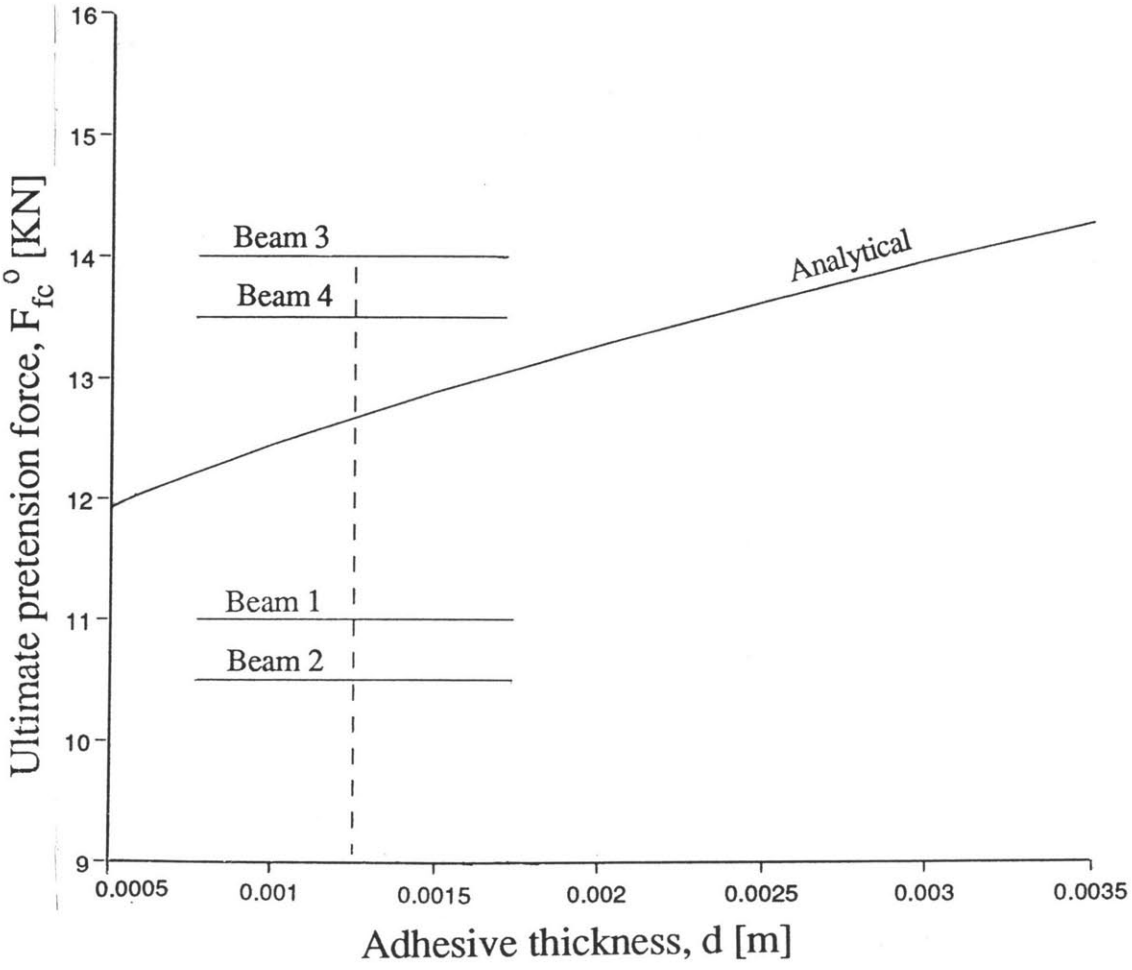

Figure 4.6 Ultimate prestress, analytical curve and experimental values.

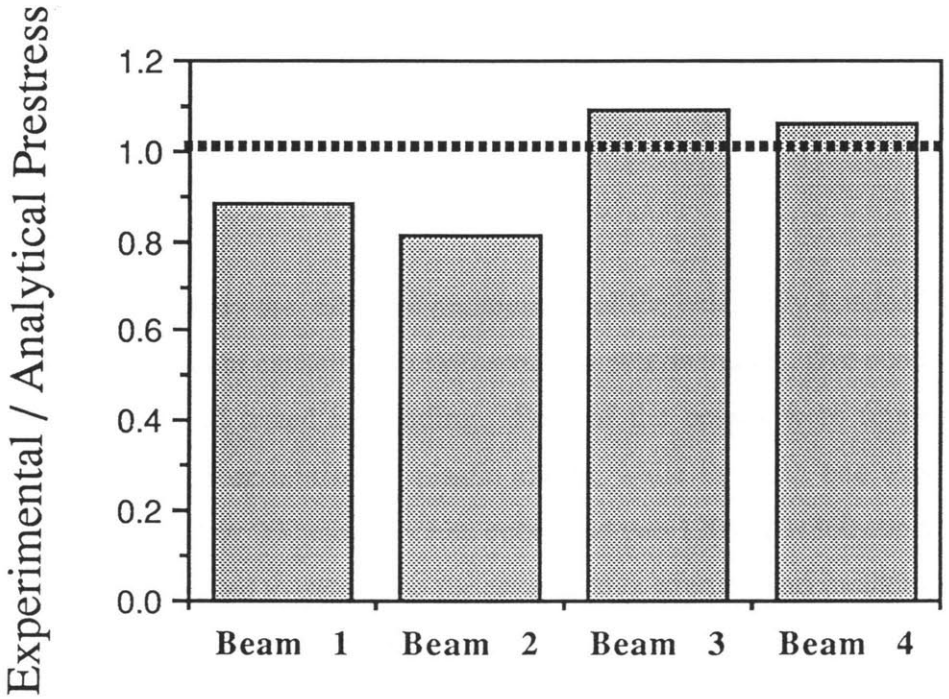

Figure 4.7 **Comparison of analytically and experimentally obtained ultimate prestress levels for adhesive thickness d = 1.25 mm.**

CHAPTER 5

FLEXURAL BEHAVIOR OF R/C -PRESTRESSED FRP SYSTEMS

5.1 INTRODUCTION

In order to study the effect of prestressing of the externally bonded FRP sheets on the ultimate moment capacity of reinforced concrete members, five concrete beams were constructed and tested in bending. Four of the beams were reinforced with prestressed carbon fiber reinforced plastic sheets, while the fifth one was used as a control specimen. Four 200 mm concrete cubes and two 120x120x360 concrete prisms were also cast and tested to determine the compressive strength and modulus of rupture of the concrete. The equations for the analysis of the bending behavior were derived for first cracking of the concrete, steel first yield and concrete crushing. Subsequently the experimentally and analytically obtained values were compared. A computer program was developed to analyze the ultimate moment capacity for various area fractions of the CFRP sheet and conclusions on the efficiency of the method were drawn.

5.2 SPECIMEN PREPARATION

For the production of the concrete test beams a standard EMPA concrete mix was employed. The proportions are given in Table 5.1 for a concrete volume of 100 l.

Table 5.1 Concrete mix components for the five test beams

Sand	0-1 mm	58.1 kg
Gravel	1-4 mm	58.1 kg
	4-8 mm	60.0 kg
Cement	PC Type I	35.0 kg
Water	(W/C ratio =0.5)	17.5 kg

Each beam had a cross section of 70x120 mm and was 1200 mm long. Beam No. 3 was reinforced with four 6 mm diameter deformed bars, while for all other beams four 4 mm diameter undeformed bars were used. For all beams, the shear reinforcement consisted of 4 mm diameter stirrups, which were placed at 40 mm spacing. The stirrups had one overlapping side which was additionally welded in order to provide for sufficient confinement and shear transfer. The shear reinforcement was designed to exclude the possibility of shear failure during the bending tests. The geometry of the beams tested is illustrated in Fig. 5.1. Following casting, the specimens were left to air-dry in a cure room at constant humidity and temperature for 28 days. At the age of 30 days the four concrete cubes and two prisms were tested to obtain the concrete properties. An average value of f'_{cube}= 33.9 MPa for the concrete cube compression strength was obtained, while the bending tests on the prisms gave an average modulus of rupture f_r= 4.2 MPa. The cylinder compressive strength was calculated from $f'_c = 0.85\, f'_{cube}$ and the elastic modulus was obtained from Beton Kalender (1987), Table 20b, to be E_c= 31.6 GPa.

5.3 PRETENSIONING OF THE BEAMS

At the age of 30 days the beams were taken out of the curing room and prepared for the prestressing process. For that purpose, the member's bottom surface was prepared to remove the layer with small particles (cement paste) as discussed in Section 4.2.2. Prestressing was applied as described in Chapter 4. The ultimate prestress force

($F_{fc}^{o} = \sigma_{fc}^{o}\ b'\ t$) was calculated using the method explained in Section 4.1.3. The analytical curves for F_{fc}^{o} corresponding to the specimens and the actually imposed prestress forces are shown in Fig. 5.2. The material and geometric properties used for the analysis are summarized in Table 5.2.

Table 5.2 Material and geometric properties

l[m]	h[m]	b[m]	E_{fc}[GPa]	E_c[GPa]	G_a[GPa]	τ_c^*[MPa]	δ^*[mm]
1.2	0.12	0.07	115	31.6	2.7	8.0	0.03

The adhesive thickness at the interface between the beam and the CFRP sheet was estimated to be 1 mm and therefore the experimental data of Fig. 5.2 were plotted at d = 1.0 mm. It should be noted that an adhesive thickness of 1.25 mm was used in the experimental part of Chapter 4, but the aggregate size for the beam used here was smaller and therefore a lower value was adopted. Different CFRP sheet thicknesses and widths were used for the prestressing of the beams. The actual prestressing level $\sigma_{fc}^{initial}$ introduced in the beams was somewhat reduced, compared to the ultimate one, to provide for some safety. Table 5.3 gives the geometric characteristics of the CFRP sheets and the prestress levels used for the beams involved in the experiments.

Table 5.3 Prestressing levels and composite sheet dimensions

BEAM	t [mm]	b' [mm]	t' [mm]	σ_{fc}^{o} [MPa]	$\sigma_{fc}^{initial}$ [MPa]	$\sigma_{fc}^{initial}/\sigma_{fc}^{o}$	Steel bars
1	0.75	50	0.53	285	280	98%	4 x ϕ4
2	1.0	50	0.71	246	180	75%	4 x ϕ4
3	1.0	50	0.71	246	230	93%	4 x ϕ6
4	1.0	70	1.0	207	190	91%	4 x ϕ4

It has to be pointed out that only one beam could be prestressed at a time and, also, the adhesive needed to be cured for 3 days. Therefore, the concrete properties changed from the time the first beam (No. 1) and the last (No. 4) were pretensioned. This, on the other hand, was not taken into account in the analysis of the ultimate pretension; the same material properties were used for all beams. It is probable that the beams pretensioned last were able to withstand higher prestress levels than predicted, due to aging of concrete; hence, the reduction percentages were gradually larger than calculated in Table 5.3. In Chapter 4 it was seen that the predicted maximum prestress values had a maximum deviation of 19% and thus, the reduction percentages have to be regarded as estimates only. After the pretensioning force was released from the hydraulic jack and transmitted to the beam, beam No. 1 showed a small horizontal crack at its vertical edge on one side, indicating that the ultimate pretension was just reached. This appears reasonable since the applied pretension was close (98%) to the theoretical ultimate value. Thus, it can be concluded, once again, that the analytical prediction of the ultimate prestress load is in good agreement with the experiment. All other beams did not shaw any visible damage or cracks. Subsequently, the beams were tested in three point bending; the results are described in the following sections.

5.4 FLEXURAL BEHAVIOR OF REINFORCED CONCRETE BEAMS WITH EXTERNAL PRESTRESSED CFRP SHEETS

In the analysis of singly R/C members in flexure, usually three important load values are reported corresponding to concrete first cracking, steel first yielding and concrete crushing. When doubly reinforced sections are used, additional modes may be encountered, depending on whether the compression steel has yielded or not. For the composite system CFRP sheet - R/C beam system described in this thesis the governing equations for all modes are derived and presented next. The following assumptions were made in the analysis:

- Plane sections remain plane.
- Adhesive thickness and its contribution to bending is neglected.
- The stresses generated in the composite sheet are uniform cross its thickness.
- The steel reinforcement is symmetrically placed and with same areas in tension and compression zones.
- The ultimate concrete strain ε_{cu} adopted is 0.0035.

First cracking

Before cracking occurs the concrete is assumed to behave in a linear elastic manner and its contribution in carrying tension is taken into account. The following equations hold:

$$\varepsilon_T = \frac{f_r}{E_c}$$
$$\varepsilon_{fc}^o + \varepsilon_T = \varepsilon_{fc} \tag{5.1}$$

where f_r and E_c are the modulus of rupture and elasticity of concrete, respectively. ε_{fc}^o and ε_{fc} are the prestress and actual strains in the fiber composite while ε_T is the strain in the concrete bottom fiber. Figure 5.3 shows the stress and strain distributions assumed herein; from the strain diagram the following compatibility relations are found:

$$\frac{\varepsilon_T}{h-c} = \frac{\varepsilon_{SC}}{c-a_o} = \frac{\varepsilon_{ST}}{h-c-a_o} \tag{5.2}$$

where ε_{SC} and ε_{ST} are the steel reinforcement strains in compression and tension, respectively, a_o is the concrete cover, c is the depth of the compressive zone and h is the height of the cross section. From eqns (5.1) and (5.2) the normal stress in the CFRP sheet is calculated:

$$\sigma_{fc} = \sigma_{fc}^o + \frac{E_{fc}}{E_c} f_r \tag{5.3}$$

where E_{fc} is the Young's modulus of the composite sheet. The equilibrium of normal forces yields the following equation:

$$F_{fc} = C_C + C_S - T_C - T_S \tag{5.4}$$

where the terms in the above represent the force in the CFRP sheet, the compressive force in the concrete, the compressive force in the compression steel, the tensile force in the concrete and the tensile force in the tensile steel reinforcement, correspondingly. The values for the forces are given in Fig. 5.3. After substituting for the forces and using the compatibility and constitutive equations given above and in Fig. 5.3, the depth of the neutral axis c, is found in the following form:

$$c = \frac{\left(\frac{\sigma_{fc}^{o}}{f_r} + \frac{E_{fc}}{E_c}\right) t\, b' + 0.5\, h\, b + A_s' \frac{E_s}{E_c}\frac{a_o}{h} + A_s \frac{E_s}{E_c}\left(1 - \frac{a_o}{h}\right)}{\left(\frac{\sigma_{fc}^{o}}{f_r} + \frac{E_{fc}}{E_c}\right)\frac{t\, b'}{h} + b + \frac{\left(A_s + A_s'\right)}{h}\frac{E_s}{E_c}} \tag{5.5}$$

where A_s and A_s' is the area of the tensile and compressive steel reinforcement, respectively, and E_s is the steel Young's modulus. Taking moments about the neutral axis we obtain the cracking moment as follows:

$$\begin{aligned} M_{cr} = {} & \sigma_{fc} b' t (h - c) + \frac{(h - c - a_o)^2}{(h - c)}\frac{f_r}{E_c} E_s A_s \\ & + f_r b \frac{(h - c)^2}{3} + \frac{(c - a_o)^2}{(h - c)}\frac{f_r}{E_c} E_s A_s' + \frac{c^3}{3(h - c)} f_r b \end{aligned} \tag{5.6}$$

where σ_{fc} and c are given by eqns (5.3) and (5.5), respectively.

Steel first yield

A parabolic stress strain relationship for concrete is considered as shown in Fig. 5.4. It is assumed that first yield is reached when the tension steel strain reaches $\varepsilon_{ST} = f_y / E_s$ (f_y = steel yield strength), while the compression steel may have yielded or not. For simplicity in this calculations it is also assumed that the maximum concrete strain is less than 0.002. The contribution of concrete in the tension zone is neglected. The stress and strain profiles along with the geometric relations are given in Fig. 5.5. Compatibility and constitutive equations yield:

$$\sigma_{fc} = \sigma_{fc}^{o} + E_{fc} \frac{(h-c)}{(h-c-a_o)} \frac{f_y}{E_s} \tag{5.7}$$

and from the geometry of Fig. 5.5 the concrete efficiency factor C_b reads:

$$C_b = \frac{f_y}{0.002E_s} \frac{c}{(h-c-a_o)} \tag{5.8}$$

Equilibrium of normal forces gives:

$$F_{fc} + T_S = C_C + C_S \tag{5.9}$$

which represents a second order polynomial equation and can be solved for c. The smaller non-negative root represents the feasible solution for stable equilibrium. Taking moments about the beam's bottom face, the moment for steel first yield can be calculated as follows:

$$M_y = C_C(h-a_f) + A_s f_y \frac{c-a_o}{h-c-a_o}(h-a_o) - A_s f_y a_o \tag{5.10}$$

where c is the root of eqn. (5.9) and a_f is the concrete compression force lever arm

shown in Fig. 5.5.

Concrete crushing

The following section aims at describing failure of the cross section by concrete crushing. The stress distribution in the compressive zone when this occures is shown in Fig. 5.6; it is that suggested by the CEB model code (1970). The CEB model was adopted in this study and not the ACI one, because it gives better agrement with test results for low reinforcement ratios, which was the case in the beams tested. For simplicity, the following analysis assumes that a_o=0.10 h, which was exactly the case for the test beams.

The stress and strain distributions along the cross section are given in Fig. 5.7. From the strain diagram, the following relations can be derived:

$$\begin{aligned} \varepsilon_{ST} &= 0.9\varepsilon_T - 0.1\varepsilon_{cu} \\ \varepsilon_{SC} &= 0.9\varepsilon_{cu} - 0.1\varepsilon_T \end{aligned} \tag{5.11}$$

Then, equilibrium of normal forces gives:

$$C_C + C_S - T_S = F_{fc} \tag{5.12}$$

which, after substituting for the forces from the relations given in Fig. 5.7 and subsequently normalizing with respect to bhE_{fc} gives the following equation:

$$\begin{aligned} &0.6885\frac{\varepsilon_{cu}}{(\varepsilon_T+\varepsilon_{cu})}\frac{f_c'}{E_{fc}} + \rho_{CS}\frac{E_s}{E_{fc}}(0.9\varepsilon_{cu} - 0.1\varepsilon_T) \\ &-\rho_{TS}\frac{E_s}{E_{fc}}(0.9\varepsilon_T - 0.1\varepsilon_{cu}) = \left(\varepsilon_T + \frac{\sigma_{fc}^o}{E_{fc}}\right)\rho_{fc} \end{aligned} \tag{5.13}$$

where $\rho_{TS} = A_s/bh$ and $\rho_{CS} = A_s'/bh$ are the area fractions of the tensile and compressive

reinforcement, respectively, while ρ_{fc} (=b't/bh) is the area fraction of the composite sheet. It should be noted that the absolute values of the second and third term in eqn. (5.12) are limited by $A_s'f_y$ and A_sf_y, correspondingly. Furthermore, the term in the parenthesis on the right hand side of eqn. (5.13) represents the strain in the composite sheet, and is limited by the ultimate CFRP sheet strain $\varepsilon_{fc}^{*} = \sigma_{fc}^{*} / E_{fc}$. Taking moments about the concrete bottom fiber and normalizing the terms with respect to bh^2f_c' the following equation is obtained:

$$\frac{M_u}{bh^2f_c'} = 0.6885\frac{\varepsilon_{cu}(\varepsilon_T + 0.585\varepsilon_{cu})}{(\varepsilon_T + \varepsilon_{cu})^2} + 0.9\,\rho_{CS}\frac{E_s}{f_c'}(0.9\varepsilon_{cu} - 0.1\varepsilon_T)$$
$$- 0.1\,\rho_{TS}\frac{E_s}{f_c'}(0.9\varepsilon_T - 0.1\varepsilon_{cu}) \qquad (5.14)$$

For given material properties and prestress level, σ_{fc}^{o}, eqn. (5.13) can be solved for ε_T which then can be substituted into eqn. (5.14) to obtain the normalized ultimate moment capacity.

A more efficient method for the solution of these equations can be obtained using a computer program. This approach was following in this thesis. The concrete bottom fiber strain ε_T was incremented as a variable and the values of σ_{fc}^{o} and M_u were calculated to satisfy eqns. (5.13) and (5.14). Through this procedure the yielding condition of both the compression and tension steel as well as the CFRP sheet tensile rupture criterion were taken into account. Figure 5.8 illustrates the results obtained for various area fractions of the composite sheet and two different reinforcement areas. Some of the curves have a slope discontinuity corresponding to yield of the top reinforcement and are interrupted for high prestress levels due to CFRP sheet failure. The material properties used to obtain the results of Fig. 5.8 are given in Table 5.4.

Table 5.4 Material properties used for the results of Fig. 5.8

f_y [MPa]	E_s [GPa]	E_{fc} [GPa]	$f_c^{'}$ [MPa]	σ_{fc}^{*} [MPa]
220	210	115	28.8	1450

From Fig. 5.8 it is seen that for higher amounts of steel reinforcement the gradient of the ultimate moment in respect to the pretension σ_{fc}^{o} is reduced. It should be added that an additional constraint from the ultimate prestress level that can be applied (as described in Chapter 3) will truncate the curves shown. Since the curves in Fig. 5.8 are general and do not depend on beam geometry, and because on the other hand the prestress cutoffs are different for various geometries, the latter are not included in the figure.

5.5 EXPERIMENTAL RESULTS

At the age of 42 days the five beams described in Section 5.2 were loaded in three point bending to failure. The span length was 960 mm and the supports were hinged cylindrical rollers allowing out of plane rotation and thus, providing a uniform load distribution along the width of the specimens. 50 mm wide and 6 mm thick steel plates were used to transmit the load to a larger area and hence, eliminate local crushing of the concrete. The tests were carried out using an Instron machine with a load capacity of 1000 KN at a displacement controlled rate of 10 mm/min. The applied load was measured through a load cell and recorded on the y axis of on xy plotter; time was recorded on the x axis. The crosshead displacement (= midspan deflection) was calculated from the known displacement speed. This method was not considered to be sufficiently accurate because of the machine compliance; the deflections obtained should only be used for comparisons among the five beams tested. The load-deflection curves obtained are shown in Fig. 5.9.

The control beam (No. 5) which was reinforced with the minimum reinforcement, failed in an expected manner, having one large flexural crack at midspan, which propagated until concrete compression failure was reached. All the other beams with the externally bonded and prestressed CFRP sheets failed at a much higher (up to 5.2 times) load level, maintaining very good displacement ductility characteristics.

Beams 1 and 2 failed in a similar manner. Inclined cracks resulted in localized peeling-off of the CFRP sheet (see Fig. 5.10a) producing a drop in the load. CFRP-concrete interface crack propagation was arrested at this point due to the high clamping forces (reactions) at the member supports. The load was further increased (another CFRP slip took place for beam 2) until crushing of the concrete occured in the compressive zone followed by complete delamination (Fig. 5.10b).

Beams 3 and 4 failed by shear through the concrete layer between the CFRP sheet and the bottom steel reinforcement, initiating near the supports (Fig. 5.10c). The failure sequence was characterized by the same slip mechanism observed in beams 1 and 2, resulting in a drop of the load followed by further increase until compressive crushing occured leading to complete delamination (Fig. 5.10d). It should be noted that no visible flexural cracks were observed almost up to the failure load.

5.6 COMPARISON OF ANALYTICAL AND EXPERIMENTAL BENDING BEHAVIOR

The analysis presented in Section 5.4 describing the bending behavior of the prestressed CFRP sheet - R/C beam system was compared to the experimentally obtained values. The theoretical moments for three different stages, namely concrete first cracking, tension steel yielding and concrete crushing, were calculated using the equations given in Section 5.4; the corresponding experimental values were obtained from the load-deflection curves given in Fig. 5.9 using the equation for three point bending:

$$M_i = \frac{P_i \, l}{4} \tag{5.15}$$

where the index i stands for the three different bending states and l is the span length (= 950 mm). All the parameters (geometric and material properties as well as prestress levels) needed for the analytical computation are listed in Tables 5.2 through 5.4. The concrete properties are discussed in Section 5.2 and the steel yield strength was given by the manufacturer as 220 MPa for the 4 mm undeformed bars and 500 MPa for the 6 mm deformed bars. The results obtained are summarized in Table 5.5.

Table 5.5 Comparison of analytical and experimental moment capacities [KNm]

	First cracking			*Steel yield*			*Concrete crushing*		
BEAM	exper.	calc.	deviation	exper.	calc.	deviation	exper.	calc.	deviation
1	1.43	1.65	15.4%	2.37	2.45	3.4%	6.9	5.6	18.8%
2	1.42	1.54	8.4%	2.43	2.47	1.6%	8.18	6.01	26.5%
3	1.68	1.83	8.9%	5.28	5.46	3.4%	9.0	8.31	7.7%
4	1.47	1.62	10.2%	2.64	2.65	0.4%	9.28	6.79	26.8%
		average	10.7%		average	2.2%		average	19.9%

The deviations in Table 5.5 were calculated from the ratio of analytical to experimental results and it is seen that the correlation is satisfactory for the first cracking and steel yielding mode, while for the case of concrete crushing the analytical solution appears conservative. It should be noted that the agreement with experimental results is better for beam No. 3, which had more reinforcing steel. This can be explained by the fact that the steel in the minimally reinforced beams experienced large deformations (more than 1%) producing hardening which was not considered in this analysis. The analytical results for the ultimate moment capacities and the corresponding experimental values are shown in Fig. 5.12. The ultimate pretension level for the test beams, calculated in

Section 5.3 and given in Table 5.3, truncates the curves shown.

The effect of the pretensioned CFRP sheets is not found to be significant when compared to unprestressed beams with the same composite area fraction (compare to values at $\sigma^{o}_{fc}/E_{fc} = 0$) and the increase in moment capacity lies in the range of 10%. This is due to the low cutoffs resulting from the ultimate prestress level that can be applied, and could be increased with proper anchorage of the composite sheets (up to 50% for beam No. 4). The efficiency of the prestress procedure is defined by the ratio of the ultimate prestress level to the pretension that would cause a CFRP sheet failure. From Fig. 5.12 it is seen that this ratio is higher for low composite area fractions ($\approx$ 50% for beam No.1 and only $\approx$20% for beam No. 4).

5.7 SUMMARY

Test results on R/C beams with external prestressed CFRP sheets showed remarkable improvement in flexural behavior when compared to members without composite reinforcement. Concrete first cracking, steel yielding and concrete crushing moment capacities were all increased, while ductility was maintained. All beams failed when concrete crushing was reached and a pullout of the CFRP sheet under the support occurred.

The calculation of the ultimate prestress level described in Chapter 3 was verified during the pretensioning procedure. The analytical prediction of the bending behavior compared well to the experimental results, although the predicted ultimate moment capacities appear conservative; this was expected since the analysis was based on code assumptions. The effect of prestressing was found to be low for the applied prestress level and produced an increase of the moment capacity of the prestressed compared to the unprestressed composite member of approximately 10%. Since the ultimate prestress level is higher for low CFRP sheet area fractions, a higher efficiency of the composite sheet is achieved in this case. In order to increase the efficiency, proper anchorage devices have to be used to allow for higher ultimate prestress forces. At the same time a

considerable increase in the moment capacity would become feasible and the effect of prestress would become significant.

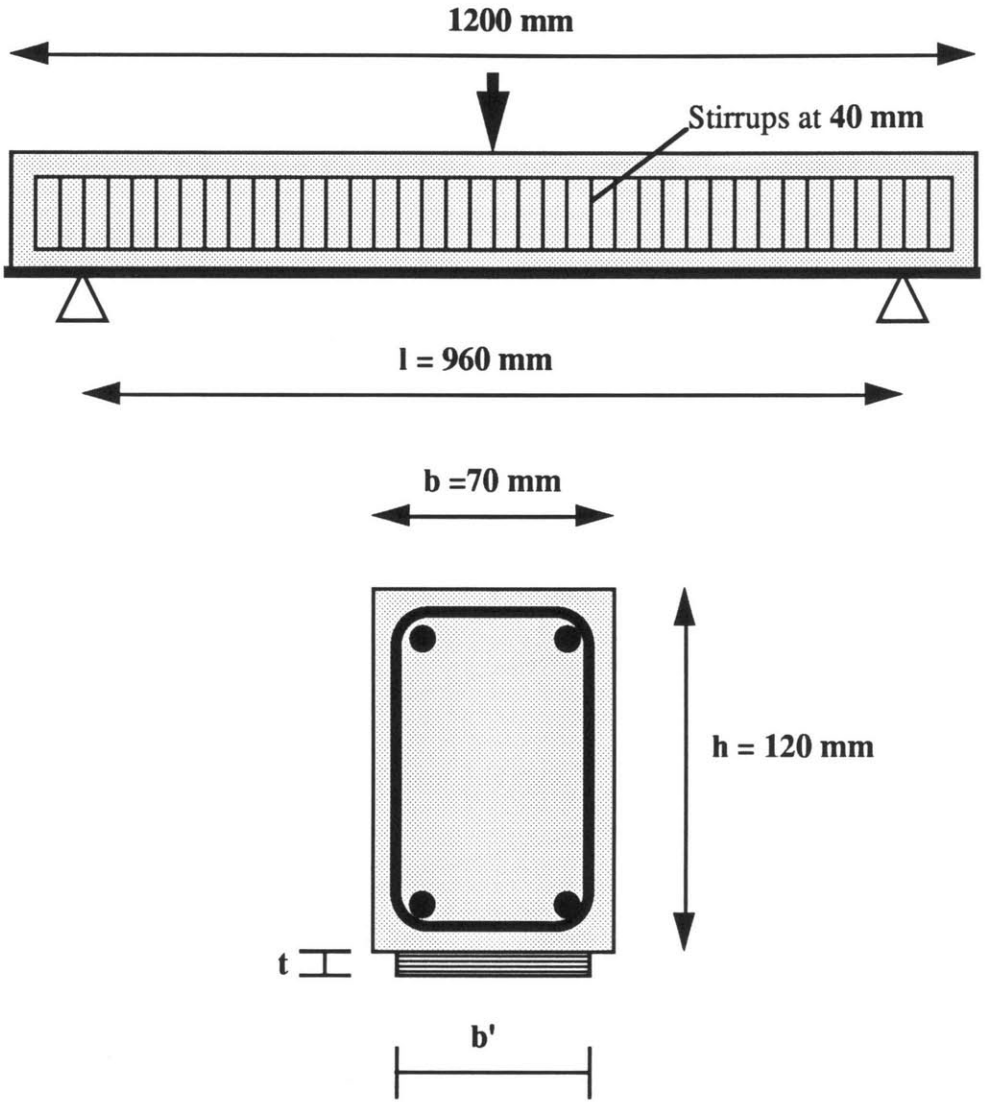

Figure 5.1 Geometry and layout of fabricated beams.

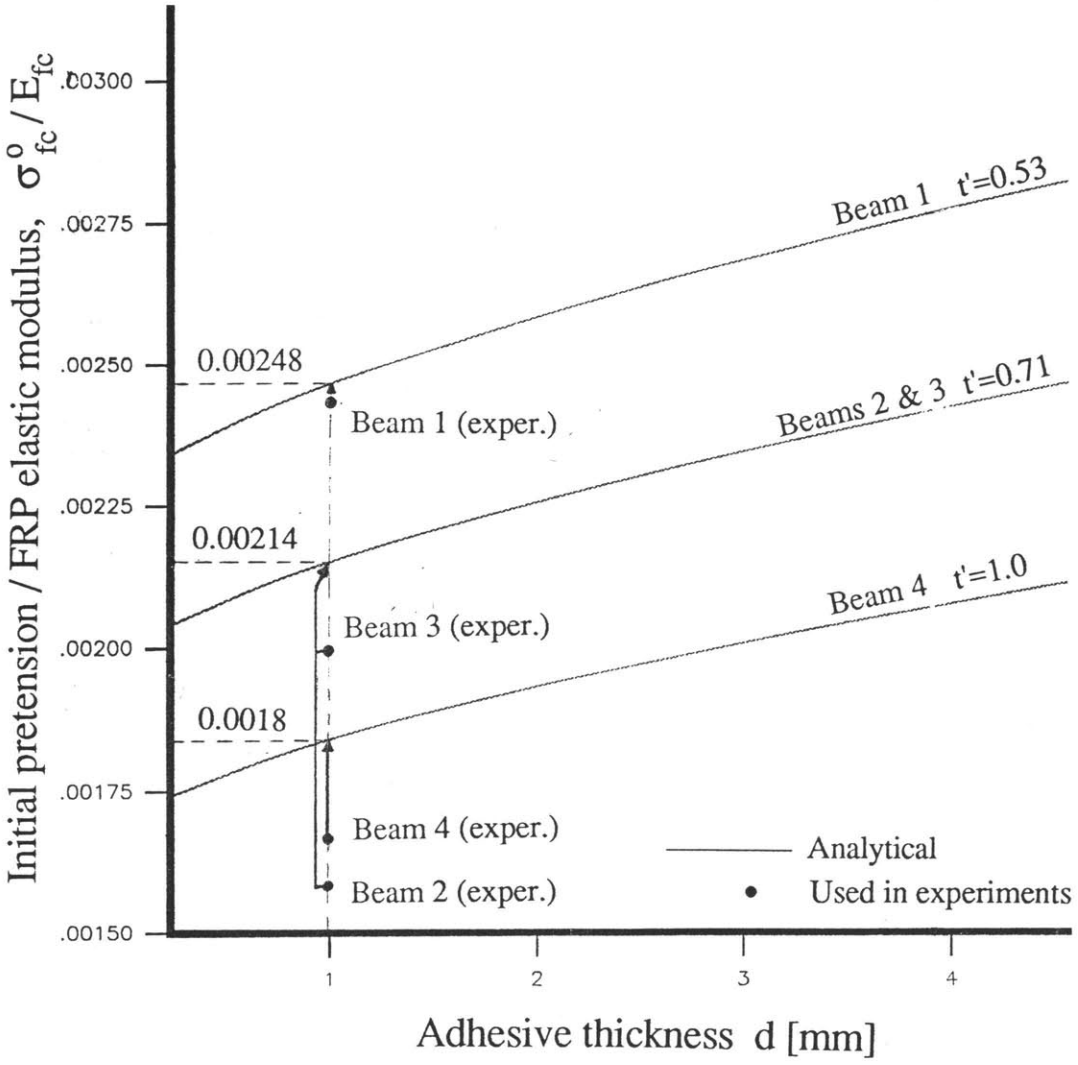

Figure 5.2 Predicted and applied prestress level.

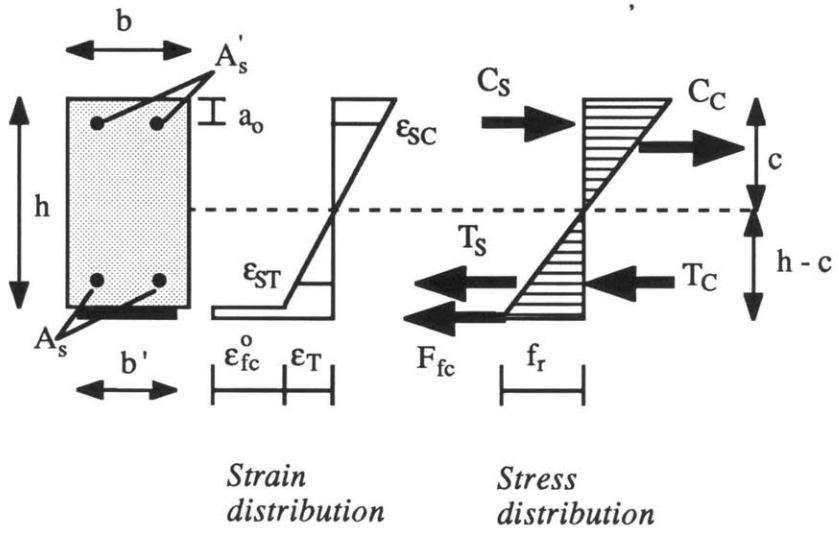

$$F_{fc} = b't\left(\sigma^{o}_{fc} + \frac{E_{fc}}{E_c} f_r\right)$$

$$C_C = \frac{c^2}{2(h-c)} f_r b$$

$$C_S = \frac{c - a_o}{h - c} f_r A_s' \frac{E_s}{E_c}$$

$$T_S = \frac{h - c - a_0}{h - c} f_r A_s \frac{E_s}{E_c}$$

$$T_C = \frac{h - c}{2} f_r b$$

Figure 5.3 Strain and stress distribution at concrete first cracking.

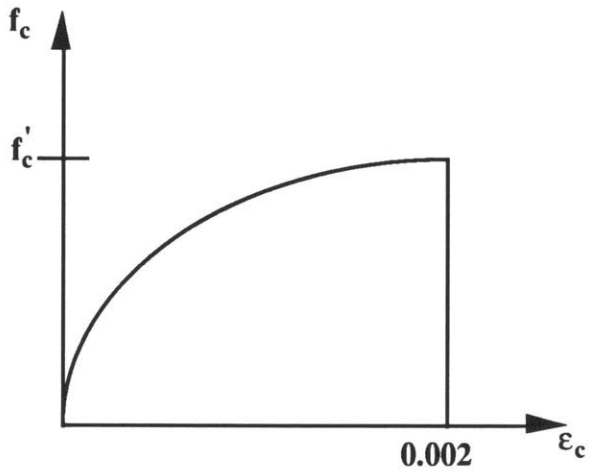

$$f_c = \frac{f_c'}{0.002}\left(2\varepsilon_c - \frac{\varepsilon_c^{\,2}}{0.002}\right)$$

Figure 5.4 Assumed concrete stress-strain relationship at steel first yield.

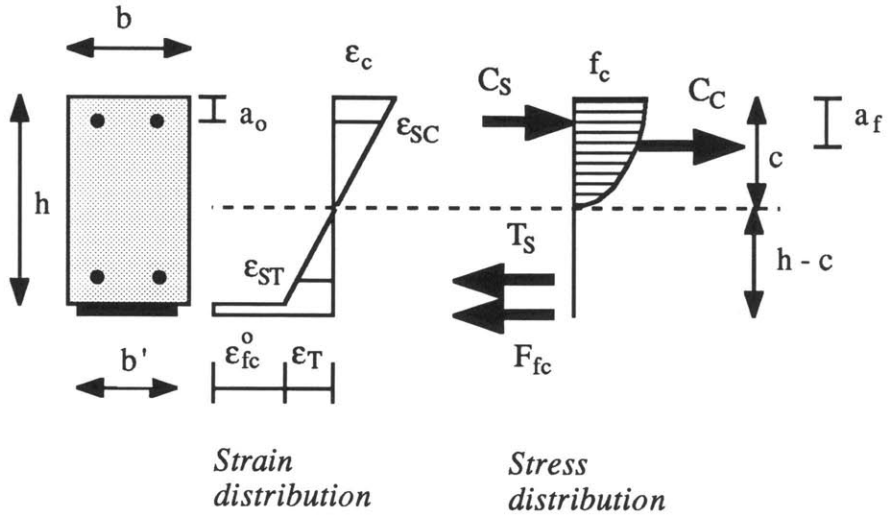

$$C_b = \frac{\varepsilon_c}{0.002}$$

$$a_f = \frac{4 - C_b}{4(3 - C_b)}$$

$$a = C_b\left(1 - \frac{1}{3}C_b\right)$$

$$f_c = \frac{f_c'}{0.002}\left(2\varepsilon_c - \frac{\varepsilon_c{}^2}{0.002}\right)$$

$$C_C = a\, b\, f_c\, c$$

$$C_S = f_y A_s \frac{c - a_o}{h - c - a_o} \le f_y A_s$$

$$T_S = f_y A_s$$

$$F_{fc} = b' t\left(\sigma^o_{fc} + \frac{E_{fc}}{E_c} f_r\right)$$

Figure 5.5 Strain and stress distribution at steel first yield.

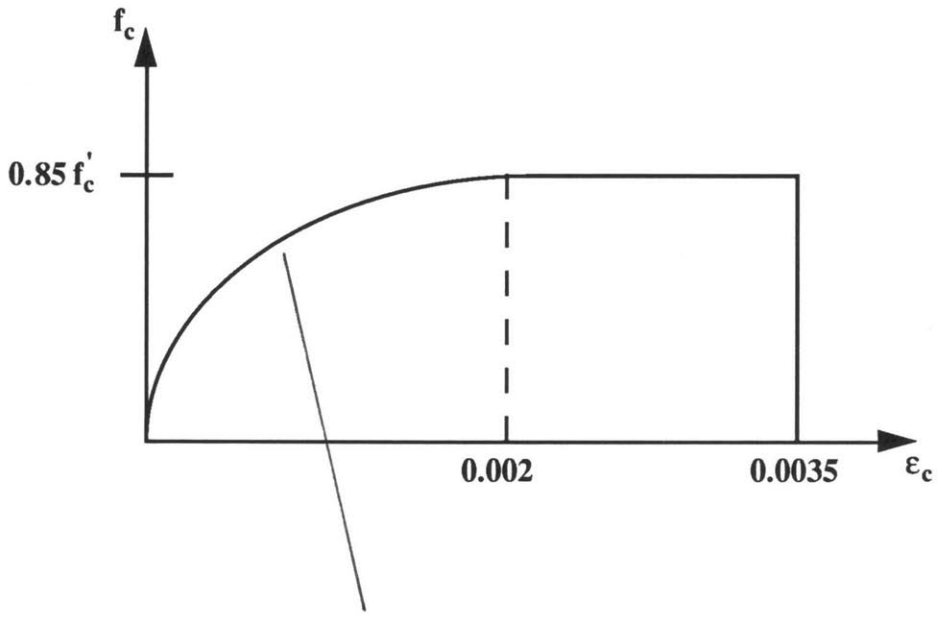

Figure 5.6 Idealized concrete stress-strain relationship at crushing failure.

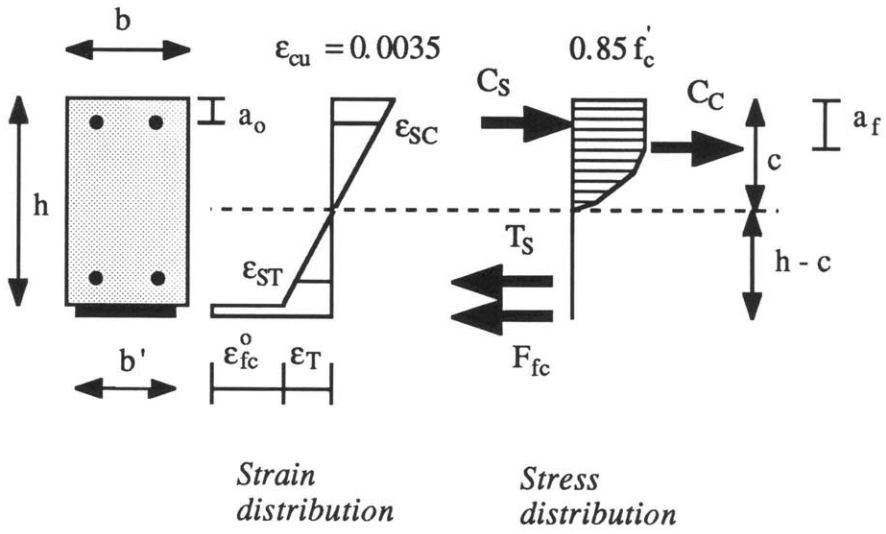

$$a_f = 0.415c$$

$$C_C = 0.6885 \frac{\varepsilon_{cu}}{\varepsilon_T + \varepsilon_{cu}} f_c' \, b \, h$$

$$C_S = E_s A_s' (0.9\,\varepsilon_{cu} - 0.1\,\varepsilon_T)$$

$$T_S = E_s A_s (0.9\,\varepsilon_T - 0.1\,\varepsilon_{cu})$$

$$F_{fc} = b' t \left(\sigma_{fc}^o + \varepsilon_T E_{fc}\right)$$

Figure 5.7 Strain and stress distribution at concrete crushing.

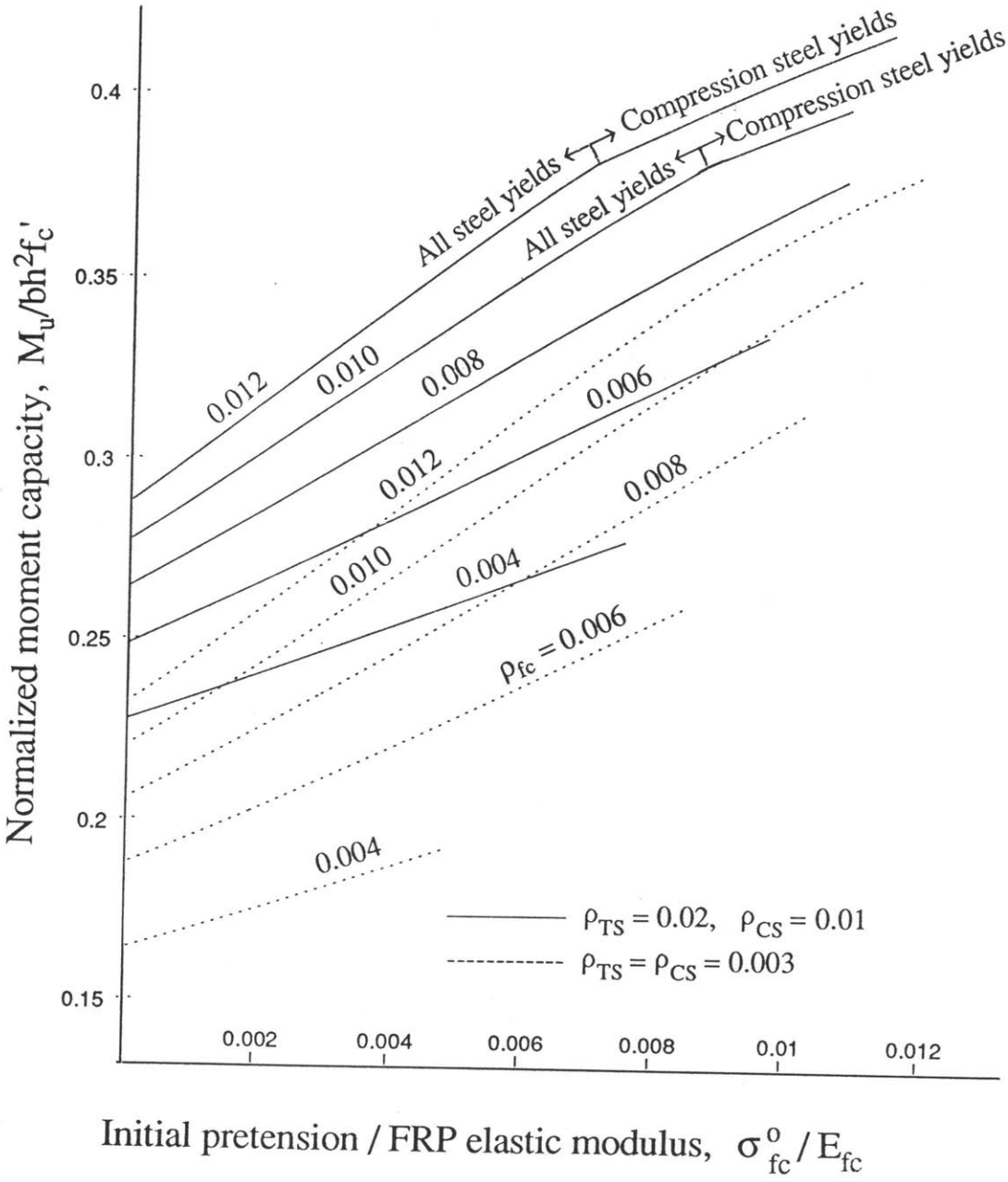

Figure 5.8 Ultimate moment capacity as a function of the prestress level.

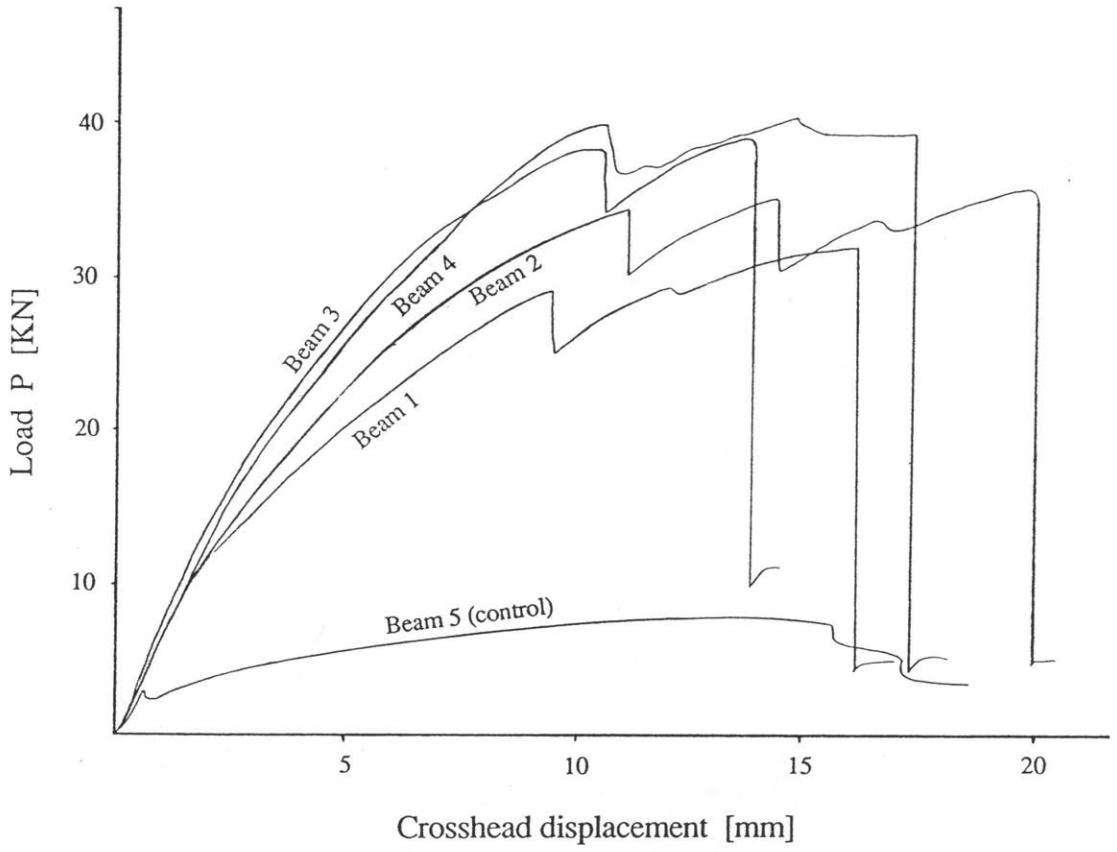

Figure 5.9 Load-deflection curves from three point bending tests.

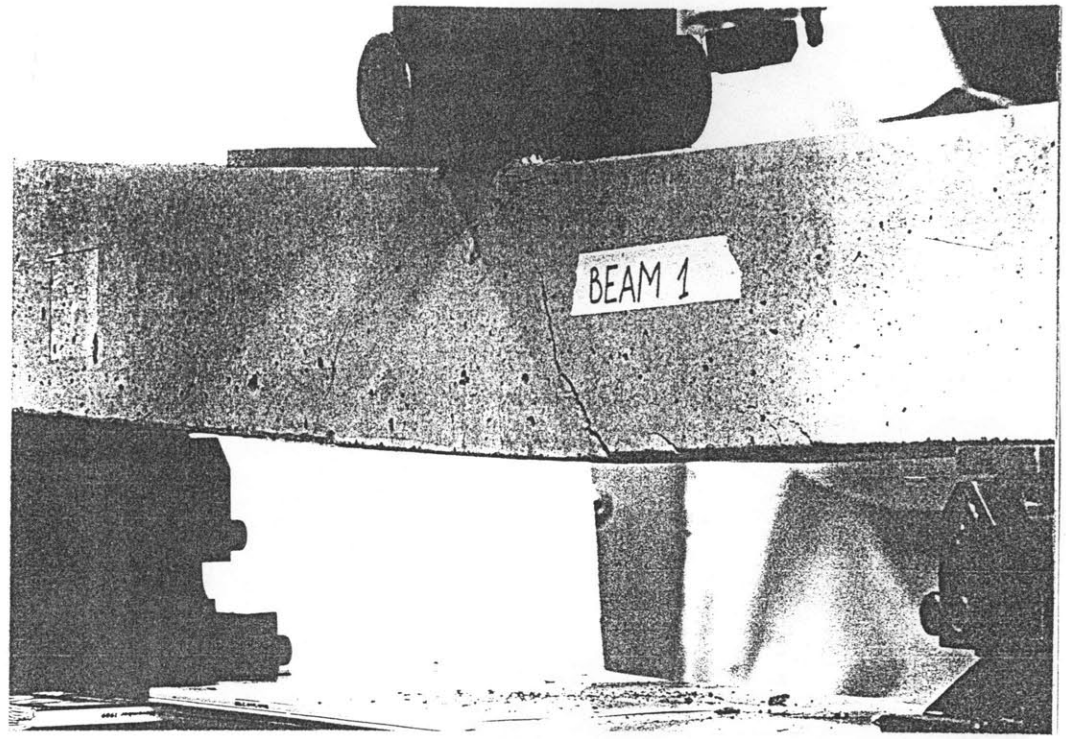

(a)

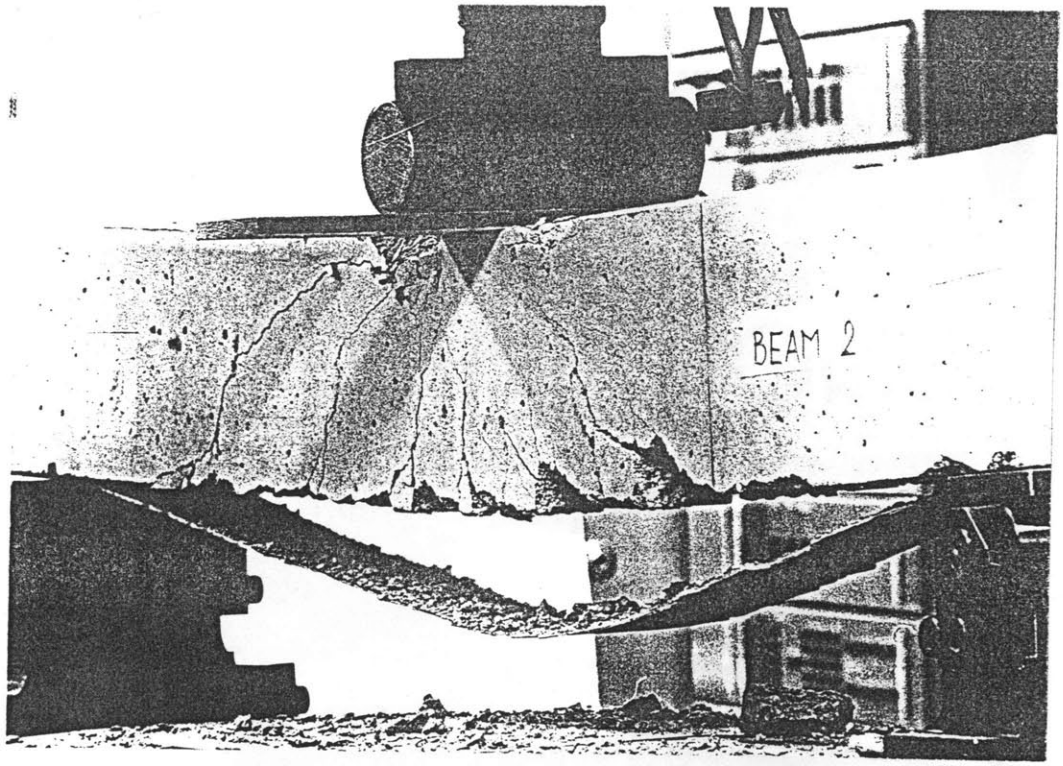

(b)

Figure 5.10 Cracking and failure patterns of beams tested.
(a) beam 1; (b) beam 2; (c) and (d) beam 4.

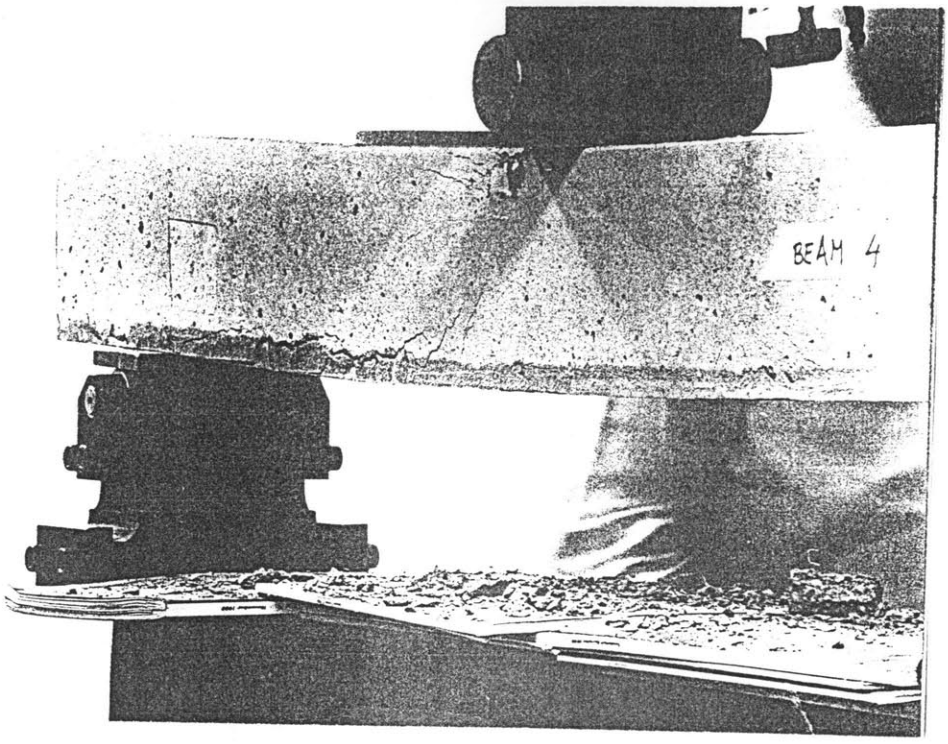

(c)

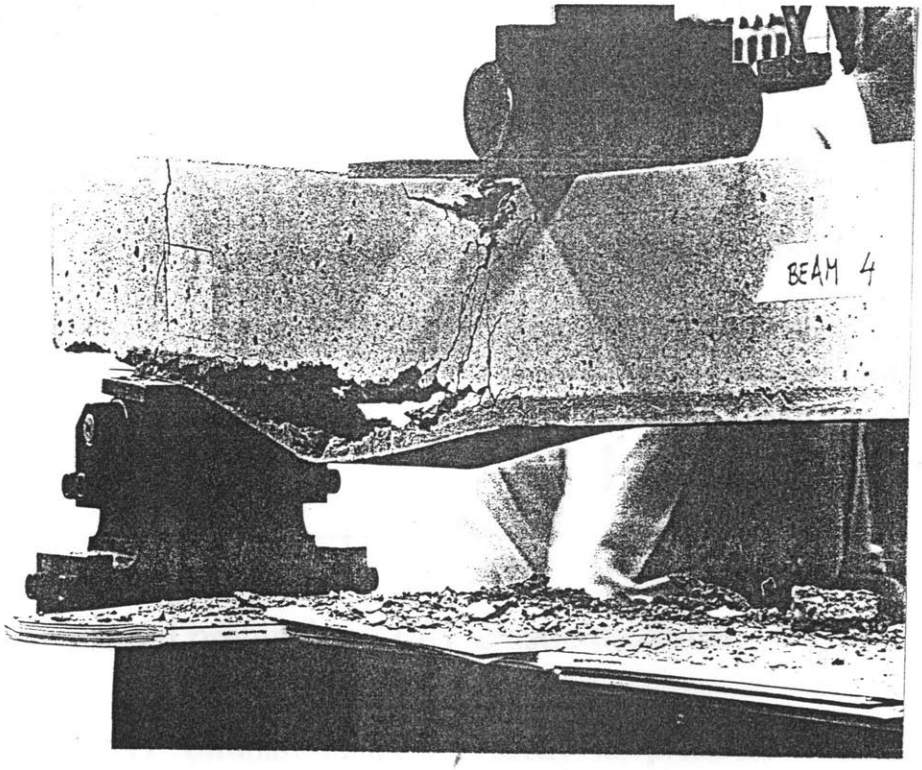

(d)

Figure 5.10 Cont'd.

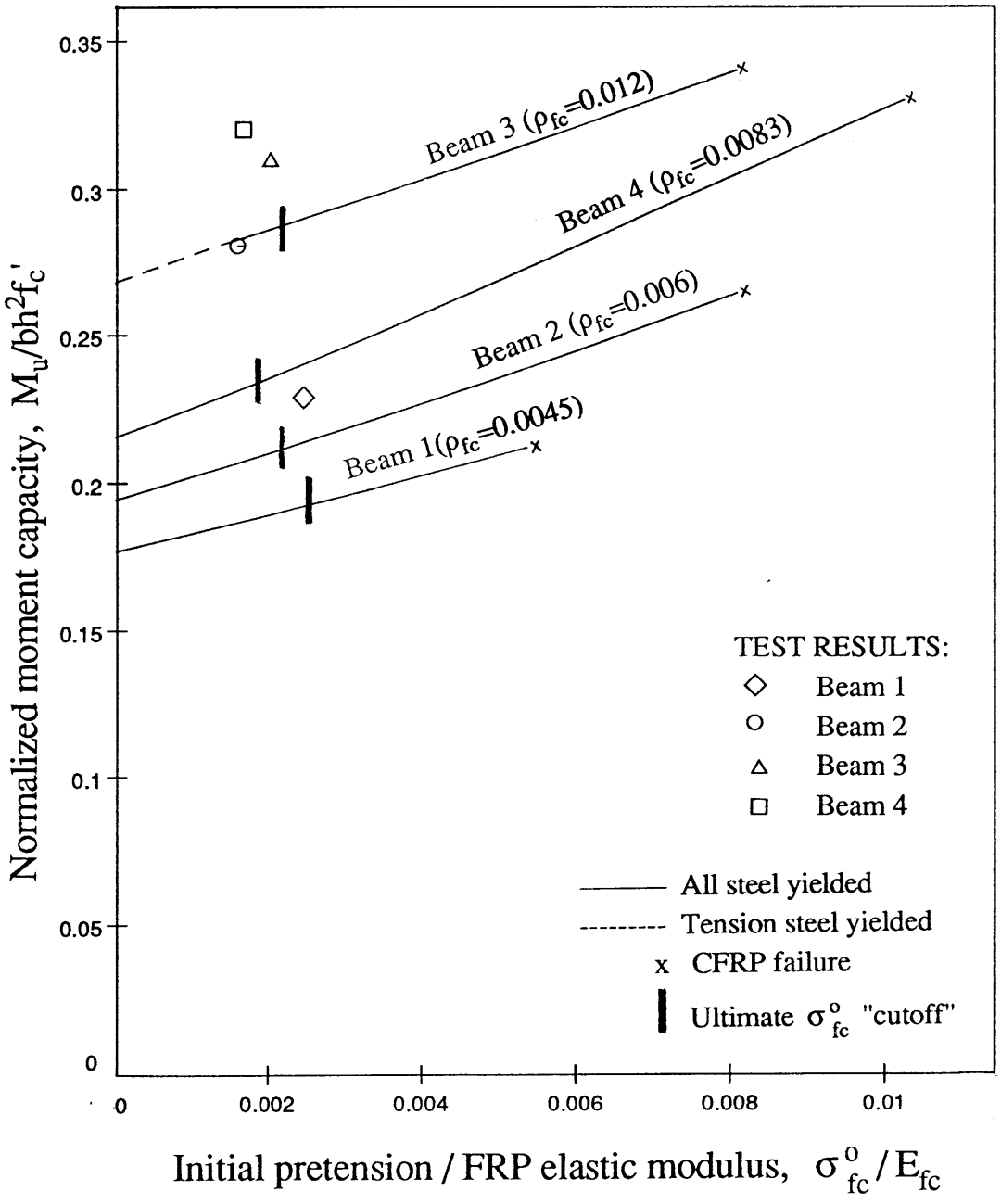

Figure 5.11 Ultimate moment capacity vs. prestress level: comparison between analysis and experiments.

CHAPTER 6

FLEXURAL BEHAVIOR OF WOOD-PRESTRESSED FRP SYSTEMS

6.1 INTRODUCTION

The flexural behavior of wood beams prestressed with externally bonded carbon fiber reinforced plastics sheets is investigated both analytically and experimentally in this chapter. The experimental program included three point bending tests on 11 beech wood beams. In the analysis, equations describing the bending behavior of the beams are derived; failure associated with wood compression yielding followed by CFRP sheet rupture (matching the experimental failures) is analyzed. A comparison between the experimental and analytical predictions is carried out and conclusions regarding the effectiveness of the proposed prestressing method are given.

6.2 TEST BEAM PREPARATION

The beams needed for the experimental program were cut out of the same quartersawed plank. The wood type was beech, belonging to the category of hardwoods. Its moisture content was initially and during the test procedure approximately 12%. Out of the 11 beams, 5 were reinforced with prestressed CFRP sheets, 3 were reinforced with unprestressed sheets, and 3 were used as control beams without any reinforcement. All the beams had a length of 800 mm but varied in cross section dimensions, composite sheet thickness and prestress level. The exact dimensions

and applied pretension are given in Table 6.1, where b and h are the width and height of the beam, respectively; t and b' are the thickness and width of the CFRP sheet used.

Table 6.1 Wood beam cross section dimensions and prestressing

BEAM	t [mm]	b [mm]	b' [mm]	h [mm]	σ_{fc}^{o} [MPa]
1	1.00	30.0	30.0	40.0	620
2	1.00	30.0	30.0	40.0	-
3	-	30.0	-	40..0	-
4	0.75	50.0	50.0	60.0	330
5	0.50	45.7	43	59.8	651
6	0.50	45.0	45.0	59.9	-
7	-	45.0	-	59.9	-
8	0.50	45.5	44.0	79.8	666
9	1.00	44.8	44.8	79.8	611
10	1.00	44..8	44.8	79.7	-
11	-	45.4	-	79.9	-

The prestress levels were chosen based on the results obtained in Chapter 4. The CFRP sheets used were from the same manufacturer as those used for the prestressing of the wood beams described in Chapter 4, for which the material properties are given in Table 4.3. The prestressing process of the beams was the same as described in Section 4.5. No damage or cracks were visible on the beams after the pretension force was released from the hydraulic jack and transmitted to them. All beams showed a center deflection due to the pretension in the bottom face, which, for beam No. 1 was as much as 5.45 mm or ≈L/145. The adhesive thickness was measured and found to be in the range of 0.6 to 0.7 mm. Subsequently, the beams were subject to three point bending tests, the results of which are presented in the following section.

6.3 THREE POINT BENDING TESTS

The 11 beams were divided in three groups based on the height of the wood cross section and tested accordingly. The testing apparatus used was that described in Section 5.5. Figure 6.1 illustrates the load deflection curves obtained for the 30×40 mm beams. Beam No.3, made of plain wood, was used as a control specimen, while beam No.1 was reinforced and prestressed with a 1.0 mm thick CFRP sheet; beam No.2 was only reinforced with the same sheet. The control beam failed by tensile fracture following compressive yielding. This was expected, since beech is a wood with a tensile strength higher than the compressive. Beam No.2 failed in a remarkably ductile manner after the compression zone yielded and a plastic hinge was formed. The CFRP sheet did not rupture in this case. Beam No.1 failed due to CFRP sheet tensile failure. The initial strain in the CFRP due to prestress was amplified with bending rotation, and when the ultimate strain ε^*_{fc} was reached failure occurred. Tensile rupture of the composite was immedietely followed by a splitting crack in the wood beam which propagated parallel to the CFRP sheet from midspan towards the support. The ultimate flexural strength of beam No.2 when compared to the control beam increased by 18%, while in the case of beam No.1 the increase was as much as 39%. Remarkable is also the increase in stiffness of 19% for beam No.2 and 42% for beam No.1, calculated at a deflection δ = 10mm. The displacement ductility of the prestressed beam was slightly higher than that of the control specimen, while the beam with the unprestressed composite sheet showed a ductility increase of approximately 200 %.

Figure 6.2 shows the results obtained from three point bending tests of the beams with h = 60 and 80 mm. Beams No.7 and 11 were control specimens and both failed after compression yielding occurred and the tensile strength of wood was exceeded. Beams No. 5, 8 and 9 (prestressed) failed with the same failure mode as beam No.1. The prestress level in these beams was approximately 40 to 45% of the ultimate tensile strength of the CFRP sheet (σ^*_{fc} = 1450 MPa) and therefore, the composite sheet ruptured before wood tensile failure occurred. For beams No.5 and 8 the displacement controlled test was continued until wood tensile failure occured, and hence, a load increase in the

load-deflection curve was obtained. All the other beams (No.4, 6, 7 and 10) failed again after the CFRP sheet strength was exhausted, but since at that point the stress in the wood bottom fiber was close to the ultimate one and also due to the sudden stress redistribution, the wood failed in tension simultaneously. The prestressed beam No.5 failed at a load slightly less than the identical, but unprestressed, beam No.6 whereas an increase in stiffness can be noticed. Similarly, beam No.9 failed at a lower load and had less stiffness than the identical unprestressed beam No.10. The explanation for the lower strength can be found in the fact that different stress distributions were generated at failure, but the lower stiffness of beam No.9 can be quantified only assuming some anomalies in the wood and/or CFRP sheet material properties.

It is seen that depending on the area fraction of the CFRP sheet, the prestressing can either increase or decrease the ultimate strength. Incidentally, when compared to the reinforced beam without prestressing, the stiffness increased with the prestress level, while the ductility decreased (since CFRP sheet failure governs).

6.4 ANALYSIS OF PRESTRESSED WOOD BEAMS WITH EXTERNALLY BONDED CFRP SHEETS IN BENDING

In all the tests described in the previous section failure of the reinforced wood beams occured at CFRP sheet tensile rupture following wood compressive yielding. This failure mode is analyzed next. The model adopted for the behavior of wood is that proposed by Bazan (1980) and modified by Buchanan (1990). According to this model, wood behaves in a linear elastic manner in tension until its tensile strength is reached; in compression, the stress-strain curve is bilinear. The Young's modulus is constant in tension and compression up to the yield stress f_c, after which a negative slope is assumed. In the analysis presented next the following assumptions are made:

- Plain sections remain plane.
- The stress across the composite sheet is uniform.
- Adhesive bending contribution is neglected.
- Wood is stronger in tension than compression.
- The compressive yield strength of wood f_c is known.
- CFRP is linear elastic to failure.

Wood yield

The behavior of wood is assumed to be linear elastic and yielding occurs when the top fiber stress reaches f_c. The stress and strain distributions in the cross section are shown in Fig. 6.3. Compatibility and constitutive relations give the equation for the stress in the CFRP sheet as follows:

$$\sigma_{fc} = f_c \frac{(h-c)}{c} \frac{E_{fc}}{E_w} + \sigma_{fc}^o \tag{6.1}$$

where E_w and E_{fc} are the Young's modulus for wood and CFRP, respectively, while σ_{fc}^o represents the applied prestress level. Equilibrium of forces gives the following relation:

$$F_{fc} + T_W = C_W \tag{6.2}$$

where F_{fc} denotes the force induced in the composite sheet while T_W and C_W represent the tensile and compressive forces carried by wood (see Fig. 6.3). From the last equation the height of the compressive zone can be found as:

$$c = \frac{\frac{h}{2} + t\frac{b'}{b}\frac{E_{fc}}{E_w}}{1 + \frac{t}{h}\frac{b'}{b}\frac{E_{fc}}{E_w} - \frac{\sigma_{fc}^o}{f_c}\frac{t}{h}\frac{b'}{b}} \tag{6.3}$$

where all the geometric parameters are defined in Fig. 6.3. Taking moments about the beam's bottom fiber the moment at which wood yield occurs is calculated as:

$$M_y = \frac{f_c b}{2}\left[c\left(h-\frac{c}{3}\right)-\frac{(h-c)^3}{3c}\right] \tag{6.4}$$

where c is given by eqn. (6.3).

CFRP sheet tension failure

The post-yield behavior of wood is assumed here perfectly plastic. The stress and strain distributions at failure of the composite sheet are shown in Fig. 6.4. From geometric and constitutive equations the following relations are obtained:

$$\frac{\left(\sigma_{fc}^{*}-\sigma_{fc}^{o}\right)}{f_c}\frac{E_w}{E_{fc}}=\frac{(h-c)}{(c-a)}=k \tag{6.5}$$

where σ_{fc}^{*} is the ultimate tensile strength of the CFRP sheet, a is the depth of the plastic zone and k is a parameter that will be used for further derivations. Equilibrium of cross section forces yields:

$$c^2\frac{(k+1)^2}{k^2}-2\,c\,h\left[1+\frac{k+1}{k^2}+\frac{\sigma_{fc}^{*}}{f_c}\frac{b'}{b}\frac{t}{h}\frac{1}{k}\right]+\frac{\sigma_{fc}^{*}}{f_c}\frac{b'}{b}\frac{t}{k}2h+\frac{h^2}{k^2}+h^2=0 \tag{6.6}$$

which can be solved for c. The ultimate moment capacity can be found taking moments about the CFRP sheet axis resulting in the following equation:

$$M_u = f_c b\left\{(h-c)^2\left[\frac{1}{3k^2}+\frac{1}{2k}-\frac{k}{6}\right]+\frac{c(k+1)-h}{k}\left[h-\frac{c(k+1)-h}{2k}\right]\right\} \tag{6.7}$$

where c is defined in eqn. (6.6).

6.5 COMPARISON OF ANALYTICAL AND EXPERIMENTAL RESULTS

In order to predict analytically the flexural behavior of the prestressed and reinforced wood-CFRP composite beams using the equations derived in Section 6.4, the material properties have to be defined first. This was achieved using the results obtained for the control specimens; the slope and first deviation from linearity of the load deflection curves gave f_c and E_w as follows:

$$f_c = \frac{3}{2}\frac{P_{el}\, l}{b\, h^2}$$
$$E_w = \frac{P_{el}\, l^3}{4\, \delta_{el}\, b\, h^3} \tag{6.8}$$

where P_{el} and δ_{el} are the load and displacement at first deviation from linearity, l is the span length and b and h are the cross section dimensions. The modulus of rupture of wood, f_t, was calculated assuming linear elastic-perfectly plastic behavior in compression and linear elastic behavior in tension. The load at failure P^* was extracted from the load-deflection curves and f_t was calculated as follows:

$$f_t = f_c \frac{\frac{P^* l}{4} + f_c \frac{bh^2}{6}}{f_c \frac{bh^2}{2} - \frac{P^* l}{4}} \tag{6.9}$$

The extracted values and the calculated material properties are summarized in Table 6.2.

Table 6.2 Calculated wood material properties

BEAM	P_{el} [KN]	δ_{el} [mm]	P^* [KN]	f_c [MPa]	E_w [GPa]	f_t [MPa]
3	3.30	9.20	6.25	72.2	16.0	191.4
7	11.5	7.83	21.25	74.1	12.9	194.9
11	18.7	6.00	32.70	68.2	11.6	143.5
			Average:	71.5	13.5	176.6

The geometric characteristics of the control beams are given in Table 6.1 and the span was l = 700 mm. For further analysis the average values from above were adopted for all beams. Using eqns (6.4) and (6.7), the moment at wood yield and failure was calculated. The material properties and prestress levels used for the calculation were given in Table 6.1. An adhesive thickness of 0.6 mm was adopted in the analysis. In order to compare the results with the experimentaly obtained moments, the proper load values were extracted from the curves in Figs 6.1 and 6.2 and substituted into $M_i = P_i l/4$. The results obtained from both approaches are shown in Table 6.3.

Table 6.3 Comparison of analytical and experimental bending moments (KNm)

	Wood yield			*CFRP sheet failure*		
BEAM	exper.	calc.	deviation	exper.	calc.	deviation
1	0.93	0.94	1.1%	1.51	1.53	1.3%
2	0.72	0.76	5.6%	1.29	-	-
4	2.71	2.75	1.5%	5.29	4.80	-9.3%
5	2.62	2.44	-6.9%	3.89	3.49	-10.3%
6	1.98	2.17	9.6%	3.94	4.23	7.4%
8	4.37	4.15	-5.0%	6.39	5.11	-20.0%
9	4.43	4.65	5.0%	6.74	7.08	5.0%
10	4.01	4.01	0%	7.89	8.01	1.5%
		Average:	1.363%		Average:	-3.171%

The deviations were calculated from the ratio of analytical to experimental results. Beam No.2 was not included in the CFRP sheet tension failure analysis since the failure mode was not of this type, as explained in Section 6.3. The largest deviation is obtained for beam No.8 where the analytical moment capacity underestimates the experimental one by 20%. Considering the small number of beams tested and the large variability in wood properties, remarkably good results were obtained. It is seen that the correlation is satisfactory and the average deviations are quite low. Therefore, the analysis presented here and the assumptions made can be considered as acceptable.

6.6 SUMMARY

Reinforcing of wood members with prestressed externally bonded CFRP sheets on the tensile face is seen to be an efficient and simple method for the production of new members. The improvement in flexural behavior of these members is closely related to the material properties of the wood itself. If wood types with brittle failure modes (tensile strength less than compressive) are used, the ultimate moment capacity will be improved with increasing prestress level, since failure will occur due to wood tensile failure. On the other hand, if ductile wood types are employed (as in the experiments performed here) the flexural moment capacity will decrease with pretension increase, since the ultimate CFRP sheet tension strain is reached sooner and as a result composite sheet failure governs. It should be noted that this statement does not hold if other failure modes, as formation of plastic hinges, were encountered and the CFRP rupture is never reached, which also depends on both wood properties and area fraction of the composite sheets used. It was found that prestressing of the externally bonded sheets increases the stiffness, regardless of wood type, while the ductility is decreased when ductile wood types are implemented and tensile failure of the composite sheet governs. Controversely, the ductility is improved when brittle wood types are sufficiently reinforced, because larger compression zones become plastic. Shear strength of wood allows for significant pretension levels (so that the system does not fail when the ends are released) and

therefore high efficiency of the prestressing method is obtained. The analytical solutions presented for wood first yielding and failure by CFRP sheet rupture were found to correlate well to experimental results and hence, represent the flexural behavior properly. Additional investigations should be carried out to analyze the flexural behavior of other failure modes and different wood types.

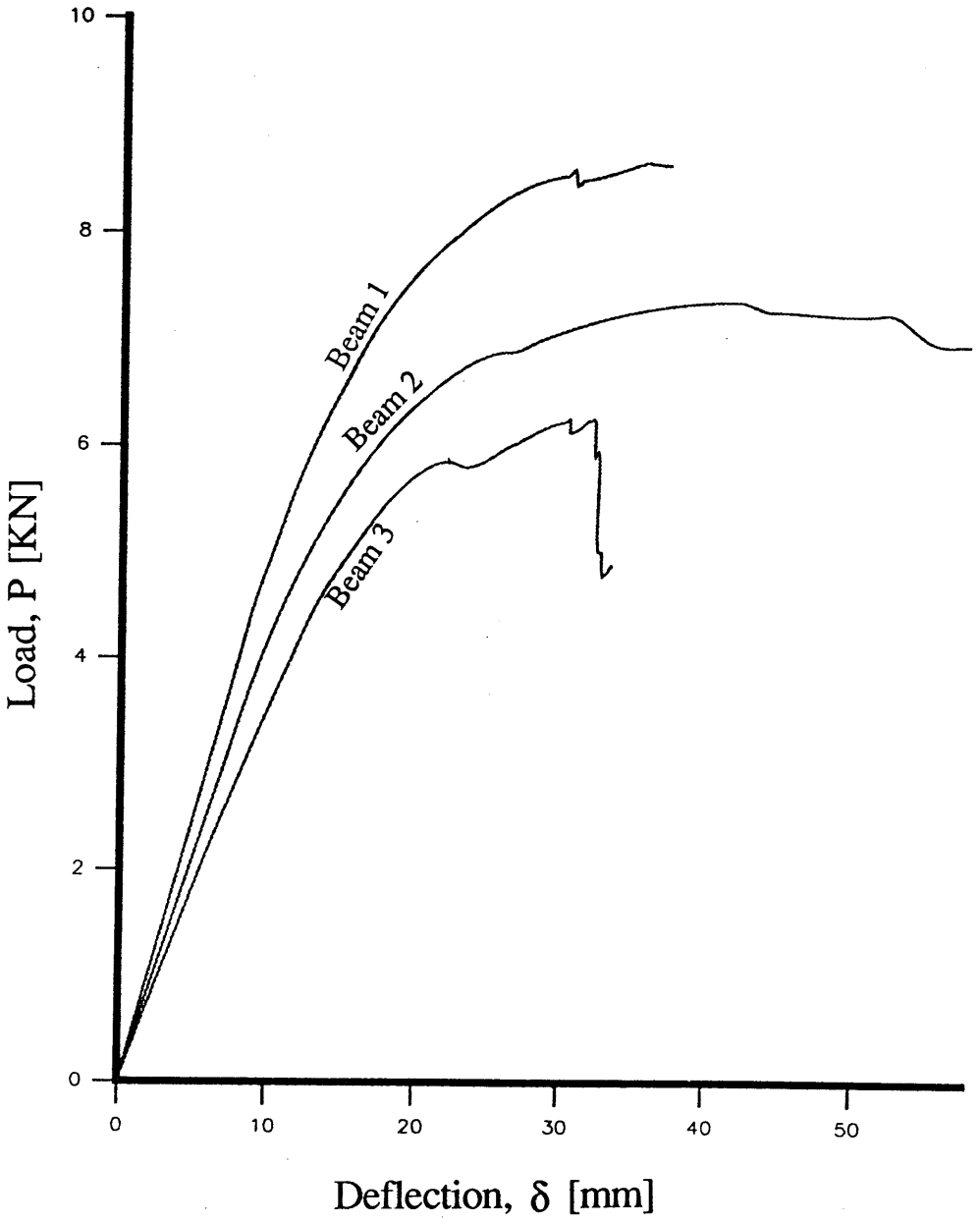

Figure 6.1 Load-deflection curves from three point bending tests of 30×40×700 mm³ beams.

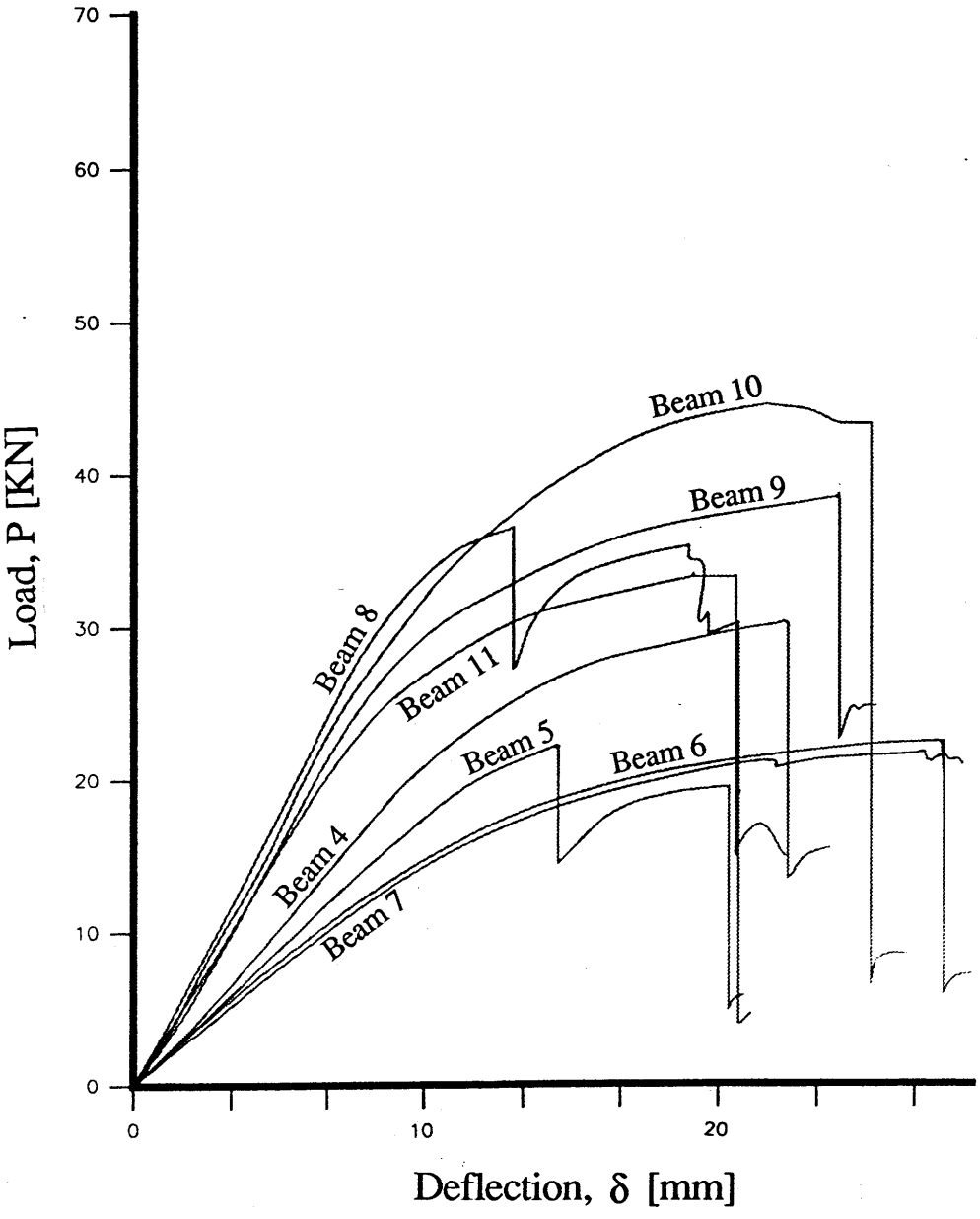

Figure 6.2 Load-deflection curves from three point bending tests of beams with h = 60 and 80 mm.

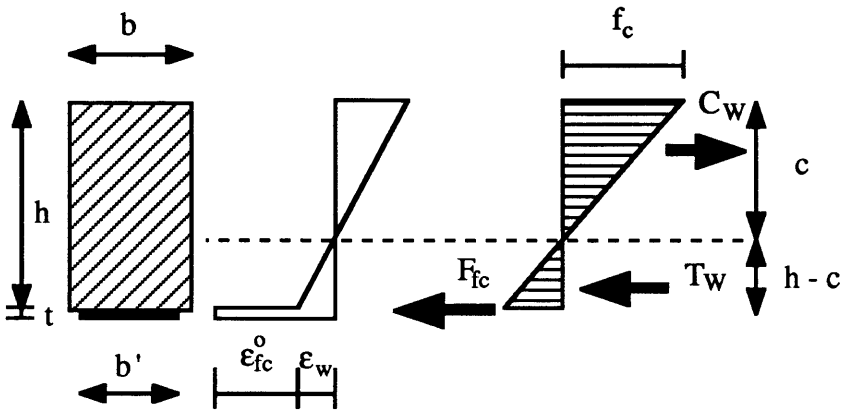

$$F_{fc} = \left(\sigma^o_{fc} + f_c \frac{(h-c)}{c} \frac{E_{fc}}{E_w} \right) b't$$

$$T_W = f_c b \frac{(h-c)^2}{2c}$$

$$C_W = \frac{1}{2} f_c bc$$

Figure 6.3 Strain and stress distributions at wood first yield.

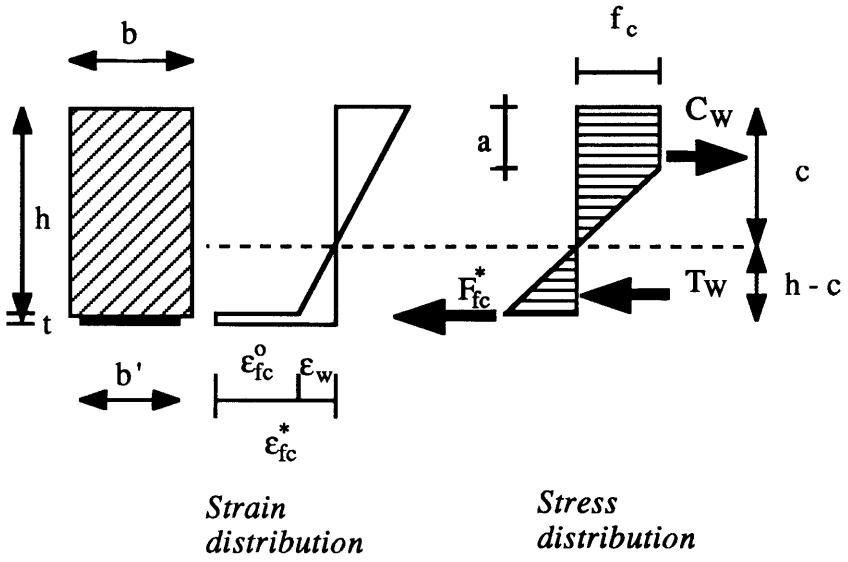

$$a = c - f_c \frac{(h-c)}{\left(\sigma^*_{fc} - \sigma^o_{fc}\right)} \frac{E_{fc}}{E_w}$$

$$F^*_{fc} = \sigma^*_{fc}\, b'\, t$$

$$T_W = f_c\, b \frac{(h-c)^2}{2(c-a)}$$

$$C_W = \frac{1}{2} f_c\, b\, (c+a)$$

Figure 6.4 Strain and stress distributions at CFRP tensile rupture.

CHAPTER 7

INNOVATIVE CONCRETE CONSTRUCTIONS WITH PRESTRESSED FRP AND SHORT FIBERS

7.1. INTRODUCTION

In this chapter a new concept of hybrid FRP-concrete structural elements is presented. The innovative idea proposes replacing the traditional steel reinforcement of concrete structures with high mechanical performance and durability materials. First, a brief review on the properties of fiber reinforced concrete is given and the equations for the ultimate strength in bending and shear are derived. Then, the behavior of fiber reinforced concrete elements with externally bonded prestressed CFRP sheets is studied. Finally, a feasibility study is carried out in order to obtain insight in the improvement in structural performance of the new concept when compared to traditional designs of reinforced concrete structures.

7.2 NEW METHOD OF REINFORCING CONCRETE STRUCTURES

The previous chapters have shown that pretensioning of reinforced concrete with externally bonded FRP sheets could be more efficient if the concrete were able to withstand higher shear stresses. This would automatically mean that the maximum pretension applied to the FPR sheet before gluing it on the concrete beam could be

increased resulting in a higher flexural capacity system. Investigations by a large number of researchers have shown that fiber reinforced concrete has a higher ultimate shear strength compared to plain concrete. Following these concepts, a new method of reinforcing concrete structures was developed; it is outlined as follows:

- The structural element is made of fiber reinforced concrete; short, randomly oriented fibers consist the only "internal" reinforcement;
- A prestressed CFRP sheet is externally bonded on the tension zone of the element;
- The existence of fibers in the concrete element increases the ultimate prestress that can be induced through the CFRP sheet because the shear strength τ_c^* of the fiber reinforced concrete increases (see eqn. (3.31));
- The CFRP sheet carries the tension resulting from the bending loads and plays the role of the main flexural reinforcement; a secondary increase of the member's flexural capacity results from the short fibers;
- The fibers in the element along with the beneficial effect of prestressing provide the primary mechanism of shear resistance.

The method suggests the application of structural members without any conventional steel reinforcement. This implies that members with excellent corrosion resistance and simple fabrication procedures could be produced. Because steel fibers result in the highest member flexural and shear capacity increase among other fibers used in fiber reinforced concrete, the following sections focus on the behavior of steel fiber reinforced concrete elements.

The corrosion of steel fibers is not a problem when considering durability of concrete. They will corrode in the presence of chlorides, but their small size precludes their being a cause of spalling. Schroff (1966) showed that insignificant corrosion by salt water on portland cement mortar reinforced with 2 percent by volume of steel fibers and no change in the flexural strength was observed for up to 90 days of rotation in and out of a saturated salt water solution.

If other types of fibers (carbon, Kevlar, polyethylene, polypropylene, nylon) were to be used, the same principles and analysis described later in Section 7.4 would

and only the corresponding equations for the ultimate tensile and shear strength would have to be modified.

7.3 BACKGROUND ON FIBER REINFORCED CONCRETE

7.3.1 General

Fiber reinforced concrete is concrete made of hydraulic cements containing fine or fine and coarse aggregate and discontinuous discrete fibers. Fibers have been produced from steel, plastic, glass, carbon, kevlar and natural materials in various shapes and sizes.

Historically fibers have been used to reinforce brittle materials since ancient times; straws were used to reinforce sunbaked bricks, horse hair was used to reinforce plaster and more recently, asbestos fibers are being used to reinforce portland cement. Patents have been granted since the turn of the century for various methods of incorporating wire segments or metal chips into concrete. The low tensile strength and brittle character of concrete have been bypassed by the use of reinforced rods in the tensile zone of the concrete since the middle of the nineteenth century. Applications of fiber reinforced concrete have been made since the mid 1960s for road and floor slabs, refractory materials and concrete products. More recently, some applications where steel fibers have been used without bars to carry flexural loads can be found. An example are the short-span elevated slabs supported on four sides of the Heathrow Airport parking garage.

The mechanical properties of fiber reinforced concrete are influenced by: the type of fiber; the fiber length-to-diameter ratio (aspect ratio); the volume fraction of fibers; the strength of the matrix; the size, shape and method of preparation of the specimen; and the aggregate size.

Steel fibers that can be mixed and placed with conventional equipment and procedures are usually in the range of 0.5 to 4.0 percent by volume. It has been found

that they increase the first cracking flexural strength of plain concrete up to 2.5 times (Williamson, 1965; Majumdar, 1970; Snyder and Lankard, 1972; Blood, 1978). The shear strength has been increased for more than 100% using steel fibers (e.g. Craig, 1983).

Asbestos fibers of 2 to 16 percent by volume were found to increase the flexural strength of the reinforced paste up to 1.6 times. Further application of these fibers has diminished with the discovery of their health hazardous properties. Extensive research has been done on the use of glass fibers in portland cement products (Grimer and Ali, 1969; Majumdar, 1970). The main problem in these applications is that of chemical attack of the glass by the high alkalinity found in hydrated portland cements. Plastic fibers, such as nylon, polypropylene and polyethylene have generally been found to contribute little, if any, to the static strength of concrete (Goldfine, 1963; Williamson, 1965). The resistance to chemical attack in concrete could not be reason enough to neglect the low increase of the shear capacity when compared to steel fibers. Fibers influence the mechanical properties of concrete and mortar in all failure modes , especially those that induce fatigue and tensile stress, e.g., direct tension, bending, impact and shear (Golopalaratnam and Shah, 1987). Fiber efficiency is controlled by the resistance of the fibers to pullout, which in turn depends on the bond strength at the fiber-matrix interface. For undeformed fibers the pullout resistance increases with the length of the fibers. Another factor is the surface area of the fibers; the fibers should have an aspect ratio such that failure of the composite occurs when they fail in tension. This indicates that high aspect ratios would be appropriate. Unfortunately, from workability constraints this is not feasible and aspect ratios larger than 100 are not practical. Therefore , failure of the composite is primarily due to fiber pullout. This is where deformed fibers such as hooked or enlarged-end steel fibers gain in significance and show superior performance compared to other fiber types.

7.3.2 Flexural Strength of Fiber Reinforced Concrete

Extensive investigations have been carried out by many researchers in order to describe the behavior of steel fiber reinforced concrete in flexure. A general literature review in the field of FRC shows that the behavior in flexure has been quantified in a very efficient manner and that very good agreement with experimental results has been obtained. Two flexural strength values are commonly reported. One, termed the first-crack flexural strength, corresponds to the load at which the load-deformation curve departs from linearity. The other corresponds to the maximum load achieved, commonly called the ultimate flexural strength or modulus of rupture. Ultimate flexural strength increases in relation to the product of fiber volume concentration V_f and aspect ratio l/d. Prismatic fibers, or hooked or enlarged-end fibers (better anchorage), have produced flexural strength increases over unreinforced matrices of as much as 100 percent (e.g. Johnston, 1980). For fiber reinforced concrete, strengths decrease with increases in the maximum size and proportion of coarse aggregate.

Several researchers have proposed different design methods and a variety of models for the flexural behavior has been established. Models have been proposed for singly and doubly reinforced FRC beams as well as for prestressed composite beams. They all refer to the fact that the presence of fibers in a reinforced concrete member will produce tensile stresses across a cracked section, and therefore, the fibers can not be neglected (as in analysis of conventionally reinforced concrete) when deriving equations for FRC. The distribution of these stresses across the section depends upon the type of fiber, its volume fraction and magnitude of strain.

The method developed by Henager and Doherty (1976) is similar to the ACI (1989) ultimate strength design method for flexure. The tensile contribution of the steel fibers is represented by a tensile stress block equal to the force required to develop the dynamic bond stress of the fibers that are effective in that portion of the beam cross section. The tension block depth is defined by the tensile strain $\varepsilon_s = \sigma_f / E_s$ where σ_f = stress in the fiber at the assumed bond stress and E_s = modulus of elasticity of the steel fibers. The tensile stress in the fiber reinforced concrete, σ_T, that can contribute to the

ultimate flexural strength is defined in the following form:

$$\sigma_T = 0.0072 \frac{l}{d_f} V_f F_{be} \tag{7.1}$$

where l / d_f is the aspect ratio, F_{be} is the bond factor and V_f is the volume fraction of the fibers. The stress-strain distribution along with the equilibrating forces at failure of a cross section are shown in Fig. 7.1.

Jindal (1984) has proposed a simplified model for the failure of reinforced fiber concrete beams in flexure, where the tensile stress block is rectangular and its depth is 0.85 times the depth of the tensile zone. This tensile stress level in steel fiber reinforced concrete is taken as 0.85 of the ultimate fiber stress in tension, which is a function of the modulus of rupture of plain concrete, the fiber content and the fiber aspect ratio.

A model developed by Craig (1987) assumes that the tensile stress that develops across a crack in the tension zone is represented by a rectangular tensile stress block across the entire tensile zone. The stress equals the number of fibers in a unit area that are effective times the average pullout force developed in a single fiber. This is similar to Williamson's (1978) method.

7.3.3 Shear Strength of Fiber Reinforced Concrete

There are considerable laboratory data indicating that fibers substantially increase the shear (diagonal tension) capacity of concrete and mortar beams. Steel fibers show several potential advantages when used to supplement or replace vertical stirrups or bent-up steel bars. These advantages are:

a) the fibers are randomly distributed through the volume of the concrete at much closer spacing than can be obtained with reinforcing bars, thus controlling cracking in a more efficient manner;

b) the first-crack tensile strength and the ultimate tensile strength are increased by

the fibers; and

c) the shear-friction strength is increased.

Although the increase in shear capacity of FRC has been quantified in several investigations, it has not yet been used in practical applications. Batson et al. (1972) conducted a series of test results to determine the effectiveness of straight steel fibers as web reinforcement in beams with conventional flexural reinforcement. In tests of 96 beams, he varied and investigated the influence of fiber size, type and volume concentration. In addition, the influence of the shear-span-to-depth ratio a/d, where a = distance between concentrated load and face of support and d = the depth to the centroid of reinforcing bars, was examined. It was found that higher fiber contents increase the shear capacity and the failure of the specimen beam can be moved from a shear to a bending failure with sufficient amounts of steel fibers used. It was also noticed that on increase in the a/d ratio decreases the ultimate shear strength.

Williamson (1978) found that with 1.1% percent by volume of steel fibers with deformed ends, the shear capacity increased 45 to 67 percent over a beam without stirrups. He concluded that steel fibers can increase the shear strength of concrete beams enough to prevent catastrophic diagonal tension failure and force the beam to fail in bending. He also proposed that fibers can present an economical alternative to the use of stirrups in reinforced concrete design. Craig (1983) has shown that crimped-end fibers can increase the shear capacity of reinforced concrete by more than 100 percent. In his tests the increase in shear capacity for the 1.0 percent by volume fiber content and with a/d =3.0 was 108 percent.

Steel fiber reinforced concrete shows improved behavior in the post-cracking resistance and tensile ductility. In addition, the presence of fibers also enhances the dowel resistance to shear. Fiber reinforced concrete, therefore, assists in shear transfer. In general, for concrete elements, there are two ways by which the shear transfer strength can develop, depending on the nature of the shear plane before the shear is applied. If there is no crack due to flexure along the shear plane, truss action plays an important role in strength development after the formation of short inclined cracks. In the presence of a crack along the shear plane prior to loading, the shear friction mechanism is primarily

responsible for stress transfer across the crack. When FRP sheets are used as externally bonded prestressed reinforcement of FRC elements, it is seen (as described in Chapter 5) that there are no significant flexural cracks in the concrete up to failure of the system. This is because the externally bonded sheet limits the strain at the extreme tension fiber of the concrete. Therefore, it can be anticipated that only the truss action can be the dominant form by which shear transfer can develop in this system, while shear friction can be neglected.

The shear strength of fiber reinforced concrete has been quantified by Sharma (1986). He tested a series of FRC beams with and without stirrups. The fibers had deformed ends. Based on these tests and those by Batson et al. (1972) and Williamson and Knab (1975), Sharma proposed the following equation for predicting the average shear strength:

$$v_{CF} = k\, f_t' \left(\frac{d}{a}\right)^{0.25} \tag{7.2}$$

where d/a is the effective depth-to-shear-span ratio; f_t' is the tensile strength of concrete obtained from indirect tension on 150x300 mm cylinders and k is a constant equal to 2/3, as suggested by Wright(1955). In literature where only the cylinder compressive strength, f_c', for beams is reported, an empirical relation recommended by the European Concrete Committee is used for calculating the tensile strength f_t':

$$f_t' = 0.75\sqrt{f_c'} \tag{7.3}$$

where f_t' and f_c' are in MPa.

Another method to calculate the ultimate shear strength for fiber reinforced concrete was given by Jindal (1984). He suggests the following relation:

$$\tau_{max} = 0.41\, \sigma_{ut} \tag{7.4}$$

where σ_{ut} is given by the following equation:

$$\sigma_{ut} = 0.97\sigma_m(1 - V_f) + 3.41V_f\frac{l}{d_f} \tag{7.5}$$

and σ_m is the ultimate flexural tensile strength of plain concrete.

7.4 STRENGTH OF FRP-PRESTRESSED FRC STRUCTURES

7.4.1 Flexural Strength

For the purpose of this section the model proposed by Henager and Doherty (1976) has been adopted and extended in order to predict the flexural behavior of fiber reinforced beams with externally bonded prestressed FRP sheets. The modification has been made by the author in order to account for the contribution to the flexural capacity by the externally bonded FRP sheet and the introduced prestress force. The following assumptions were made for the analysis method:

1. The maximum usable strain at the extreme concrete compression fiber is 0.003. There are some data indicating that 0.003 might be conservative. Work by Williamson (1973) and Pearlman (1979) indicates that 0.0033 may be more realistic for steel fiber concrete. Swamy and Al-Ta'an (1981) recommend 0.0035.

2. The compressive stress is represented by a rectangular stress block as used in the ultimate strength method and defined in ACI (1989).

3. The tensile contribution of the steel fibers is taken as proposed by Henager and Doherty (1976), which is described in Section 7.3.2.

4. The dynamic bond stress is taken equal to 2.3 MPa, which is based on reported values in the range of 1.5 to 4.0 MPa for smooth, straight, round, high-strength fibers with embedment lengths of 12 to 32 mm (Aleszka and Beaumont, 1973; Williamson, 1974; Naaman and Shah, 1976).

5. A bond efficiency factor F_{be} of 1.0 is applied, even though this value is

appropriate for smooth, straight, round or rectangular fibers while for other types (deformed) higher values could be assigned.

6. The fiber aspect ratio of 75 is adopted, since Jindal (1984) has recommended this value as the optimal in to order achieve maximum shear strength.

7. The influence of the fiber volume fraction V_f on the flexural strength has been investigated by Balaguru and Ezeldin (1987). They noticed that prestressed beams with narrow webs can be cast without difficulty using hooked fibers up to a fiber content of 1.5%, hence a conservative value of 1.0 % is adopted.

The mathematical formulation for the ultimate flexural strength is based on the following assumptions:

(i) The system fails due to concrete crushing;

(ii) The design will check for FRP failure;

(iii) Four point bending is assumed throughout the calculations as the governing loading pattern;

(iv) The stress and strain distribution at failure is assumed as shown in Fig. 7.2.

Constitutive relations

The minimum tensile strain required to invoke tensile stresses in the fiber reinforced concrete is:

$$\varepsilon_s(\text{fibers}) = \frac{\sigma_f}{E_S} \tag{7.6}$$

where σ_f is the tensile stress developed in the fibers during pullout and can be derived as:

$$\sigma_f = \frac{2\tau_d F_{be} l}{d_f} \tag{7.7}$$

where τ_d is the dynamic bond stress = 2.3 MPa (as described above), F_{be} is the bond efficiency factor = 1.0, and l / d_f is the aspect ratio = 75.

The tensile stress in the fiber reinforced concrete, σ_T, that can contribute to the ultimate flexural strength can be calculated in the following form:

$$\sigma_T = 0.0072 \frac{l}{d_f} V_f F_{be} \tag{7.8}$$

where V_f represents the volume fraction of the fibers in the composite = 1.0 %.

Compatibility equations

From Fig. 7.2 the following geometric relations can be derived:

$$c = \frac{\varepsilon_{cu} h}{\varepsilon_T + \varepsilon_{cu}} \tag{7.9}$$

and

$$e = \frac{(\varepsilon_s + \varepsilon_{cu}) h}{\varepsilon_T + \varepsilon_{cu}} \tag{7.10}$$

were c is the height of the compressive zone and e is the depth at which the fiber pullout starts.

Equilibrium Equations

Referring to the stress-strain distributions given in Fig. 7.2 and taking equilibrium of horizontal forces we find:

$$C - T = F_{fc} \tag{7.11}$$

and using the compatibility eqns (7.9) and (7.10) we obtain the following equation :

$$0.85^2 \frac{\varepsilon_{cu}}{\varepsilon_T + \varepsilon_{cu}} - \frac{\sigma_T}{f_c'} \frac{\varepsilon_T - \varepsilon_s}{\varepsilon_T + \varepsilon_{cu}} - \rho_{fc} \varepsilon_T \frac{E_{fc}}{f_c'} = \frac{\sigma_{fc}^o}{f_c'} \rho_{fc} \tag{7.12}$$

where ρ_{fc} represents the area fraction of the FRP sheet and σ_{fc}^{o} is the initial pretension. If we take moment equilibrium about the bottom fiber in Fig. 7.2, we obtain the following equation:

$$\frac{M_u}{bh^2 f_c'} = 0.85^2 \frac{(\varepsilon_T + 0.575\varepsilon_{cu})}{(\varepsilon_T + \varepsilon_{cu})^2}\varepsilon_{cu} - \frac{\sigma_T}{f_c'}\frac{1}{2}\frac{(\varepsilon_T - \varepsilon_s)^2}{(\varepsilon_T + \varepsilon_{cu})^2} \tag{7.13}$$

where M_u represents the ultimate moment capacity for the given cross section and material properties and the values ε_s and σ_T are defined in the constitutive equations. The solution of the last two equations can be obtained in the easiest way through an iteration process, where the value of ε_T is incremented as a variable and the corresponding value of M_u obtained. FRP failure can be checked by calculating the first two terms in eqn. (7.12) and comparing their sum to the given ultimate strain for the particular FRP material used. In this application the value of 1.22 % is adopted as the limiting strain, which is a common value for carbon FRP sheets.

Once the procedure was established it was implemented in a computer program; and the results are shown in Fig. 7.3. The values for the material properties and the geometric characteristics used in this part are given in Table 7.1:

Table 7.1 Material properties used to obtain the numerical results

Parameter	ε_{cu}	$\frac{1}{d_f}$	τ_d	V_f	F_{be}	E_s	f_c'	E_{fc}
Units	-	-	GPa	%	-	GPa	GPa	GPa
Value	0.003	75	2.3	1.0	1.0	210	28.8	115

Figure 7.3 shows the ultimate flexural moment capacity as a function of the applied pretension. The relationship is given for different values of the area fraction, ρ_{fc}, of the FRP sheet. Similar curves were established for various values of the dynamic bond

stress and fiber volume content and it was found that they do not change the curves significantly. This can be explained by the fact that the tension in the FRP dominates the contribution of the tensile forces to the ultimate moment of the cross section. The curves are terminated at a certain point which is a result of the constraint that the FRP strain is limited.

The applied pretension stress, σ_{fc}^{o}, has to be limited, too, by the calculated maximum pretension that can be applied so that the FRP does not peel-off due to shear failure in the concrete when the ends of the prestressing apparatus are released. This limits the validity of the curves shown in Fig. 7.3 and produces a cutoff to them.

In order to determine the maximum pretension stress that can be applied, the procedure described in Chapter 3 was employed. The contribution of the fibers in the concrete matrix was taken into account by using higher values for the ultimate shear stress parameter, τ_c^*. The value of 8.0 MPa used in Chapter 3 was increased to a value of 15 MPa. Note that this is just an estimated value based on the fact that the shear strength of FRC is of the order of two times that of plain concrete. In addition, the ultimate shear crack slip δ^* has been increased from the value of about 30 μm expected for plain concrete to 100 μm since the fibers contribute to the shear softening in an effective manner and the aggregate smoothening is not as dominant as in plain concrete. Using the same computer program as in Chapter 3 and the new values for τ_c^* and δ^*, the ultimate pretension stress was found for different beam lengths. Figure 7.4 shows the normalized ultimate pretension as a function of the FRP sheet area fraction ρ_{fc}. The adhesive thickness was kept constant at 1.5 mm and the height of the beam was taken as 0.1 of its length. The curves in Fig. 7.4 correspond to beam lengths of 1.2, 3 and 5 m. The adhesive shear modulus is taken, as in Chapter 4, to be equal to G_a = 2.7 GPa. Figure 7.4 can be used to obtain the maximum prestress level, σ_{fc}^{o}, truncating the curves of Fig. 7.3. The discussion on these results is presented in the last section of this Chapter, hence no further comments will be given here.

7.4.2 Shear Strength

In this section, a simple method to analyze the shear capacity of externally FRP-prestressed fiber reinforced concrete beams is presented. The methodology used is an extension of the ACI-code (ACI 318-89, eqn. 11.4) method of analysis; both the influence of the pretension induced through the FRP sheet and the contribution of the steel fibers is taken into account. According to the ACI procedure, the shear strength of the beam is decribed as:

$$V_u = V_C + V_S + V_F \tag{7.14}$$

where V_C, V_S and V_F are the parts of shear corresponding to the contribution of concrete, stirrups and prestress effect, respectively. It is seen that since our model has no shear reinforcement (stirrups) $V_S = 0$. The contribution of the two other terms is described next.

Effect of Fiber Reinforced Concrete to Shear Capacity

The contribution of concrete is described by the shear transfer strength of fiber reinforced concrete. For the analytical method developed in this work the model developed by Sharma (1986) was adopted (see eqn. (7.2)). The shear capacity of FRC is obtained multiplying the shear strength of eqns (7.2)-(7.3) by the shear area bh:

$$V_C = 0.5\, b\, h\, \sqrt{f_c'}\left(\frac{h}{a}\right)^{0.25} \tag{7.15}$$

Note that the effective section depth for the calculation of the shear area is equal to the total section height, h.

Effect of Prestress Level to Shear Capacity

To analyze the effect of prestress on the shear strength (V_F), the same principle as used in the ACI formulation was implemented. This method assumes that the prestress force effect is associated with a shear capacity corresponding to the first cracking load. This gives the following relation:

$$V_F = \frac{V_u}{M_u} M_{CR} \tag{7.16}$$

where:

V_u = ultimate shear force corresponding to the load P_u;

M_u = ultimate moment capacity corresponding to the load P_u;

M_{CR} = cracking moment.

In the method proposed herein it is assumed for simplicity that the loading condition is a four point loading case, and therefore the ratio M_u/V_u = a (shear span). M_{CR} is calculated based on a tensile flexural strength of the fiber reinforced concrete (first-crack composite strength) which can be expressed as follows (ACI, 1986):

$$\sigma_T = 0.843\, f_r \left(1 - V_f\right) + 2.93\, V_f \frac{l}{d_f} \tag{7.17}$$

where f_r represents the stress in the matrix (modulus of rupture of plain concrete) and l/d_f is the aspect ratio of fibers. Wright(1955) found that the indirect tension test on 150x300 mm cylinders gave values of tensile strength of the order of 2/3 of the values of the modulus of rupture of 100 mm beams tested under third-point loading. Hence it is seen:

$$f_r = \frac{2}{3} f_t' \tag{7.18}$$

Inserting eqns (7.3) and (7.18) into eqn. (7.17) yields:

$$\sigma_T = 0.422\sqrt{f_c'}\ (1-V_f) + 2.93\ V_f \frac{1}{d_f} \tag{7.19}$$

Next we solve for the first cracking moment, M_{CR}. It is assumed that the bottom fiber stress in the fiber reinforced concrete is equal to σ_T given by eqn. (7.19) and that the fiber reinforced concrete behaves linearly. Figure 7.5 gives the assumed stress-strain distribution corresponding to first-cracking of the externally prestressed fiber reinforced concrete beam. From the material constitutive relations we have:

$$\varepsilon_T = \frac{\sigma_T}{E_c} \tag{7.20}$$

and

$$\sigma_{fc} = \left(\varepsilon_T + \varepsilon_{fc}^{o}\right) E_{fc} \tag{7.21}$$

where ε_{fc}^{o} is the initial pretension induced in the FRP sheet. Furthermore, the compatibility equations yield:

$$c = \frac{h\varepsilon_c}{\varepsilon_T + \varepsilon_c} \tag{7.22}$$

and

$$h - c = \frac{h\varepsilon_T}{\varepsilon_T + \varepsilon_c} \tag{7.23}$$

From force equilibrium we obtain C - T = F_{fc}, which using eqns (7.20)-(7.23) transforms into the following form:

$$\frac{1}{2}(f_c - \sigma_T) - \rho_{fc}\frac{\sigma_T}{E_c}E_{fc} = \rho_{fc}\,\sigma_{fc}^{o} \tag{7.24}$$

Taking equilibrium of moments about the bottom fiber we find:

$$M_{CR} = \frac{bh^2}{6}\frac{\left(3\sigma_T f_c^2 + 2f_c^3 - \sigma_T^3\right)}{\left(\sigma_T + f_c\right)^2} \tag{7.25}$$

where f_c is described by eqn. (7.24). Then, the contribution to the shear force due to the prestressing effect can be summarized as follows:

$$V_F = \frac{h}{a}\frac{bh}{6}\frac{3\sigma_T f_c^2 + 2f_c^3 - \sigma_T^3}{(\sigma_T + f_c)^2} \tag{7.26}$$

where f_c is given by eqn. (7.24) and σ_T is defined in eqn. (7.19).

Finally, the total shear force capacity can be calculated. Inserting the expressions for V_C and V_F from eqns (7.15) and (7.26) into eqn. (7.14) and normalizing the resulting expression with respect to the shear area bh, the relation for the ultimate shear capacity is obtained in the following form:

$$\frac{V_u}{bh} = 0.5\sqrt{f_c'}\left(\frac{h}{a}\right)^{0.25} + \frac{h}{a}\frac{\left(0.5\sigma_T f_c^2 + \frac{1}{3}f_c^3 - \frac{1}{6}\sigma_T^3\right)}{(\sigma_T + f_c)^2} \tag{7.27}$$

where f_c and σ_T are given by eqns (7.24) and (7.19).

In order to study the influence of the pretension level and the efficiency of the system fiber reinforced concrete - FRP sheet, the normalized shear capacity defined by eqn. (7.27) was plotted vs. the normalized pretension stress σ_{fc}^o / E_{fc}. The procedure was implemented in a computer program and the variable f_c was used as the incremental unknown. Each value of f_c gave both σ_{fc}^o from eqn. (7.24) and the shear strength from eqn. (7.27). The incrementation was initiated for the value of f_c that would require no prestress to satisfy equilibrium. Hence:

$$f_c^{initial} = \sigma_T\left(1 + 2\rho_{fc}\frac{E_{fc}}{E_c}\right) \tag{7.28}$$

The resulting curves are truncated because of the following two constraints:

a) The compression stress in the top concrete fiber was limited by the value of $0.5\, f_c'$, so that the linear behavior of concrete is still a relatively good

approximation ($f_c \leq 0.5f_c'$);

b) The strain in the FRP sheet was limited by the ultimate strain of the FRP material to 1.22% (see Section 7.4.1).

The results are shown in Fig. 7.6. The figure shows the relation between V_u and σ_{fc}^o for three different shear-span-to-depth ratios (0.4; 1.0; 3.3). Each of those a/h values defines a family of curves, depending on the area fraction of the FRP sheet used. Again, similarly to the ultimate flexural capacity, the curves are truncated by the ultimate prestress level resulting in concrete horizontal shear FRP peeling-off. Figure 7.7 shows the family of curves for the shear-span-to-depth ratio 3.3.

7.5 DISCUSSION

7.5.1 Example of Analysis and Design

To evaluate the effectiveness of the new proposed concept for reinforcing concrete structures, the structural behavior of a fiber reinforced concrete beam with an externally bonded FRP prestressed sheet and a traditionally reinforced concrete beam is examined and compared. The analysis presented earlier was aimed at evaluating the flexural and shear capacities of FRP-prestressed FRC members and only these will be studied in the following comparison. For the design of the conventionally reinforced beam the ACI 318/318R-89 (ACI, 1989) code has been used. The application of the new concept is mainly intended for prefabricated structural elements, which justifies the use of simply supported beams for the study. Only four point loading cases with varying shear span-to-depth ratios are considered but it is believed that the results for other loading configurations will follow the same general trends.

The same geometry and material properties for both beam designs have been used and are given in Table 7.2.

Table 7.2 Geometric and material properties of the beams for design comparison

Length l [m]	Height h [m]	Width b [m]	Concrete cover a_o [mm]	Concrete strength f_c' [MPa]	Steel yield stress f_y [MPa]
5.0	0.5	0.25	25	28.8	500

Traditional Design Method

For the design of the reinforced concrete beam in flexure, the amount of reinforcement is limited to 75 % of the balanced failure value. From Park and Paulay (1975) the maximum steel area fraction ρ_s^{max} is calculated according to the following equation:

$$\rho_s^{max} = \frac{0.638\, f_c' \,\beta_1}{f_y} \frac{600}{600 + f_y} \tag{7.29}$$

where β_1 (=0.85 for 28 MPa concrete) represents the compressive block height ratio. Substituting for the parameters from Table 7.2, this equation yields ρ_s^{max}= 0.017 (2018 mm^2, 4 # 8 rebars). The ultimate flexural capacity of a singly reinforced cross section can be found from the following equation:

$$M_u = \rho_s^{max}\, b\, d^2\, f_y \left(1 - 0.59 \frac{\rho_s^{max}\, f_y}{f_c'}\right) \tag{7.30}$$

where d is the effective cross section depth (= h - a_o= 0.475 m). For the values given above, eqn. (7.30) yields an ultimate flexural capacity of 396 KNm.

The shear capacity of a given reinforced concrete cross section can be expressed as the summation of the concrete and shear reinforcement contribution. Equation 11-6 of ACI 318/318R-89 (ACI 1989) for the ultimate shear stress provided by plain concrete for

unprestressed members reads:

$$f_c^{initial} = \sigma_T\left(1+2\rho_{fc}\frac{E_{fc}}{E_c}\right) \quad \leq \quad 0.29\sqrt{f_c'} \tag{7.31}$$

where ρ_s is the area fraction of the longitudinal steel reinforcement (ρ_s^{max} here) and a/d represents the shear span-to-depth-ratio. The stress units are in MPa. The contribution of shear reinforcement v_s is limited by ACI 11.5.5.8, expressed in MPa, with:

$$v_s \leq 0.6637\sqrt{f_c'} \tag{7.32}$$

and hence the shear capacity V_u is obtained by adding eqns (7.31) and (7.32) in the following form:

$$V_u = \left(0.8214\sqrt{f_c'} + 17.22\,\rho_s\frac{d}{a}\right) b\,d \tag{7.33}$$

Innovative Design Method

The method described in Section 7.4 was employed for the design of the given beam. From Fig. 7.3 the ultimate flexural capacity can be obtained for a given CFRP sheet area fraction and a given prestress level. For the comparison here the two rather extreme area fractions of 0.004 and 0.012 were chosen. The prestress level was defined at its ultimate value resulting in flexural capacities of 306 and 450 KNm for the two CFRP sheet area fractions, respectively.

Similarly, the ultimate shear strength V_u was obtained from Fig. 7.6 for the same two CFRP sheet area fractions as above and for three different shear span-to-depth ratios, namely 0.4, 1.0 and 3.3, respectively. The values were again chosen corresponding to the ultimate prestress level. It should be noted that for practical applications these values should be chosen with a certain safety factor to account for prestressing losses, unless

special anchorage devices are used minimizing the undesirable viscoelastic effect of the adhesive. The values of the normalized shear capacity, V_u/bh, for the different beam designs are summarized in Table 7.3.

Table 7.3 Ultimate shear stress V_u/bh [MPa]

		Shear span-to-depth ratio		
		0.4	**1.0**	**3.3**
ρ_{fc}	**0.004**	7.75	4.4	2.5
	0.012	9.65	5.15	2.75

7.5.2 Comparison of Results

The comparison between conventional design and the method proposed herein is evaluated in Fig. 7.8. Since the loading case considered here is that of four point bending, the ratio of the ultimate moment to shear capacity is constant and equal to the shear span, a. In Fig. 7.8 the ultimate load P_u ($= M_u/a = V_u$) is plotted as a function of the shear span-to-depth-ratio for the two design methods. The full lines represent the behavior when moment capacity controls while the dashed lines are valid when shear is critical. Results for three beam designs are given: one corresponds to the traditional design (case A) and the other two represent the new proposed designs for two area fractions of the CFRP sheet ρ_{fc}, 0.004 (case B) and 0.012 (case C), respectively.

It is seen that for low values of the shear span-to-depth ratio the ultimate shear capacity governs, while for higher values of the same ratio the flexural strength becomes dominant. The transition from shear to flexural strength occurs at a/h ratios of approximately 1.7, 1.3, and 2.1 for the design cases A, B and C, respectively. Regarding flexural capacity, it can be noted that the traditional design can be adequately substituted by the new design method using the appropriate area fractions of the CFRP

sheet, ρ_{fc}, while when the shear capacity is of concern, the innovative design can provide higher shear strength than the traditional one, even if low ρ_{fc} values are used. Only for high values of a/h the traditional method gives higher shear strengths, but in this region the flexural behavior governs and hence the shear capacities do not affect the member's structural behavior. It should be noted that the load case considered here assumes that the ultimate moment and the shear capacities are reached at the same cross section, which in practice is rarely the case, and therefore the analysis presented is rather conservative. If more uniformly distributed loads were to be considered, flexural behavior would govern in most practical cases, and as shown above the prestressed FRP design is quite efficient in this respect.

7.5.3 Effect of Prestressing

Figure 7.3 shows that the increase in the ultimate moment for the two limiting values of the CFRP sheet area fractions (ρ_{fc} = 0.004 (case I) and 0.012 (case II)) due to the prestressing is not more than 9 %. On the other hand, the CFRP sheet is used much more efficiently in case I, where the ultimate achievable prestress level σ_{fc}^{o} reaches almost 50 % of that causing the CFRP sheet to fail in tension (curve end), than in case II, where, while much more prestress potential is accumulated, the ultimate prestress level, σ_{fc}^{o}, is quite low.

The beneficial effect of the CFRP prestressing to a member's capacity can be studied in Figs 7.6 and 7.7. It is seen that the increase in shear strength is more significant for smaller shear span-to-depth ratios and higher CFRP sheet area fractions. The increase for a/h = 0.4 is 30% and 54% for case I and II, respectively, while for a/h = 3.3 the increase in shear strength is only 10% and 18%, correspondingly. The relatively low increase in shear capacity for the latter case is not of concern, since at high shear span-to-depth ratios flexural behavior governs. Again it can be noted that for the lower ρ_{fc} values the CFRP sheet has been used more efficiently comparing the applicable ultimate prestress σ_{fc}^{o} to the stress required to fail the CFRP sheet in tension

(approximately 50% efficiency), while for higher values of ρ_{fc} the efficiency is of the order of 30%.

The issues discussed above indicate that the maximum achievable prestress levels (governed by failure of the two concrete end zones in horizontal shear when the force is released) are not high enough to use the benefits of the prestressed CFRP sheets in the most efficient manner. Therefore, it is of interest to improve the method by providing for some anchorage devices which would carry the high shear stresses induced in the end zones and transmit them to the fiber reinforced beam through a different loading path. Application of end plates with a certain type of bolt connectors to the beam appears to be one possible solution.

7.6 CONCLUSIONS

The proposed innovative method of designing concrete structures represents a successful way to eliminate the traditional steel reinforcement without losing on structural performance. The ultimate flexural and shear capacities of the elements designed according to the proposed method are at least equal to and sometimes exceed the corresponding values for conventional reinforced concrete designs. The new concept of design consists of fiber reinforced concrete elements that are reinforced along their tensile faces with externally epoxy-bonded prestressed CFRP sheets. Corrosion resistance and simple fabrication are the most important properties of this system. While efficiency of prestressing is higher when thinner CFRP sheets are used, thicker sheets provide more strength. The efficiency could be much higher if the prestress level were not limited due to shear stress concentrations at the far ends of the externally bonded CFRP sheet. This problem should be addressed in the future through the design of adequate anchorage devices.

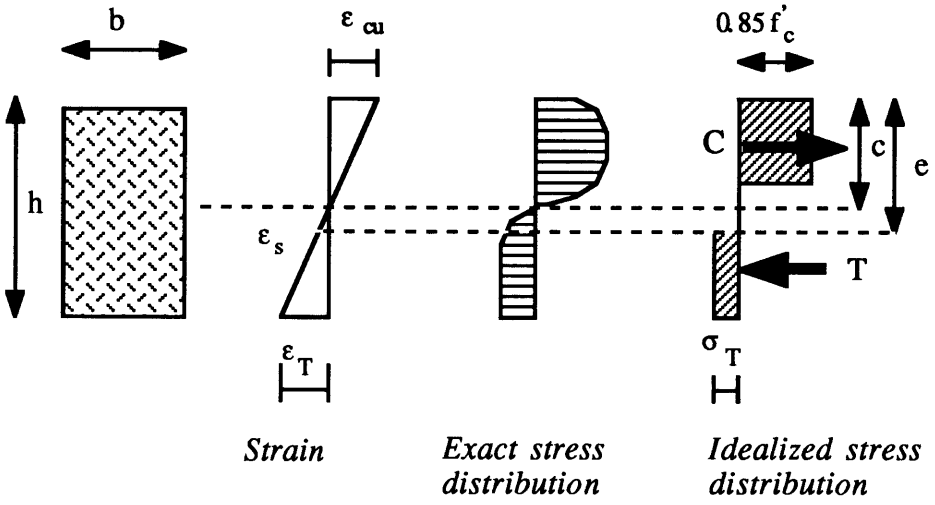

Figure 7.1 Stress/strain distributions for the Henager and Doherty (1976) model.

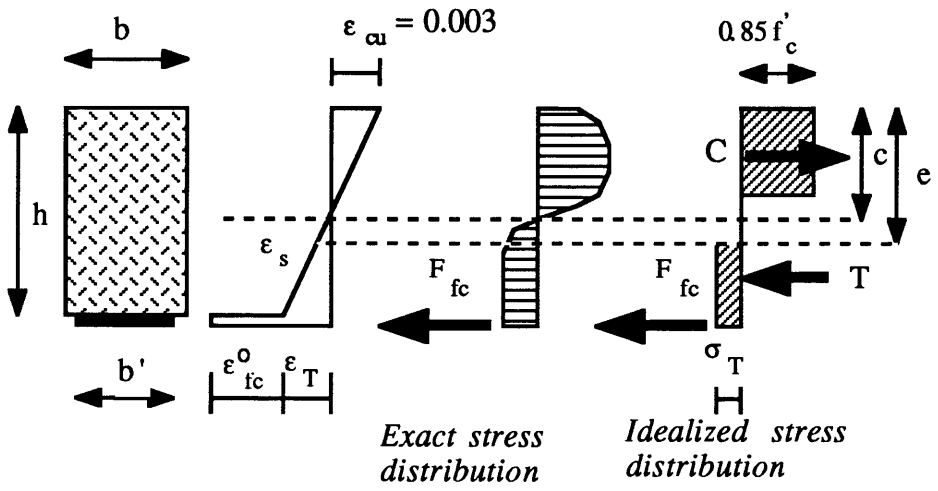

Figure 7.2 Stress/strain distribution at failure for FRP-prestressed FRC beam.

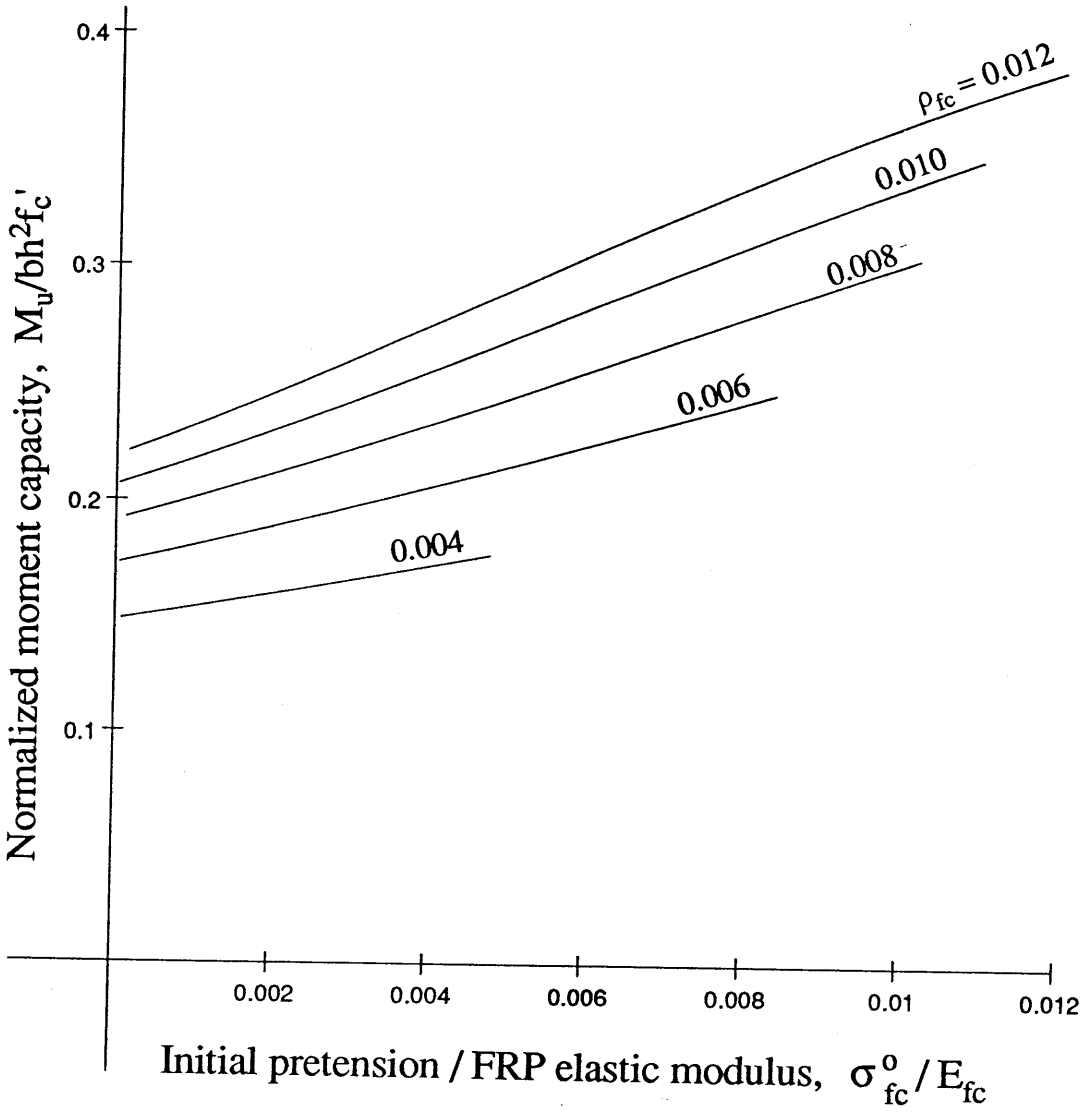

Figure 7.3 Normalized moment capacity vs. normalized prestress level for various FRP area fractions.

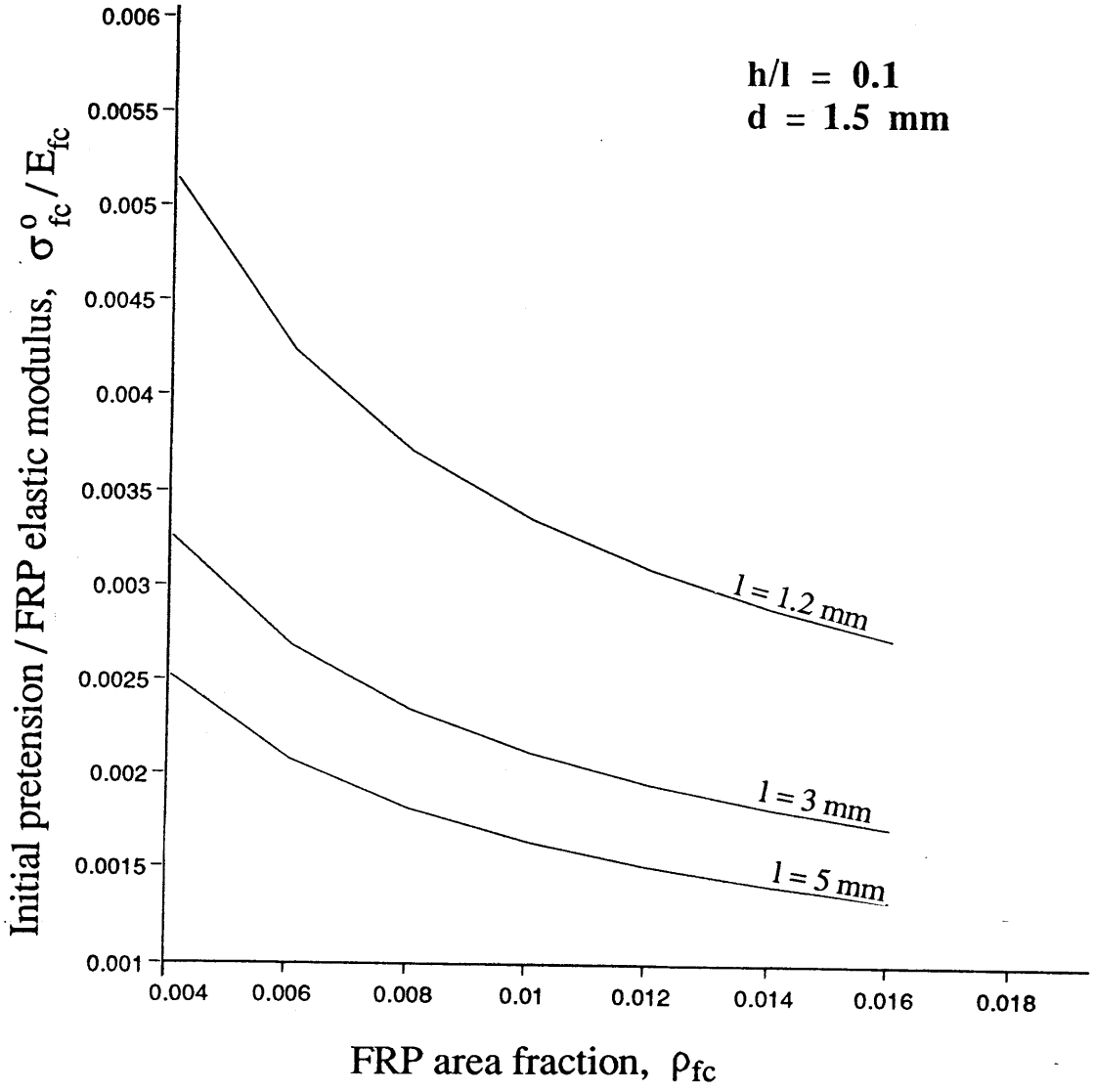

Figure 7.4 Normalized prestress level as a function of the FRP area fraction for three different beam lengths.

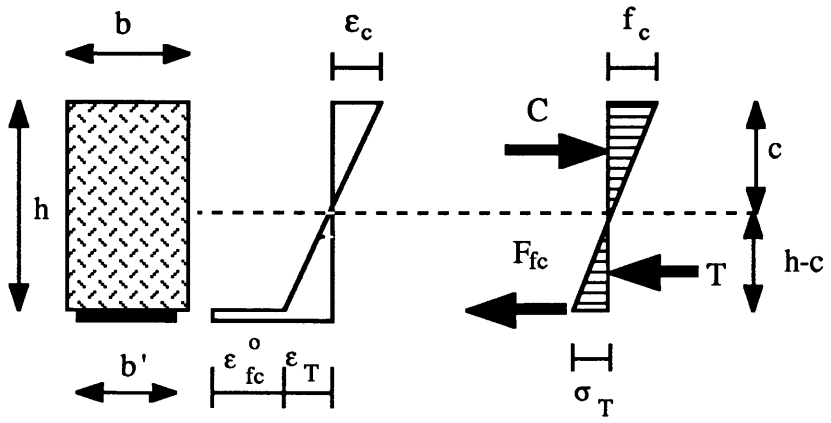

Figure 7.5 Stress/strain distribution at first cracking of a FRP-prestressed cross section.

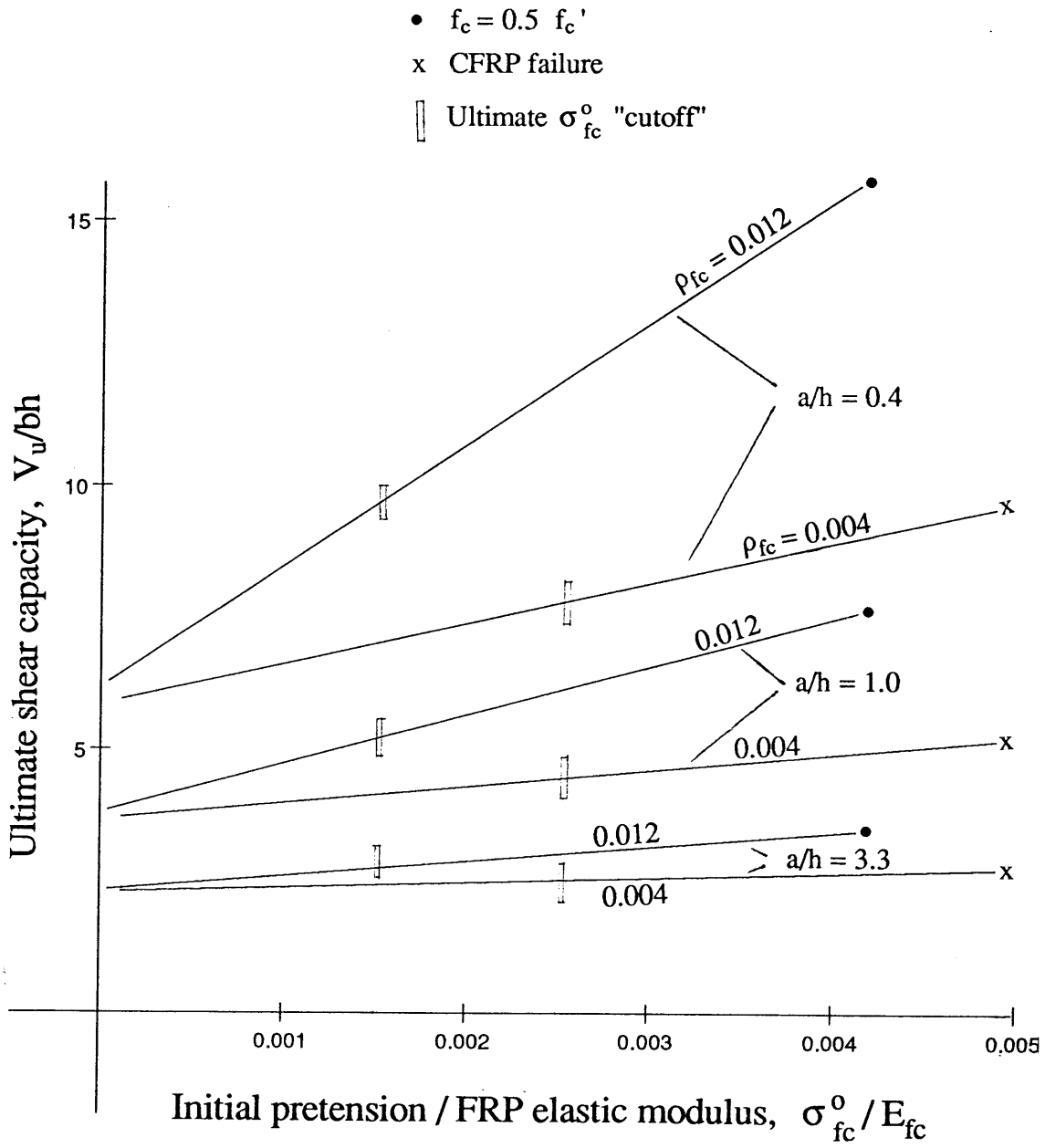

Figure 7.6 Normalized shear capacity vs. normalized prestress level for various FRP area fractions and shear-span-to-depth ratios.

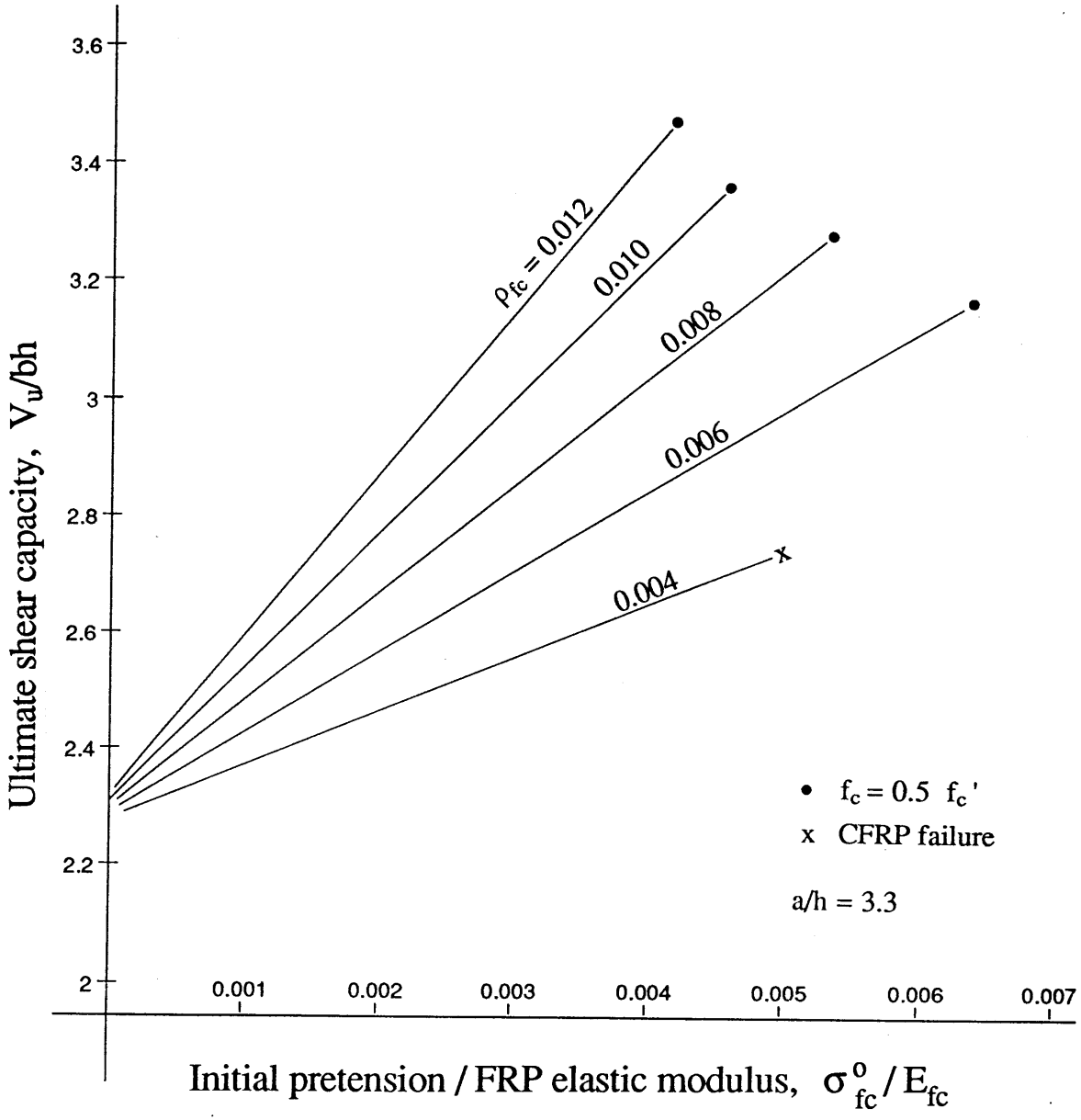

Figure 7.7 Normalized shear capacity vs. normalized prestress level for various FRP area fractions and a/h =3.3.

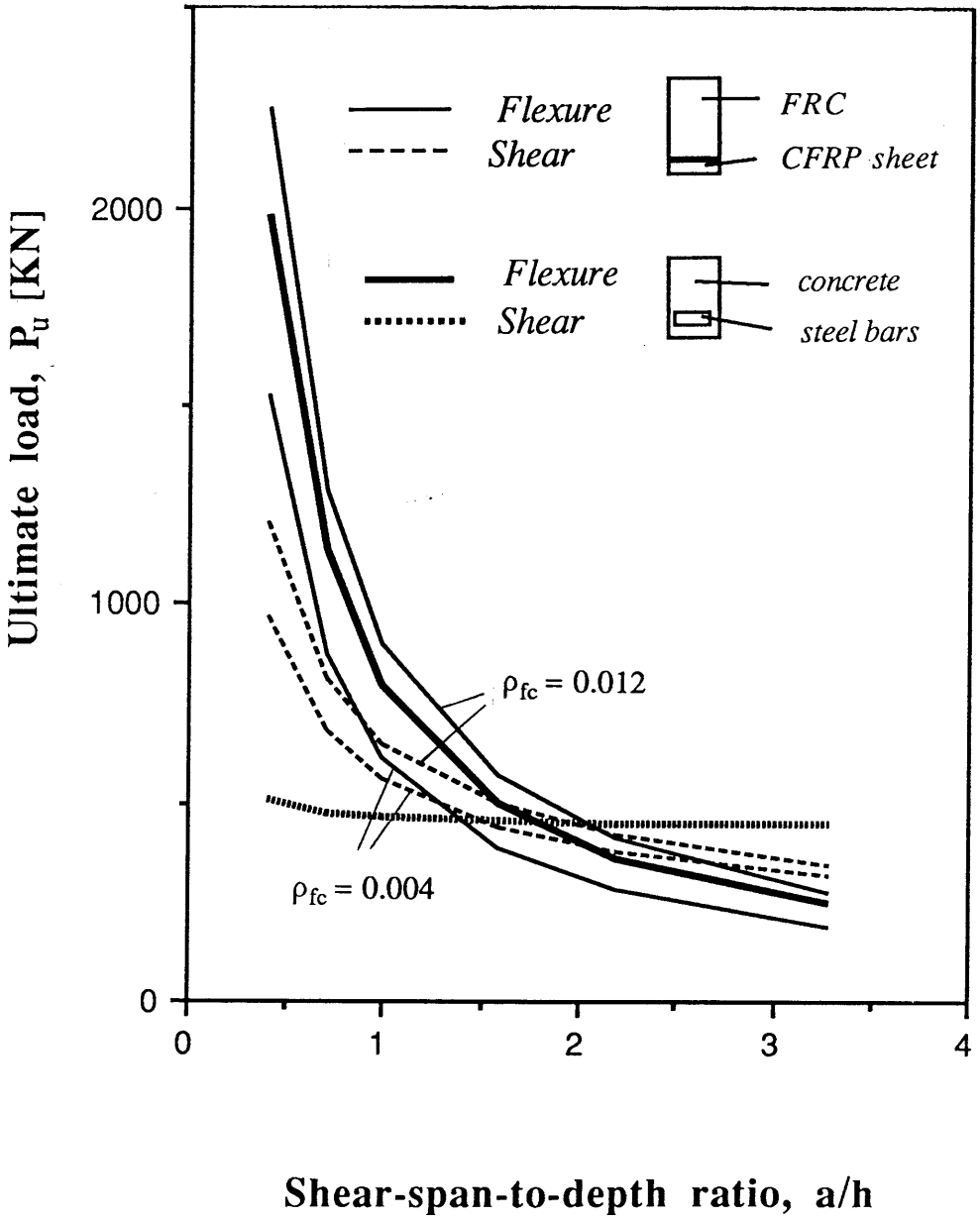

Figure 7.8 Comparison of design methods.

CHAPTER 8

SUMMARY - CONCLUSIONS - RECOMMENDATIONS

8.1 SUMMARY

An innovative method of prestressing structures is presented in this work. The technique involves external bonding of pretensioned fiber-reinforced plastic composite sheets on the tension zones of structural elements. The mechanics associated with the short term behavior of this novel prestressing scheme was investigated.

First, analytical models describing the maximum achievable prestress level so that the FRP-prestressed system does not fail near the anchorage zones were developed. Account was taken for the failure of either the adhesive layer or the beam material, depending on which of the two is characterized by the lowest shear strength. In the latter case, analytical solutions for concrete and wood beams were derived considering both linear and nonlinear material behavior. In addition, equations for the beam-FRP interface shear and beam bottom fiber normal stress were obtained. Based on experimental results it was shown that the proposed analytical solutions give good estimates of the ultimate pretension when concrete beams are prestressed with the new technique. It was demonstrated that the surface preparation at the interface plays an important role for the achievable prestress level and should be carefully taken into account in practical applications. The experiments showed that prestressing of externally bonded CFRP sheets on concrete and wood beams represents a viable and promising method for strengthening and/or reinforcing structures.

Next, the short term flexural behavior of reinforced concrete beams externally

prestressed with FRP sheets was investigated both analytically and experimentally. Equations for the bending moment at first cracking, steel yielding and concrete crushing were derived. Comparison of the analytical solutions with experimental data obtained from three point bending tests verified the validity of the strain compatibility method used in the analysis. The analytical prediction of the bending behavior compared well to the experimental results, although the predicted ultimate moment capacities appear rather conservative; this was expected, since the analysis was based on code assumptions for the concrete model. The efficiency of the innovative prestressing method was investigated using a computer program to analyze the ultimate moment capacity as a function of the FRP sheet area fraction.

Similarly, the flexural behavior of FRP-prestressed wood beams was investigated and equations for the bending moment at wood first yield in compression and CFRP rupture were derived. The analytical solutions were verified experimentally in three point bending tests and good agreement between experiment and analysis was obtained. It was shown that this method of prestressing wood members appears to be a simple, efficient and in some cases cost effective method to strengthen existing or produce new structural members.

Finally, a new concept of hybrid FRP-concrete structural elements was presented. The innovative idea proposes replacing the traditional steel reinforcement of concrete structures with high mechanical performance and durability materials. The behavior in flexure and shear of fiber-reinforced concrete elements with externally bonded prestressed CFRP sheets was studied and a feasibility study was carried out comparing the traditional designs of R/C structures to the new concept. It was demonstrated that the innovative method of designing concrete structures represents a successful design concept which, given experimental verification, could be implemented in the industry of prefabricated structural elements.

8.2 CONCLUSIONS

The novel prestressing technique involving external bonding of prestressed CFRP sheets on the tension zones of structural elements represents an applicable method for strengthening existing structures as well as reinforcing new ones. The results from the analysis of the ultimate achievable prestress level suggest that the latter increases by increasing the thickness of the adhesive layer and/or decreasing the area fraction of the composite material. On the other hand, the prestress introduced in the beam's bottom fiber is improved by increasing the adhesive thickness and/or the FRP area fraction. It is remarkable that the prestress is almost constant along the beam and drops almost suddenly to zero near the two ends (anchorage zones).

When concrete beams are prestressed with this method, the length of the nonlinear zone increases with the FRP area fraction and decreases with the adhesive thickness, unless extremely thin adhesive layers are used and adhesive shear failure starts to govern. The nonlinear zone also increases when the length of the member decreases. When, on the other hand, high shear strength wood beams are prestressed with FRP sheets, the nonlinear zone decreases with adhesive thickness.

The flexural behavior of R/C beams reinforced with externally prestressed CFRP sheets shows remarkable improvement when compared to members without composite reinforcement. Concrete first cracking, steel yielding and concrete crushing moment capacities are all increased, while ductility is maintained if the composite sheets are extended into the supports. The effect of pretensioned CFRP sheets was not found to be significant when compared to unprestressed beams with the same composite area fraction; the increase in the moment capacity lies in the range of 10% only. This is due to the constraint imposed by the ultimate prestress level that can be applied. To relax this constraint additional anchoring mechanical devices may be needed or the shear strength of the member should be increased (at least near the bottom zone) through, for instance, the use of short fiber reinforcement. If efficiency of the prestress procedure is defined by the ratio of the ultimate prestress level to the pretension that would cause a CFRP sheet failure, low composite area fractions appear more efficient and the high performance

material is properly explored. On the other hand, if high composite area fractions are required for flexure, high efficiency can be achieved only if appropriate anchoring devices are employed.

Reinforcing wood structures with externally bonded prestressed CFRP sheets appears to be an efficient and simple method for strengthening existing members and/or fabricating new ones. Since wood materials are characterized by a variety of different types and the flexural behavior is closely related to the material properties of the wood itself, the improvements in bending behavior resulting from the new prestressing method also vary. If wood types with brittle failure modes are used, the ultimate moment capacity will be improved with increasing prestress level, since failure will occur due to wood tensile failure. On the other hand, if ductile wood types are employed the flexural moment capacity will decrease with pretension increase, since the ultimate CFRP sheet tension strain is reached sooner and as a result composite sheet failure governs. Prestressing of the externally bonded sheets increases the stiffness, regardless of wood type. When ductile wood types are employed and tensile failure of the composite sheet governs, the ductility is inversely proportional to the degree of prestress while in the case of sufficiently reinforced brittle wood types the ductility increases with prestressing since larger compression zones become plastic. The shear strength of wood allows for significant pretension levels and therefore high efficiency of the prestressing method can be achieved.

The innovative prestressing technique can be implemented efficiently in the fabrication of new concrete structures. A new design concept, consisting of fiber-reinforced concrete prestressed by externally bonded CFRP sheets can substitute the traditional R/C design. Corrosion resistance and simple fabrication are the main advantages of this system. The ultimate flexural and shear capacities of the elements designed according to the proposed method are at least equal to and sometimes exceed the corresponding values for conventional reinforced concrete designs when ultimate prestress levels (such that the system does not fail when the ends are released) are applied. Furthermore, when adequate anchorage devices are used, the efficiency of the innovative design will increase making it possible to employ more economical CFRP area

fractions.

The relatively high expense of the CFRP material used in the new method can be justified in both strengthening of existing structures and the fabrication of new ones: The low weight and high stiffness of CFRP sheets allows for simpler application procedures eliminating the expensive scaffolding needed for traditional strengthening techniques with steel plates. Corrosion and fatigue resistance are additional cost saving aspects. For new constructions, the innovative method finds its advantages through a simple fabrication process, electromagnetic neutrality (important for structures supporting magnetic levitation railroads) and again high corrosion resistance where long term savings are imminent. On the other hand, the market price of CFRP materials should decrease in the future due to increased demand and production and hence, it can be anticipated that the method proposed in this work will be employed in future applications.

8.3 RECOMMENDATIONS FOR FUTURE RESEARCH

The short term behavior of an innovative method of prestressing structures was investigated in this work. The technique's range of applicability includes the rehabilitation/strengthening of structures as well as the construction of new prefabricated ones. However, in view of the viscoelastic nature of the epoxy adhesives, it is imperative that creep and relaxation behavior of the constituent materials be examined in detail before the method can be applied in construction practice. Work needs to be carried out to obtain an understanding and model the long term characteristics (creep, fatigue) of the technique. The author believes that the system's long term behavior response will be quite satisfactory with some detailing of the end anchorage zones. An experimental verification of the proposed innovative design concept for concrete structures has to be performed. In conjunction to these experiments, shear pullout tests of CFRP sheets bonded to fiber-reinforced concrete need to be carried out to characterize the softening behavior of FRC in shear. The design of efficient anchorage device mechanisms needs further research and additional failure modes of concrete and wood members in flexure

have to be investigated. A cost efficiency analysis needs to be carried out in order to prove and justify the method's perspective and its application potential.

REFERENCES

ACI (1986) Design Consideration for Steel Fiber Reinforced Concrete, *ACI Structural Journal*, Committee Report 544, 4R **85**(6), pp. 563-580.

ACI (1989) *Building Code Requirements for Reinforced Concrete* (ACI 318-89), *and Commentary* (ACI 318-89), Detroit, Michigan.

Aleszka, J. C., and Beaumont, P. W. (1973) The Fracture Behavior of Plain, Polymer-Impregnated, and Fiber-Reinforced Concrete, *Regist No. UCLA-ENG- 7396*, University of California, Los Angeles.

Aminian, P. K. and White, J. K. (1988) A review of the properties of type F (Kevlar 29) Parafil cables with reference to the design of cable structures, *Symposium on Engineering applications of Parafil ropes*, Imperial College of Science and Technology, January 6, London, UK.

Bakeri, P. A. (1989) *Analysis and Design of Polymer Composite Bridge Decks*, S.M. Thesis Submitted to the Department of Civil Engineering, Massachusetts Institute of Technology, Cambridge, MA.

Balaguru, P. and Ezeldin, A. (1987) Behavior of Partially Prestressed Beams Made with High Strength Fiber Reinforced Concrete, *Fiber Reinforced Concrete-Properties and Applications*, SP 105-24, American Concrete Institute, pp. 419-436.

Bank, L. C. and Mosallam, A. S. (1990) Structural Performance of a Fiber Reinforced Plastic Pultruded Frame, *Proceedings of the 8th Structures Congress '90*, ASCE.

Batson, G., Jenkins, E. and Spatney, R. (1972) Steel Fibers as Shear Reinforcement in Beams, ACI JOURNAL, *Proceedings*, **69**(10), pp. 640-644.

Bazan, I. M. M. (1980) *Ultimate Bending Strength of Timber Beams,* thesis presented to Nova Scotia Technical College, at Halifax, Nova Scotia, in partial fulfillment of the requirements for the degree of Doctor of Philosophy.

Beton Kalender (1987) Verlag fur Architektur und Technische Wissenschaften, Ernest & Sohn, Berlin.

Blood, G. W. (1978) *Properties of Fiber Reinforced Concrete,* MS Thesis, the University of Calgary, Alberta.

Brown, V. L. and Bartholomew, F. (1990) FRP Rebar in Reinforced Concrete Members, *Proceedings of the 8th Structures Congress '90*, ASCE.

Buchanan, A.H. (1990) Bending Strength of Lumber, *Journal of Structural Engineering*, ASCE, **116**(5), pp. 1213-1229.

Burgoyne, C. J. (1988) Structural applications of Type G Parafil, *Symposium on Engineering applications of Parafil ropes*, Imperial College of Science and Technology, January 6, London, UK.

CEB-FIP (1970) International Recommendations for the Design and Construction of Concrete Structures.

Chambers, J. J. (1986) *Parallel-lay aramid ropes for use as tendons in prestressed concrete*, Ph.D. Thesis submitted to the University of London, UK.

Craig, R. J. (1983) Design Procedures for Fibrous Concrete-Shear, Moment and Torsion *Proceedings, Structural Concrete Design Conference*, New Jersey Institute of Technology , Newark, March 4, pp. 253-284.

Craig, R. J. (1984) Structural Applications of Reinforced Fibrous Concrete, *Concrete International: Design & Construction,* **6** (12), pp. 28-32.

Deuring, M. (1990) Personal communication.

Dunker, K. F., Klaiber, F. W., Beck, B. L. and Sanders, W. W., Jr. (1985) Strengthening of Existing Single-Span Steel Beam and Concrete Desk Bridges, *Report No. ISUERI-Ames-85231*, Department of Civil Engineering, Iowa State University, Ames.

Faza, S. S. and GangaRao, H. (1990) Behavior of Fiber Reinforced Plastic Rebar Under Bending, *Proceedings of the 8th Structures Congress '90*, ASCE.

Fleming, C. J. and King, G. E. M. (1967) The Development of Structural Adhesives for three original uses in South Africa, *RILEM International Symposium, Synthetic Resins*

in Building Construction, Paris, pp. 75-92.

Fu, S. H., Prucz, J. C. and Spyrakos, C. C. (1990) Structural Performance of I-Beams Made of Fiber Reinforced Plastics (FRP) *Proceedings of the 8th Structures Congress '90*, ASCE.

Fujisaki, T., Matsuzaki, Y., Sekijima, K. and Okamura, H. (1987) New Material for Reinforced Concrete in Place of Reinforcing Steel Bars, *IABSE Symposium, Concrete Structures of the Future,* Paris-Versailles, pp. 695-696.

Gerritse, A., Maatjes, E. and Schurhoff, H. J. (1987) Prestressed Concrete Structures with High Strength Fibers, *IABSE Symposium, Concrete Structures of the Future*, Paris-Versailles, pp. 425-432.

Goldfine, S. (1963) Plastic Fibrous Reinforcement for Portland Cement, *Technical report No. 1757-TR*, U.S. Army Engineering Research and Development Laboratory, Fort Belvoir, Va.

Golopalaratnam, V. S. and Shah, S. P. (1987) Failure Mechanisms and Fracture of Fiber Reinforced Concrete, *Fiber Reinforced Concrete-Properties and Applications*, SP 105, American Concrete Institute, pp. 1-25.

Grimer, F. J. and Ali, M.A. (1969) The Strength of Cements Reinforced With Glassfibers, *Magazine of Concrete Research* (London), **21** (66), pp. 23-30.

Henager, C. H. and Doherty, T. J. (1976) Analysis of Reinforced Fibrous Concrete Beams, *Proceedings*, ASCE, **12** (ST1), pp. 177-188.

Hull, D.(1981) *An Introduction to Composite Materials*, Cambridge University Press, UK.

Jindal, R. L. (1984) Shear and Moment Capacities of Steel Fiber Reinforced Concrete Beams, *Fiber Reinforced Concrete-International Symposium*, SP-81, American Concrete Institute, pp. 1-16.

Johnston, C. D.(1980) Properties of Steel Fiber Reinforced Mortar and Concrete, *Proceedings, International Symposium on Fibrous Concrete (CI-80)*, Construction Press, Lancester, pp. 29-47.

Jones, R., Swamy, R.N., Bloxham, J. and Bouderbalah, A. (1980) Composite

Behavior of Concrete Beams With Epoxy Bonded External Reinforcement, *International Journal of Cement Composites and Lightweight Concrete*, **2** (2), pp. 91-107.

Kaifasz, S. (1963) Some Tests on Beams Prestressed by Fiberglass Cords, *Magazine of Concrete Research*, **15**, pp. 91-98.

Kaifasz, S. (1967) Concrete Beam with External Reinforcement Bonded by Gluing, *RILEM International Symposium, Synthetic Resins in Building Construction,* Paris, pp. 141-151.

Kaiser, H. (1989) *Strengthening of Reinforced Concrete with Epoxy-Bonded Carbon-Fiber Plastics*, Doctoral Thesis, ETH (in German).

Kinloch, A. J. (1987) *Adhesion and Adhesives*, Chapman and Hall.

Klaiber, F. W., Dunker, K. F.; Wipf, T. J. and Sanders, W. W., Jr. (1987) Methods of Strengthening Existing Highway Bridges, *NCHRP Research Report* No. 293, Transportation Research Board.

Ladner, M. and Weder, C. (1981) Concrete Structures with Bonded External Reinforcement, *EMPA Report* No. 705.

Leonhard, F. (1973) Procede de construction par cycles de betonnage en coffrage fixe et cycles de poussage. *Annales de l'I.T.B.T.P.*, pp. 46-63.

Lerchenthal, C. H. (1967) Bonded Steel Reinforcement for Concrete Slabs, *RILEM International Symposium, Synthetic Resins in Building Construction*, Paris, pp. 165-173.

L'Hermite, R. and Bresson, J. (1967) Concrete Reinforced with Glued Plates, *RILEM International Symposium, Synthetic Resins in Building Construction*, Paris, pp. 175-203.

MacDonald, M. D. and Calder, A. J. J. (1982) Bonded Steel Plating for Strengthening Concrete Structures, *International Journal of Adhesion and Adhesives,* **2** (2), pp. 119-127.

Magnel, G. (1953) Le beton precontraint, Vol. IV, Serie Pratique du calcul du beton

arme.

Majumdar, A. J. (1970) Glass Fiber Reinforced Cement and Gypsum Products, *Proceedings*, Royal Society of London, No. A 319, pp. 69-78.

McCormick, F. C. (1978) Laboratory and Field Studies of a Pedestrian Bridge Composed of Glass Reinforcement Plastic, *Transportation Research Record 665, National Research Council,* Washington, DC., pp. 99-107.

Meier, U. (1986) Future Use of Advanced Composites in Bridge Construction Engineering, *Proceedings of the Institution of Mechanical Engineering,* C46, pp. 217-223.

Meier, U. (1987a) Proposal for a carbon fibre reinforced composite bridge across the Strait of Gibraltar at its narrowest site, *Proceedings of the Institution of Mechanical Engineers,* **201**(B2), pp. 73-78.

Meier, U. (1987b) Bridge Repair with High Performance Composite Materials, *Material and Technik,* **4**, 125.

Meier, U. (1990) Personal communication.

Muller, J. (1980) Construction of the Long King Bridge, *PCI Journal*, pp. 97-111.

Naaman, A. E., and Shah, S. P. (1976) Pullout Mechanism in Steel Fiber Reinforced Concrete, *Proceedings*, ASCE, **102** (ST8), pp. 1537-1548.

Park, P., and Paulay, T. (1975) *Reinforced Concrete Structures*, John Wiley & Sons, New York.

Pearlman, S. L. (1979) *Flexural Performance of Reinforced Steel Fiber Concrete Beams*, MS Thesis, Carnagie-Mellon University, Pittsburgh.

Plecnik, J. (1989) Chapter 7 of a Draft Technical Report.

Plecnik, Joseph M., Hamoud, A. S., Ballinger, C. and Plecnik, John M. (1989) Development of High Strength Composite Cables, *Proceedings of the sessions related to structural materials at Structures Congress '89*, ASCE.

Preis, L. and Bell, T. A. (1986) Fiberglass Tendons for Posttensioning Concrete

Bridges, *Transportation Research Record 1118, National Research Council,* Washington, DC., pp. 77-82.

Ranisch, E. H. and Rostasy, F. S. (1986) Bonded Steel Plates for the Reduction of Fatigue Stresses of Coupled Tendons in Multispan Bridges, in *Adhesion between Polymers and Concrete, RILEM ISAP 86*, pp. 561-570.

Rehm, G. and Franke, L. (1974) Synthetic-Resin Reinforced Bundled Glass Fiber Rods as Reinforcement in Concrete Construction, *Die Bautechnik*, **115**, 132 (in German).

Rehm, G. and Franke, L. (1979) Reinforced GRP-Rods as Reinforcement of Concrete, *Deutscher Ausschuss for Stahlbeton*, **304** (in German).

Rubinsky, I. A. and Rubinsky, A. (1954) A Preliminary Investigation of the Use of Fiberglass for Prestressed Concrete, *Magazine of Concrete Research*, **6**, pp. 71-78.

Saadatmanesh, H. and Ehsani, M. (1989) Application of Fiber-Composites in Civil Engineering, *Proceedings of the sessions related to structural materials at Structures Congress '89*, ASCE.

Saadatmanesh, H., Albrecht, P. and Ayyub, B. M. (1989) Experimental Study of Prestressed Composite Beams, *Journal of Structural Engineering*, ASCE, **115** (9), pp. 2344-2364.

Schroff, J. K. (1966) *The Effect of a Corrosive Environment on the Properties of Steel Fiber Reinforced Portland Cement Mortar*, MS Thesis, Clarkson College of Technology, Potsdam, NY.

Sharma, A. K. (1986) Shear Strength of Steel Fiber Reinforced Concrete Beams, ACI JOURNAL, *Proceedings*, **83** (4), pp. 624-628.

Somes, N. F. (1963) Resin-Bonded Glass-Fiber Tendons for Prestressed Concrete, *Magazine of Concrete Research*, **15**, pp. 151-158.

Swamy, R. N. and Al-Ta'an, A. A. (1981) Deformation and Ultimate Strength in Flexure of Reinforced Concrete Beams made with Steel Fiber Concrete, ACI JOURNAL, *Proceedings*, **78** (5), pp. 395-405.

Swamy, R. N., Jones, R. and Bloxham, J. W. (1987a) Structural Behavior of Reinforced Concrete Beams Strengthened by Epoxy-Bonded Steel Plates, *The Structural*

Engineer (London), **65A** (2), pp. 59-68.

Snyder, M. J. and Lankard, D. R. (1972) Factors Affecting the Flexural Strength of Steel Fibrous Concrete, ACI JOURNAL, *Proceedings*, **69** (2), pp. 96-100.

Triantafillou, T. and Plevris, N. (1990) Strengthening of R/C Beams with Epoxy-Bonded Fiber-Composite Materials, *submitted to Materials and Structures,* RILEM.

Virlogeux, M. P. (1990) External Prestressing: from Comstruction History to Modern Technique and Technology, *External Prestressing in Bridges*, American Concrete Institute, SP 120-1, pp. 1-61.

Waaser, E. and Wolff, R. (1986) A New Material for Prestressed Concrete-HLV High-Performance Glass Fiber Connecting Rods, *Beton*, **36**, pp. 245-250.

Weiser, M. and Preis, L. (1984) Synthetic-Resin Reinforced Bundled Glass Fiber Rods-A Corrosion-Resistant Alternative to Prestressed Steel, *Fortschritte im konstruktiven Ingenieurbau*, pp. 79-85.

Williamson, G. R. (1965) Fibrous Reinforcement for Portland Cement Concrete, *Technical Report No. 2-40*, U.S. Army Corps of Engineers Ohio River Division Laboratories, Cincinnati.

Williamson, G. R. (1973) Compression Characteristics and Structural Beam Design Analysis of Steel Fiber Reinforced Concrete, *Technical Report No. M-62*, U.S. Army Construction Engineering Researsh Laboratory, Champain.

Williamson, G. R. (1974) The Effect of Steel Fibers on the Compresive Strenght of Concrete, *Fiber Reinforced Concrete*, SP-44, American Concrete Institute, pp.195-207.

Williamson, G. R. and Knab, L. I. (1975) Full Scale Fiber Concrete Beam Tests, *Fiber Reinforced Cement and Concrete*, RILEM Symposium 1975, Construction Press, Lancaster, pp. 209-214.

Williamson, G. R. (1978) Steel Fibers as Web Reinforcement in Reinforced Concrete, *Proceedings*, U.S. Army Science Conference, West Point, **3**, pp. 363-377.

Wolff, R. and Miesseler, H. (1987) Heavy Duty Composite Material for Prestressing, *IABSE Symposium, Concrete Structures of the Future,* Paris-Versailles, pp. 695-696.

Wright, P. J. F. (1955) Comments on an Indirect Tensile Test on Concrete Cylinders, Magazine of Concrete Research (London), **7** (20), pp. 87-96.